AD-A130 998 MEASUREMENTS OF ATMOSPHERIC AEROSOLS: EXPERIMENTAL METHODS AND RESULTS OF..(U) NAVAL RESEARCH LAB WASHINGTON DC W A HOPPEL ET AL. 19 JUL 83 NRL-8703 1/1

UNCLASSIFIED F/G 4/1 NL

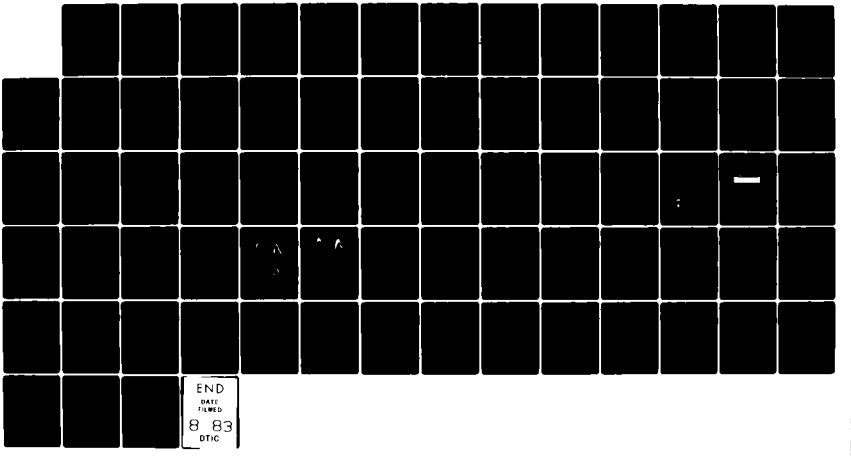

END
DATE FILMED
8 83
DTIC

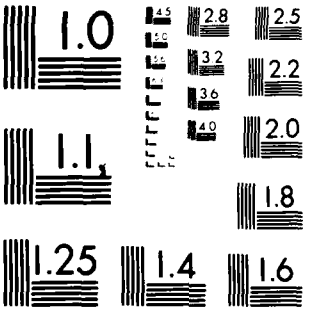

NRL Report 8703

Measurements of Atmospheric Aerosols: Experimental Methods and Results of Measurements Off the East Coast of the United States

WILLIAM A. HOPPEL, JAMES W. FITZGERALD, AND REGINALD E. LARSON

Atmospheric Physics Branch
Environmental Sciences Division

July 19, 1983

NAVAL RESEARCH LABORATORY
Washington, D.C.

SECURITY CLASSIFICATION OF THIS PAGE (When Data Entered)

REPORT DOCUMENTATION PAGE	READ INSTRUCTIONS BEFORE COMPLETING FORM
1. REPORT NUMBER NRL Report 8703	2. GOVT ACCESSION NO. AD-A130948
3. RECIPIENT'S CATALOG NUMBER	
4. TITLE (and Subtitle) MEASUREMENTS OF ATMOSPHERIC AEROSOLS: EXPERIMENTAL METHODS AND RESULTS OF MEASUREMENTS OFF THE EAST COAST OF THE UNITED STATES	5. TYPE OF REPORT & PERIOD COVERED Interim report on continuing NRL problems.
	6. PERFORMING ORG. REPORT NUMBER
7. AUTHOR(s) William A. Hoppel, James W. Fitzgerald, and Reginald E. Larson	8. CONTRACT OR GRANT NUMBER(s)
9. PERFORMING ORGANIZATION NAME AND ADDRESS Naval Research Laboratory Washington, DC 20375	10. PROGRAM ELEMENT, PROJECT, TASK AREA & WORK UNIT NUMBERS 61153N, RR033-02-42 61153N, WR033-02-001 NRL Problems 43-1110-0-3 and 43-1111-0-3
11. CONTROLLING OFFICE NAME AND ADDRESS Office of Naval Research, Arlington, VA 22217 Naval Air Systems Command, Arlington, VA 20361	12. REPORT DATE July 19, 1983
	13. NUMBER OF PAGES 70
14. MONITORING AGENCY NAME & ADDRESS(if different from Controlling Office)	15. SECURITY CLASS. (of this report) UNCLASSIFIED
	15a. DECLASSIFICATION/DOWNGRADING SCHEDULE

16. DISTRIBUTION STATEMENT (of this Report)

Approved for public release; distribution unlimited.

17. DISTRIBUTION STATEMENT (of the abstract entered in Block 20, if different from Report)

18. SUPPLEMENTARY NOTES

19. KEY WORDS (Continue on reverse side if necessary and identify by block number)

Atmospheric aerosols
Visibility
Marine aerosols
Particle size distributions
Electromagnetic extinction

20. ABSTRACT (Continue on reverse side if necessary and identify by block number)

Accurate measurements of the size distribution of atmospheric aerosols in the size (radius) range from 0.006 to 2.2 micrometers made along the east coast of the United States both at a shore site (Wallops Island) and from a ship within 300 km of the coast are presented. Some measurements at Washington, D.C., are included to contrast urban aerosols with aged continental air off the east coast. As air advects from land to sea, there is a rather rapid decay of particles smaller than 0.05 micrometers during the first day or so. After this initial decay of small particles the size distribution

(Continued)

DD FORM 1 JAN 73 1473 EDITION OF 1 NOV 65 IS OBSOLETE
S/N 0102-014-6601

SECURITY CLASSIFICATION OF THIS PAGE (When Data Entered)

20 ABSTRACT (Continued)

was often found to remain remarkably stable for hours. Significant changes in the size distribution were often associated with changes in air masses and meteorological conditions. Some of the changes can be explained qualitatively. Others, such as a pronounced double peak which occurred occasionally in the fine-particle range, are difficult to understand.

Measurements of the activation parameter for submicrometer particles were also made and yield values in the range of 0.1 to 0.55.

Using the measured size distribution, electromagnetic extinction was calculated for the wavelength range 0.3 to 12 micrometers. The calculations compare favorably to the measured scattering coefficient at 0.55 micrometers in wavelength. Particles in the radius range 0.1 to 0.3 micrometer made the largest contribution to the total extinction at optical wavelengths on nearly all occasions.

The instrumentation and methods which were developed at NRL are described in some detail in the report.

CONTENTS

PREFACE

This report is written for two audiences, with the first being our sponsors at NRL, ONR, and NAVAIR, whom we wish to provide with a self-contained document of our accomplishments in the area of aerosol measurements over the last several years without their need to consult numerous other publications in scientific journals. Sufficient background is given so that our sponsors can place our work in perspective and distinguish NRL's unique contributions. The second audience consists of specialists in atmospheric aerosols. The third section of the report is a review of the instruments and methods developed at NRL. Much of this material can be found in the publications referenced. The latter part of the report contains the results obtained on three field deployments, which are for the most part not yet reported in the open literature. A reader not interested in the measurement techniques or already familiar with NRL's capabilities may want to skip directly to the results and the discussion.

MEASUREMENTS OF ATMOSPHERIC AEROSOLS: EXPERIMENTAL METHODS AND RESULTS OF MEASUREMENTS OFF THE EAST COAST OF THE UNITED STATES

INTRODUCTION

Atmospheric aerosols are the population of particles suspended in the atmosphere and range in radius between atmospheric ions (about 1 nm) to precipitation-size particles (about 1 mm). Few studies deal with this entire size range, and the use of the term "aerosol" can often be confusing until the subset under discussion is further specified. Furthermore size is only one way to classify aerosols. For example, a meteorologist may refer to the total number of particles, regardless of size, as condensation nuclei (or Aitken nuclei), or the meteorologist may refer to the smaller subset which is active in natural clouds and fogs at low supersaturations ($<1\%$). The particles in this cloud-active subset are called cloud condensation nuclei (CCN). Aerosols can also be classified by their mode of formation, chemical composition, or method of measurement. All of the properties of aerosols are important in the total evaluation of aerosol effects, and many of the properties are interrelated. Thus, the scattering and absorption of electromagnetic (EM) radiation by aerosol particles depends on both their size and composition, as does their nucleating effectiveness in clouds and fogs.

Some reasons aerosols are important to the Navy are the following:

- Extinction of EM radiation used in surveillance, guidance, and communication systems is due both to the absorption bands of gaseous components of the atmosphere and to scattering and absorption by aerosols. Gaseous absorption is more predictable and better understood than scattering and absorption by aerosols in the atmosphere. Further research on the geographical distribution of aerosol properties is necessary in order to better design and evaluate systems. A capability to predict aerosol effects during military operations is also important.

- Weather modification and fog-visibility prediction depend on aerosols. All cloud and fog droplets form on aerosol particles; thus cloud microstructure, colloidal stability, and visibility are largely determined by the aerosol load prior to cloud formation. Cloud seeding is an effort to change the cloud properties by changing the aerosol on which it forms.

- Artificial aerosols generated by pyrotechnic devices to obscure naval operations are constantly being reevaluated and updated.

- Aerosols affect the solar radiation balance directly by scattering and absorption and indirectly by changing the cloud cover and the reflectivity (albedo). Although a change in the radiation balance may have no immediate effects on military operations, it is significant in projecting global climate changes and could affect military planning.

BACKGROUND

In 1977 the field of aerosol research was surveyed to determine which area of atmospheric aerosols was least understood, which area is the most important to the Navy, and where the NRL research

Manuscript approved February 14, 1983

effort could make the most significant contribution. It was readily concluded that little was known about particles smaller than 0.2 um in radius. Larger particles could be sized with optical particle counters and impactors, and single particles bigger than 1 μm in radius could be chemically analyzed using special techniques. The size distribution, chemical nature, geographical distribution, and mechanism of formation were all poorly understood for particles smaller than about 0.2 μm. This understanding was particularly poor for the marine environment but less poor for the urban environment, where small particles exist in much larger concentrations and where a larger effort in pollution studies has been supported (Hidy, 1972, and others). After reviewing the few submicrometer-size distribution measurements made in the marine environment, Jaenicke (1978) stated, "It is difficult to decide whether observed differences are due to differences in time and location of the measurements or whether the distributions are biased by the method of measurement."

Prior to 1976 NRL had extensively studied those atmospheric particles (CCN) which are active in cloud and fog formation where the supersaturations is rarely greater than 1%. During the early 1970s NRL made significant advances in instrumentation to measure CCN and made measurements of CCN concentrations and supersaturation spectra at many geographical locations from NRL aircraft and ships. From these data much information about the geographical and altitude distribution of CCN was obtained. Although the sizes of CCN were not determined precisely, it was shown that CCN were in the radius range of about 0.02 to 0.09 μm and were composed of a large fraction of soluble material (Twomey, 1965, and Hoppel, 1979). The composition was originally thought to be sea salt. However, volatility measurements made by NRL indicated the material was much too volatile to be sea salt (Twomey, 1968, 1971, Dinger, et al., 1970, and Hoppel et al., 1973) and was most likely to be substances such as ammonium sulfate formed by gas-to-particle conversion within the atmosphere itself (Hoppel et al., 1973, and Hoppel, 1975).

The dependence of visibility on relative humidity has been of considerable importance within the Navy. This humidity dependence is caused by the uptake of water by soluble aerosols at relative humidities above 50%. NRL developed a theoretical model of the growth of particles with increasing relative humidity using measured data on the chemical composition of larger particles (Fitzgerald, 1975, 1978). This model has been used in a number of Navy programs. More recently NRL has developed a unique method to measure the solubility (hygroscopicity) of submicrometer aerosols (Hoppel, 1979, and Fitzgerald and Hoppel, 1982). This method will be discussed later.

With NRL's historical interest in CCN, which are a subset of the submicrometer particles, it was quite natural to turn our attention to the entire population in that difficult and little explored region below 0.3 μm. It is a difficult region experimentally because the particles are below the optically detectable range and are too volatile to be probed by conventional methods such as electron microscopy. Since the particle sizes are of the order of the molecular mean free path (Fig. 1), neither continuum mechanics nor kinetic theory is applicable, and special theoretical methods are required.

In 1977 the NRL mobility analyzer was developed (Hoppel, 1978). This instrument (to be described later) has given us a unique capability to size particles in the range 0.006 to 0.5 μm. It has been used in two ways: primarily as a size spectrometer and secondarily as a means to segregate particles of nearly monodisperse size for further study. It was first used on a USNS *Hayes* cruise in 1977 but with limited sensitivity; even so, the results were unique (Hoppel, 1979). In 1978 a new instrument was developed (Hoppel et al., 1980) to detect and count single particles transmitted by the analyzer. When used with the mobility analyzer, this instrument gave us an extremely sensitive system which could be automated. The results of size distribution measurements to be given in this report are those obtained with the automated system. For particles larger than about 0.4 μm in radius, commercially available optical particle counters were used.

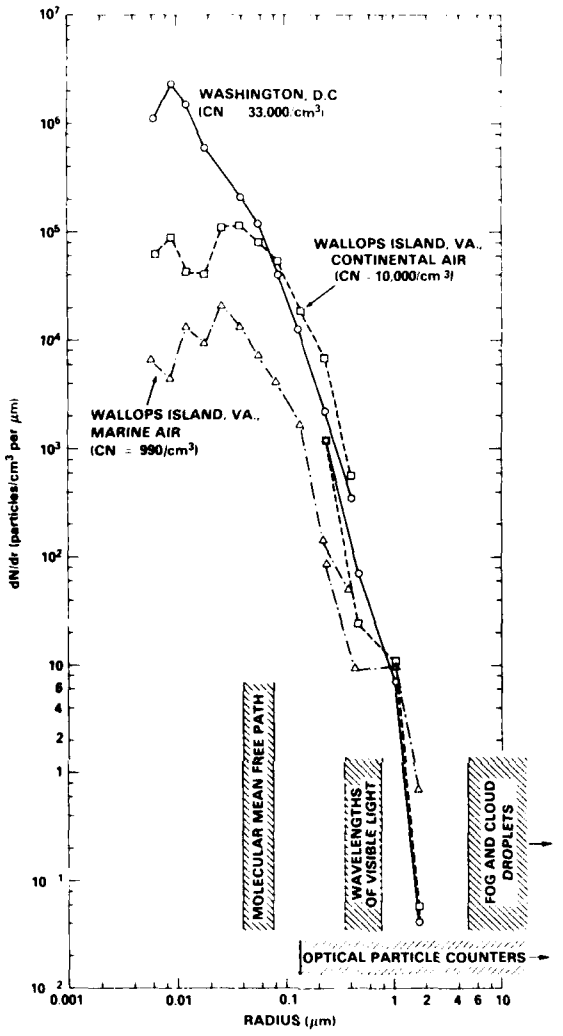

Fig. 1 — Typical size distributions of condensation nuclei (CN) for urban, continental, and coastal marine environments. Also shown are some benchmark dimensions.

Figure 1 illustrates the large concentration of particles in the size range below 0.2 μm as opposed to the larger size range accessible to optical probes. These size distributions were taken with the NRL mobility analyzer and are typical of the size distributions to be discussed in this report.

The ability to segregate small particles of nearly monodisperse size from a polydisperse sample is of prime importance in determining particle composition. If the chemical composition and dry size of a particle are known, then according to Köhler's theory it is possible to predict its size at higher relative humidities as well as the critical supersaturation at which the particle will be nucleated. Simultaneous data on the size distribution and supersaturation spectrum of known pure-salt aerosols taken at the Second International Workshop on Cloud and Ice Nuclei in 1970 (Grant, 1971) implied a relationship between dry size and critical supersaturation which deviated significantly from the relationship predicted by Köhler's theory. The acceptance of Köhler's theory and its extensive use in cloud physics was subsequently questioned in the literature (Katz and Kocmond, 1973). One of the first uses of the mobility analyzer was to segregate a narrow size range of particles and transmit it to the thermal-gradient

diffusion cloud chamber, where the critical supersaturation for nucleation could be measured. The results agreed with those predicted by Köhler's theory for known salts (Gerber et al., 1977) and were readily accepted as validating that theory. The difficulty in the earlier experiments was that the measurements were much less accurate than was claimed. Extension of these measurements to natural aerosols has led to the first measurements of the solubility of natural particles smaller than 0.1 μm. Some of these data have recently been published (Fitzgerald et al., 1982) and will also appear in this report.

In 1979 and 1980 a number of field measurements were made with the automated system together with supporting measurements. During June 1979 12 days of measurements were made on the Atlantic coast at NASA's Wallops Island rocket launching site. The purpose of these measurements was to differentiate the size distribution of marine and continental aerosols. In July 1979 several weeks were spent making measurements at NRL's Potomac River waterfront to test the system and to sample urban air. Then in April 1980 we participated in a 2-week cruise off the coast of the United States with scientists from the NRL Environmental Biology Branch. The object of our participation was to study the change in the aerosol size distribution in air masses advecting off the east coast. Then in the fall of 1980 we participated in the International Cloud Condensation Nuclei Workshop. In addition to taking the thermal-gradient diffusion cloud chamber (TGDCC) and the newly developed isothermal haze chamber (IHC) for comparison with other such instruments, NRL was invited to bring the NRL mobility analyzer to characterize the size distribution of aerosols used at the workshop.

In this report the results of the first three field trips mentioned will be presented with emphasis on the data obtained on the 1980 *Hayes* cruise. The results of measurements at the International Workshop have been adequately reported in the workshop proceedings and in four articles by NRL personnel (Fitzgerald et al., 1981, Hoppel, 1981a, 1981b, and Hoppel and Wojchiechowski, 1981) in the special issue of the Journal de Recherches Atmospheriques devoted to the workshop.

The primary purpose of this field work has been to obtain a data base which will lead to an understanding of submicrometer aerosols, their mode of formation, and the mechanisms which shape the size distribution and are responsible for the dynamic evolution of the size distribution in air masses advecting over the ocean. Emphasis will be on the submicrometer particles as opposed to the larger sea-salt particles which have been the subject of many other investigations. New data on the solubility of submicrometer particles will be presented as will supporting data such as visibility and radon concentrations. Extinction of EM radiation in the wavelength range 0.3 to 12 μm due to aerosols is calculated from the size distributions and compared to the scattering coefficient at 0.55 μm measured with a nephelometer. Instrumentation which has been developed at NRL will be described in some detail, since it represents relatively new technology.

INSTRUMENTATION AND METHODS

The goal of the work reported herein has been to increase our understanding of atmospheric aerosols. We would have preferred to accomplish this goal by using commercially available instruments. Unfortunately, however, one reason so little is known about submicrometer particles has been the absence of a measurement technology. During the past few years much effort has been expended in developing a capability for submicrometer aerosol measurement. This effort has been profitable and has resulted in the NRL mobility analyzer, a variable-humidity nephelometer, and an isothermal haze chamber. It has also made possible the unique results given in the next main section of this report and in recently published papers.

The Mobility Analyzer

The size distribution of small particles can be measured with an electron microscope by first electrostatically precipitating the particles onto an electron-microscope grid. This method is not only tedious but is of doubtful validity when applied to atmospheric aerosols which contain a large fraction of

volatile material that will not survive the vacuum environment of the electron microscope. In the atmosphere most size distributions of particles below 0.2 μm have been obtained by measuring the transmission of particles through a diffusion bank as a function of airflow. The number of particles lost to the walls depends on the diffusion coefficient of the particles. The inversion of the transmission characteristic gives the distribution of diffusion coefficients, from which the size distribution can be calculated. The inversion technique essentially involves taking two derivatives of experimental data, a process which is inherently inaccurate. Still other measurements have been made with a commercial instrument called the electric aerosol analyzer, originally due to Whitby (and described by, for example, Lundgen et al., 1979). This instrument sizes particles down to radii below 0.01 um and has been used in a number of air-pollution and laboratory studies but lacks the sensitivity and accuracy required in our studies.

The NRL mobility analyzer (Fig. 2) is a system for measuring the size distribution of particles between 0.006 and 0.5 μm in radius. The aerosol sample is first brought to charge equilibrium by passing the sample through a region of bipolar ionization. The sample air enters the mobility analyzer through a slit in the outer cylindrical wall and is confined to a thin laminar layer along the wall by filtered sheath air. A small amount of filtered air is extracted through a slit in the inner electrode. When a voltage is applied to the inner electrode, those particles which are charged and which lie in a narrow mobility range will be withdrawn with the air extracted through the inner electrode. The particles in the extracted air are counted in a cloud chamber after they are nucleated and have grown to optically detectable sizes. From these data on the particle concentration in the extracted air as a function of voltage, the mobility distribution of the charged fraction is obtained. Knowing the mobility distribution of the charged fraction (of one polarity) and knowing that the particles are in charge equilibrium and have a Boltzmann charge distribution, one can obtain the size distribution by an iterative procedure. The iterative procedure corrects for multiply charged particles which have the same mobility as smaller singly charged particles. The theory of the mobility analyzer and the analytical method for recovering the size distribution is given in Hoppel (1978).

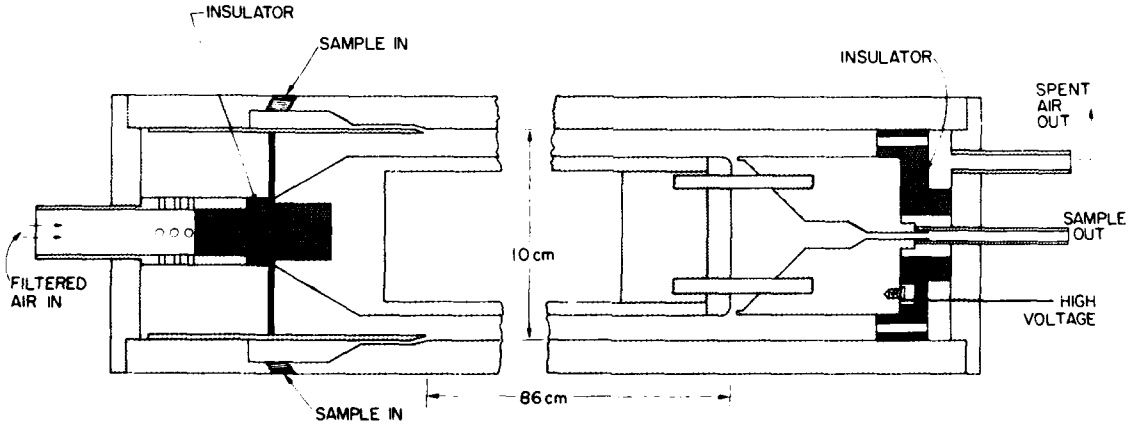

Fig. 2 — Basic portion of the NRL differential mobility analyzer

This instrument can be referred to as a differential mobility analyzer of second order. It differs from a simple aspirated condenser (for example a Gerdien chamber) which measures integral properties of the mobility distribution such as conductivity and total ion count. In the case of an integral counter two derivatives of the experimental current-voltage curve must be taken to obtain the mobility distribution function. Second-order chambers (such as the NRL mobility analyzer) are chambers where both derivatives are taken instrumentally by dividing the incoming air into sheath and sample air and

measuring the ionic current to only a small segment of the electrode. In a second-order chamber the data are directly related to the mobility distribution itself.

In mobility chambers the ions are usually detected by the electrical current generated when their charge is transferred to an electrode upon contact. For atmospheric aerosol measurements this current is too small to be measured; therefore second-order chambers have not been used. An important feature of the NRL mobility analyzer is that the electrical current is not measured but rather the particles are removed, nucleated in a cloud chamber, and counted individually. This increases the sensitivity vastly over that obtainable from an ionic current measurement. (Some history on this type of instrument is given by Knutson and Whitby, 1975, and Liu and Pui, 1974.)

The concentration of particles in the extracted air is much lower than in the sample air. The first data from the mobility analyzer were obtained by measuring the concentration in the extracted air with a Pollak counter. Although the long-tube Pollak counter is probably the most sensitive of the light-scattering condensation-nucleus (CN) counters, its use imposed rather severe limitations on the sensitivity of the system. Useful size distributions were obtained only when particle concentrations were high. When the total count dropped below about 1000 particles/cm^3, the system could not be used. Even at high concentrations the sensitivity was not adequate to detect particles in all 11 of the size (mobility) channels. Despite these limitations, this early version demonstrated the usefulness of the mobility analyzer and produced useful results (Hoppel, 1979).

In an attempt to increase the sensitivity of the system, a single-particle CN counter was developed at NRL. This CN counter now allows much greater sensitivity and has made it possible to automate the system. Although this new continuous particle counter is used as part of the mobility analyzer system, it is novel and will possibly have other applications. Therefore the new continuous CN counter will be described in some detail here.

Figure 3 shows the design of the new single-particle CN counter. The sample air enters along the axis of the chamber and is surrounded by filtered, humidified sheath air. The walls are water saturated; alternate segments are maintained at alternating temperatures. The basic principle is similar to that employed in the TGDCC, where a supersaturation exists between horizontally oriented hot and cold plates with saturated walls. The TGDCC is limited to measuring particles activated in a narrow range of supersaturations between about 0.2% and 1.0% because of well-documented reasons related to fallout during the time required to establish the equilibrium supersaturation in the TGDCC. The advantage of the segmented chamber is that particles falling vertically are not lost and the segmented geometry suppresses large-scale convective motions which would occur between vertically oriented hot and cold walls. The criterion in the segmented chamber is that the airflow rate must be such that the residence time in a single segment is short compared with the time required for moisture or heat to diffuse in from the walls to the center, whereas the residence time of the sample in the entire chamber must be longer than the diffusion time. When this criterion is met, the air along the axis will reach a temperature and vapor pressure which is approximately midway between the temperature and vapor pressure of each segment. Along the axis the asymptotic supersaturation is the same as that existing in the center of a TGDCC working at the same temperature difference. Figure 4 shows the development of the supersaturation within the chamber. Since the sheath air is prehumidified, so that the supersaturation begins at 0%, the upper curves are applicable to our mode of operation. Details of the design and analysis of the chamber appear in Hoppel et al. (1979).

In practice the temperature difference is set such that the asymptotic (maximum) supersaturation is about 20%, so that all atmospheric particles in the size range of interest are nucleated and grow larger than 1 μm in radius. The particles are then individually counted by a commercially available optical particle counter (a Royco optical particle counter, which was used in this application only to count the activated droplets and not to size them).

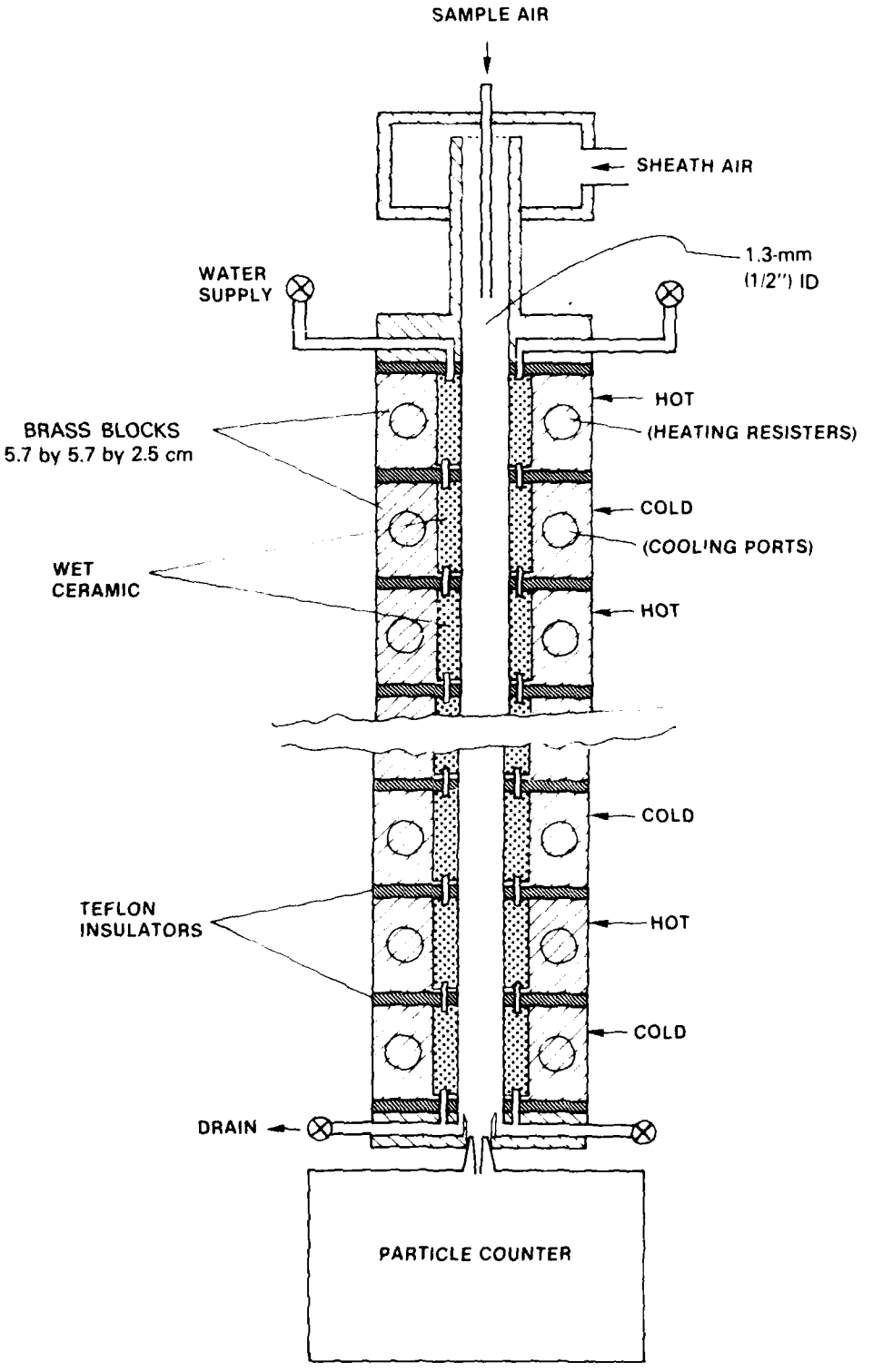

Fig. 3 — NRL segmented thermal-gradient condensation-nuclei counter

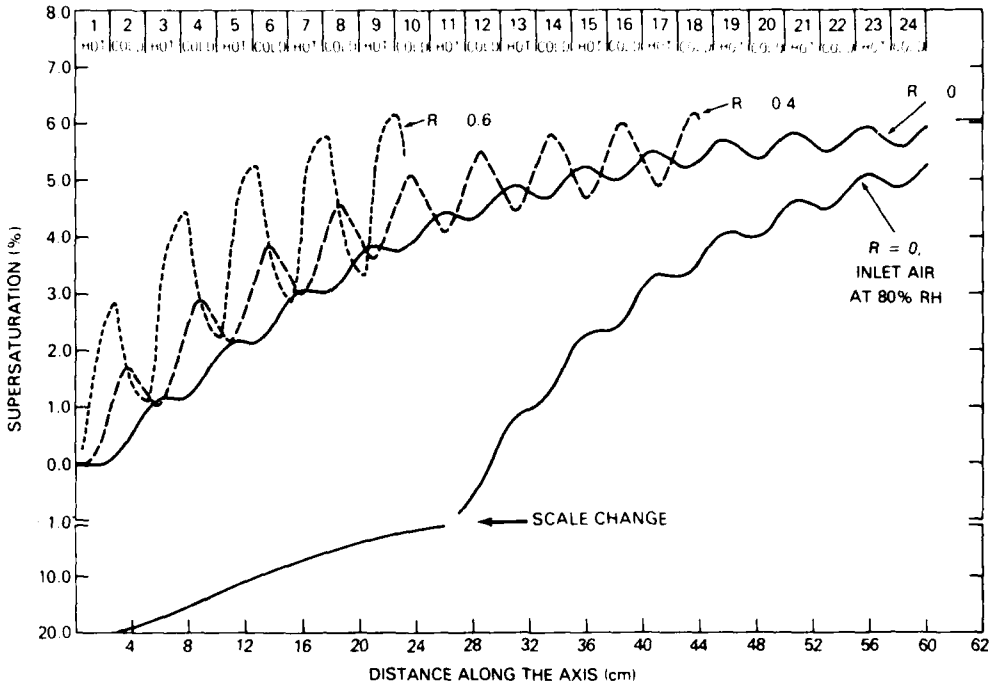

Fig. 4 — Development of supersaturation in the segmented chamber (Fig. 3). The radial distance in the chamber is indicated as the normalized distance R such that $R = 0$ is along the axis and $R = 1$ is along the wall.

In the winter of 1979 the mobility analyzer was automated using an HP-9825 desktop calculator and appropriate interfaces. A 16-bit binary interface was used to control a high-voltage power supply (0 to 5000 V) which supplied the polarizing voltage to the mobility analyzer. Another interface controlled and read the Royco optical particle counter at the output of the segmented chamber. A real-time clock in the HP-9825 controlled the timing such that the voltage cycled through 12 voltage steps between 0 and 5000 V. After each voltage change, 60 s are allowed for a new equilibrium to be established, and then two consecutive 12-s counts are obtained from the particle counter for each voltage. The average of the counts is stored, and at the end of the run the size distribution is calculated, printed out, and stored on a magnetic-tape cartridge. A plotter has been added to the system so that the size distribution can be plotted after each run. A single size distribution takes about 15 minutes. The increased sensitivity of single-particle counting now allows particles to be counted in all 11 channels under all conditions encountered to date.

In field work we have consistently used only 11 channels to cover the stated size range. More channels could be used to improve the size resolution, but this would increase the time required to obtain the size distribution. The selection of 11 channels has been a good compromise between resolution of sizes and resolution of temporal changes.

The size distribution $n(r)$ is defined as the number of particles dN in a radius interval dr:

$$n(r) = \frac{dN}{dr}. \tag{1}$$

In calculating the size distribution from the mobility analyzer data, the infinitesimals of differential calculus must be replaced by finite differences. The procedure is given in Hoppel (1978). The size distribution is usually plotted on log-log paper and can be displayed in a number of alternate ways depending

on the application. Since $n(r)$ decreases so rapidly with increasing size (Fig. 1), it has become quite common to plot the logarithmic derivative instead:

$$\frac{dN}{d(\log r)} = \ln_e(10)\ r\ \frac{dN}{dr} = 2.303\ r\ \frac{dN}{dr}. \tag{2}$$

This form of the size distribution gives more weight to the larger particles and hence makes the distribution less steep.

The area distribution is intimately related to optical properties of aerosols and is defined as the size distribution weighted by the geometric cross section:

$$\frac{dA}{dr} = \pi\ r^2\ n(r). \tag{3}$$

The integral of the area distribution function over all radii is the total cross-sectional area presented by the entire population of particles in 1 cm^3.

The manner in which the volume (or mass) is distributed among the various sizes is given by the volume distribution

$$\frac{dV}{dr} = \frac{4}{3}\ \pi\ r^3\ n(r). \tag{4}$$

Integration of the volume distribution over all sizes gives the total volume in 1 cm^3.

In the area and volume distributions the larger particles are given increasingly more weight and hence skew the distribution toward larger sizes. In this report log-log plots of size distributions (dN/dr) and area distributions (dA/dr) will be the display forms used.

Thermal-Gradient Diffusion Cloud Chamber (TGDCC)

The TGDCC is an instrument which records the concentrations of particles nucleated at low supersaturations (0.2 to 1%). Since supersaturations in natural clouds rarely exceed 1%, the TGDCC measures the subset of particles upon which natural clouds form. This subset of condensation nuclei (CN) is referred to as cloud condensation nuclei (CCN). The TGDCC was developed largely at NRL in the late 1960s by Twomey (1967) and is now widely used to measure CCN. In addition to using the instrument to obtain the supersaturation spectrum between 0.2% and 1.0% supersaturation, the instrument was used in conjunction with the mobility analyzer to obtain information on the solubility of small particles during the field operations. This novel use of the instrument will be described in the next subsection. Since the NRL TGDCC has been described in several papers (Hoppel and Wojciechowski, 1981), only a brief description is given here.

The TGDCC chamber consists of two plates 7.5 cm in diameter separated by 1.25 cm and covered with saturated filter paper. A cylindrical glass wall at the circumference of the plates and separating them forms the chamber. The top plate is at room temperature, and the bottom plate is cooled with a thermoelectric cooler. The temperature difference is measured with several sets of thermocouples imbedded in the plates. A high-intensity mercury-arc lamp with appropriate lens and collimating slits which are imaged in the chamber produce an illuminated volume which is viewed at a 90° scattering angle by an 8-mm camera and a video camera system.

The video system permits immediate playback and stop-frame counting of the cloud droplet concentration in the chamber. The 30-cm (12-in.) monitor screen is marked off to identify the viewing dimensions for ease in counting the droplet images.

Air to be analyzed is drawn into a 10-liter holding chamber by drawing down a metalized Mylar diaphragm. This air is then continuously circulated through the holding chamber until a measurement

is made. To make a measurement, the circulating air is shut off, and a slight pressure is applied to the diaphragm to force air from the holding chamber to the TGDCC. The count is recorded both on video-tape and a number of frames of 8-mm movie film. The 8-mm Bolex camera is operated manually while the chamber is viewed through the camera. The first frame is taken 1 to 2 s after the valve is closed, and ten to 15 frames are taken manually until it is clear that the maximum particle count has passed. Two or three successive samples are recorded at each of four supersaturations (as established by changing the temperature differences between the plates).

The video-tape count is quicker and easier to obtain and is the count given in this report. However, it has always been our experience with atmospheric aerosols that the photographic count is always about 10 to 15% higher. We attribute this to the smaller detectable size obtained with the photographic method. The minimum detectable size for our photographic system is estimated to be about 0.5 μm, whereas the minimum detectable size for the video system is estimated to be just under 1 μm.

There are definite limits on the supersaturation range for which the results of the TGDCC are valid. The range of validity is usually given as 0.2 to 1%. However, even within this range there can be significant errors, depending on the nuclei spectrum (size distribution) being measured. The accuracy limitations of TGDCCs in general, and of our chamber in particular, were investigated by Hoppel and Wojciechowski (1976).

The smaller particles which have critical supersaturations about the same as the maximum supersaturation in the TGDCC are not nucleated until the chamber has reached its steady-state value and then grow more slowly than the larger particles which are nucleated before the chamber has reached equilibrium. The object is to find an interval of time when the less active particles have grown to minimum detectable size and the larger (more active) particles have not yet started to fall out. A time which satisfies both criteria may not exist for all size distributions. If such an interval of time does exist, then it should evidence itself by a plateau in the curve of number of particles detected versus time. A well-defined plateau was not found to exist in the data on natural continental aerosols presented by Hoppel and Wojciechowski (1976). Alofs and Carstens (1976) did a numerical simulation of the TGDCC which predicted large errors, depending on the nuclei distribution and minimum detectable size.

Our method for obtaining the count was as follows: two (or three) successive samples were recorded at each supersaturation. The recordings from these samples were played back and visually examined to obtain the succession of frames for each sample where the maximum count occurred. Several of these frames were counted, and the maximum count was obtained. The maximum counts from two (or three) samples were averaged to obtain the CCN count given in this report.

Measurements of the Hygroscopicity (Solubility) of Submicrometer Particles

Theory

The relationship between the saturation ratio S (relative humidity/100) of the air and the equilibrium radius r of an aqueous solution droplet may be expressed as (Pruppacher and Klett, 1978)

$$S = a_w \, e^{2\sigma/\rho_w r R_v T}, \tag{5}$$

where a_w is the water activity of the aqueous solution, σ is the surface tension of the droplet, R_v is the specific gas constant of water vapor, and T is the temperature. The water activity describes the reduction in vapor pressure due to the dissolved material and is equal to the equilibrium saturation ratio over a plane surface of the solution. The exponential factor in Eq. (5) describes the increase in vapor pressure above that of a plane surface due to the curvature of the droplet.

Atmospheric aerosol particles consist of water-soluble and water-insoluble substances, the soluble component normally being a complex mixture of different salts (Winkler, 1973, Junge and McLaren, 1971, and Hänel, 1976). For droplets formed upon such particles we may write (Hänel, 1976)

$$a_w = e^{-(\bar{\nu}\,\bar{\phi}\,\epsilon\,\gamma\,M_w/\bar{M}_s)(m_0/m_w)}, \tag{6}$$

where $\bar{\nu}$ is the mean number of moles of ions and undissociated molecules per mole of salt mixture, $\bar{\phi}$ is the observed practical osmotic coefficient, ϵ is the mass fraction of soluble material in the aerosol particle, $\bar{M}_s$ is the mean molecular weight of the salt mixture, M_w is the molecular weight of water, m_0 is the dry mass of the particle, m_w is the mass of water condensed on the particle, and γ is correction factor taking into account absorption (or desorption) of ions by the insoluble portion of the particle, which is assumed to be totally submerged in the aqueous solution.

We denote the coefficient of m_0/m_w in Eq. (6), which is referred to as the exponential mass-increase coefficient (Hänel, 1976), by η:

$$\eta = \frac{\bar{\nu}\,\bar{\phi}\,\epsilon\,\gamma\,M_w}{\bar{M}_s}. \tag{7}$$

Thus in terms of η the expression for a_w becomes

$$a_w = e^{-\eta\,(m_0/m_w)}. \tag{8}$$

The coefficient η is a function of solute concentration and can be expressed as a function of either a_w or m_0/m_w. If we make the simplifying approximation that the volume of the solution drop is equal to the sum of the volumes of the dry particle and of the pure water condensed on it, we can write

$$\frac{r^3}{r_0^3} = 1 + \frac{\rho_0 m_w}{\rho_w m_0}, \tag{9}$$

where r_0 is the equivalent volume radius of the dry particle and ρ_0 and ρ_w are the densities of the dry particle and water respectively. Using Eq. (9) to express m_0/m_w in terms of r/r_0 and substituting the result into Eq. (8) leads to

$$a_w = e^{-B/(r^3/r_0^3 - 1)}, \tag{10}$$

where $B = \rho_0\eta/\rho_w = \rho_0\bar{\nu}\bar{\phi}\,\epsilon\gamma\,M_w/\rho_w\bar{M}_s$. We refer to B as the aerosol hygroscopicity parameter. The value of η, and hence the value of B, is not constant, owing to the variation of $\bar{\phi}$ with the concentration of the solution. We can express η and B as functions of m_w/m_0 or a_w.

Since η and B are related by the constant factor ρ_0/ρ_w, we can write

$$B(a_w) = \frac{\eta(a_w)}{\eta^0}\,B^0, \tag{11}$$

where η^0 and B^0 are the values of η and B for an infinitely dilute solution, that is for $a_w = 1$. For $a_w = 1$, $\bar{\phi} = 1$.

Hänel and Lehmann (1981) have determined (via Eq. (8)) η as a function of water activity for atmospheric aerosol samples by measuring the relative mass increase (m_w/m_0) as a function of a_w using a microbalance system. Figure 5 is based on their measurements and shows the ratio η/η^0 as a function of a_w for an industrial aerosol sample (curve 4) and several samples composed of background aerosol combined with particles from industrial and local sources. The key to the curves (the list in the figure title) gives the values of η^0 and B^0 in addition to the chemical composition of the soluble portion of each of the samples. To obtain the value of η^0, Hänel and Lehmann used the mixture rule for semi-ideal mixtures of electrolytes to extrapolate the value of η measured at $a_w = 0.96$. Several features of these curves are noteworthy. First, the curves show a relative maximum in η/η^0 in the range $0.75 \leqslant a_w \leqslant 0.8$. At values of a_w above this maximum the soluble material can be presumed to be

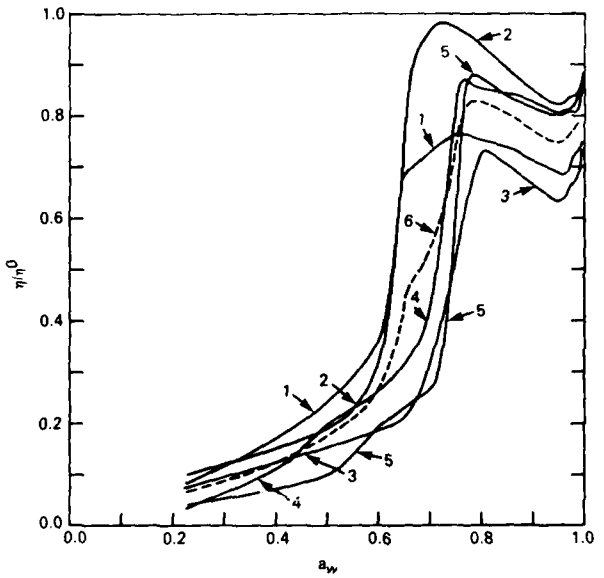

Fig. 5 — Normalized exponential mass-increase coefficient η/η^0 versus water activity a_w for five continental aerosol samples, based on measurements by Hänel and Lehmann (1981) for increasing relative humidity. The chemical compositions of the soluble components of the samples along with the η^0 and B^0 values, keyed to the curves, are as follows:

1. 0.57 $(NH_4)_2\,SO_4$ + 0.23 NH_4NO_3 + 0.20 H_2SO_4; $\eta^0 = 0.12$ and $B^0 = 0.23$;
2. 0.57 sea salt + 0.43 $NH_4\,NO_3$; $\eta^0 = 0.27$ and $B^0 = 0.90$;
3. 0.93 $(NH_4)_2\,SO_4$ + 0.07 $H_2\,SO_4$; $\eta^0 = 0.32$ and $B^0 = 0.59$;
4. 0.76 N_aNO_3 + 0.24 H_2SO_4; $\eta^0 = 0.18$ and $B^0 = 0.34$;
5. 0.5 NH_4N0_3 + 0.37 sea salt + 0.13 $(NH_4)_2\,SO_4$; $\eta^0 = 0.24$ and $B^0 = 0.61$;
6. average of curves 1 through 5.

totally dissolved. Second, above $a_w \approx 0.78$, the value of η/η^0 at a given water activity shows a maximum variation of only 30% and a deviation of $\pm 15\%$ from the mean curve. The value of B^0, on the other hand, is known to vary by as much as about a factor of 5, due to variations in ϵ, ρ_0, $\bar{M}_s$, and $\bar{\nu}$. Third, for a given sample (a given mixture of electrolytes) the value of η/η^0 is fairly constant over the range $0.78 \leqslant a_w \leqslant 0.99$. Thus over the range $0.78 \leqslant a_w \leqslant 0.99$ the value of B as a function of a_w can be obtained with reasonable accuracy from Eq. (11) by measuring the value of B^0 and using the mean curve of η/η^0 versus a_w in Fig. 5 or, even more simply, by using $B = 0.8\,B^0$.

In computing particle size as a function of relative humidity from Eqs. (5) and (10), the dependence of surface tension on the concentration of the solution must be taken into account. The surface tension of an aqueous solution can be described by (Hänel, 1976)

$$\sigma = \sigma_w + b\epsilon\,\frac{m_0}{m_w}, \tag{12}$$

where σ_w is the surface tension of pure water and b is constant for each solute. In terms of the hygroscopicity parameter B, σ may be expressed as

$$\sigma = \sigma_w - \frac{\beta \ln a_w}{B}, \tag{13}$$

where $\beta = b\epsilon\rho_0/\rho_w$. The surface tension of water can be approximated by

$$\sigma_w(T) = 117.4 - 0.153T,$$

where σ_w is in micronewtons per millimeter (dynes per centimeter) and T is in kelvins.

An error in σ does not have a large influence on the equilibrium size of a particle until S exceeds 0.95 if $r_0 > 0.1$ or until S exceeds 0.9 if r_0 is as small as 0.05 μm. However, at these high values of S the second term in Eq. (13) is sufficiently small compared to σ_w that an uncertainty in the value of β of as much as 50% will result in an error in σ of less than 5 to 10%. Hänel and Lehmann (1981) have also determined the values of b, ϵ, and ρ_0 for their atmospheric aerosol samples. The value of β calculated from these data ranges from 9.4 to 47.7 μN/mm and has the average value of 20.2 μN/mm. This value of β is reasonable one to use in computing the equilibrium size of atmospheric aerosol particles as a function of relative humidity.

At values of the saturation ratio at and above unity, a solution droplet may be assumed to be sufficiently dilute (such that $\sigma \approx \sigma_w$ and $B \approx B^0$) so that $r^3/r_0^3 - 1$ can be approximated by r^3/r_0^3 and the exponential terms in Eqs. (5) and (10) can be expanded to yield

$$S = 1 + \frac{A}{r} - \frac{B^0 r_0^3}{r^3}, \tag{14}$$

where $A = 2\sigma_w/\rho_w R_v T \approx 4.33 \times 10^{-7}\, \sigma_w/T$.

The relationship between the dry size and critical supersaturation (S_c) of an aerosol particle is obtained by differentiating Eq. (14) and setting $\partial S/\partial r \approx 0$, yielding

$$S_c = \left(\frac{4A^3}{27B^0}\right)^{1/2} r_0^{3/2} = K r_0^{3/2}. \tag{15}$$

Since the parameter B^0 ($\equiv \rho_0\eta^0/\rho_w$) determines the supersaturation at which particles of a given size are activated, it will be referred to as the particle activation parameter. In this study Eq. (15) was used to determine the values of B^0 and K of natural aerosol particles from measurements of the critical supersaturation and dry size of the particles. Knowing the value of B^0, we computed the equilibrium size of the aerosol particles as a function of relative humidity (over the range $0.8 \leqslant S$ 0.99) from Eqs. (5), (10), and (11), using the approximate values $B = 0.8B^0$ and $\beta = 20.2\ \mu$N/mm.

Experimental Method

The critical supersaturation of particles of known size was measured by using the mobility analyzer in tandem with the thermal-gradient diffusion cloud chamber (TGDCC). The mobility analyzer is designed to measure the size distribution of aerosol particles and is described elsewhere in this report. However, its use in these experiments is in principle the same as the electrical aerosol classifier described by Liu and Pui (1974).

The first step in the experimental procedure is to bring the aerosol sample to charge equilibrium by means of a radioactive source. The sample is then passed through the mobility analyzer. Particles in a preselected narrow size range are segregated from the total aerosol population by the mobility analyzer and are transmitted to the TGDCC, where the critical supersaturation of the particles is measured. This method was employed by Gerber et al. (1977) to verify Köhler's theory for pure salt particles of known composition.

To determine the critical supersaturation of particles transmitted by the mobility analyzer, the supersaturation in the TGDCC is slowly increased by gradually raising the temperature difference ΔT between the plates of the chamber. Typically five to ten determinations of the number of activated nuclei are made in the time it takes ΔT to increase by 0.25°C. The average number of particles activated in each 0.25°C interval of ΔT is then plotted as a function of the mean supersaturation for that temperature interval. Averaging is necessary to obtain a statistically significant count, because of the small number of particles in the narrow size range transmitted to the TGDCC and because of the small sensitive volume (0.067 cm^3) used in the TGDCC. Next, the number of multiply charged larger particles, which are transmitted along with the more numerous singly charged particles of the desired size, is estimated from the particle size distribution (which is measured immediately before or after each B^0 measurement) and is subtracted from the number activated at each supersaturation. The corrected number of particles at each supersaturation is then normalized to the maximum number activated.

As an illustration of the method, Fig. 6 shows the normalized number of activated nuclei as a function of supersaturation for a run made on 30 July 1979. The transmitted size range in this case was from 0.0427 to 0.052 μm in radius. Particle size is computed from particle mobility on the assumption that the particles are singly charged. The range of critical supersaturation of the particles in the transmitted size interval is taken to be between the points where 10% and 90% of the particles are activated. These points are identified by the arrows on the curves. (Ninety percent rather than 100% was chosen because statistical fluctuations in the number of droplets in the small viewing volume used in the TGDCC make it impossible to determine the exact supersaturation at which all particles are activated.) Critical supersaturation is plotted against particle size as shown by the blocks in Fig. 7 for the three transmitted size ranges used in the run of 30 July. The widths of the blocks are the transmitted size intervals, and the heights of the blocks are measured ranges of critical supersaturation. The values of critical supersaturation and particle radius at the center of a block are used to compute the values of B^0 and K from Eq. (15). For reference Fig. 7 also shows the theoretical relationship between critical supersaturation and dry radius for pure ammonium sulfate particles and for particles characterized by $B^0 = 0.10$.

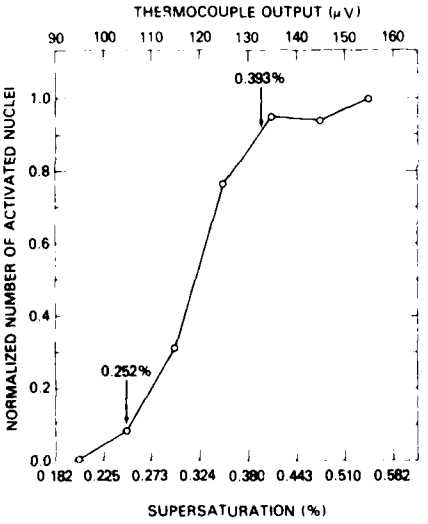

Fig. 6 — Normalized number of activated nuclei as a function of supersaturation for the experimental run made on 30 July 1979 (T = 31°C)

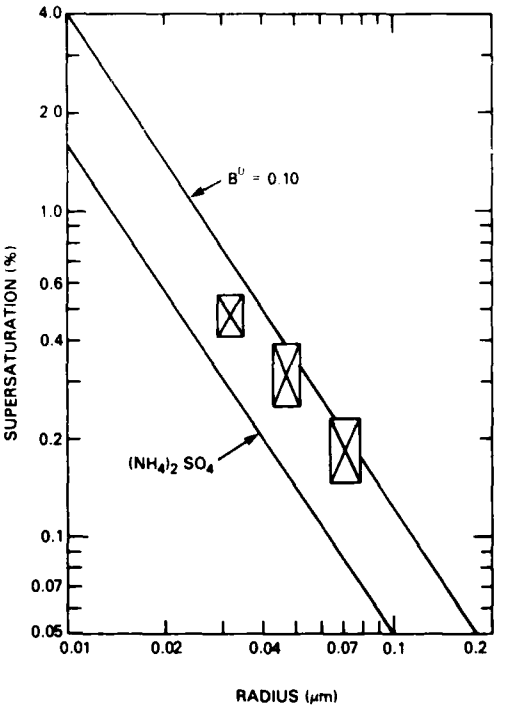

Fig. 7 — Critical supersaturation as a function of particle radius. The boxes show the range of supersaturation required to activate particles in the transmitted size intervals on the run of 30 July ($T = 31$°C). The continuous lines are theoretical curves for ammonium sulfate particles and for particles characterized by $B^0 = 0.10$.

The results of the solubility measurements (B^0 measurements) will be discussed later in this report.

Calculation of Aerosol Extinction in the Wavelength Range 0.3 to 12 μm

Electromagnetic extinction at any wavelength depends on the aerosol size distribution, the nature of the aerosol, and the relative humidity. The relative extinction at different wavelengths largely depends on the shape of the aerosol size distribution and the variation of the complex refractive index with wavelength.

The general expression for the aerosol extinction coefficient is

$$k_e = \int_0^\infty \pi r^2 \, Q_e(m, \alpha) \, n(r) \, dr, \tag{16}$$

where r is the particle radius, $n(r) = dN/dr$ is the number of particles per cubic centimeter per micrometer radius interval, and Q_e is the Mie-theory extinction efficiency factor. Q_e is a function of the particle size parameter $\alpha = 2\pi r/\lambda$ and the complex index of refraction of the particle $m = n - i\kappa$. Exact values of Q_e are computed from Mie-theory codes. However, to facilitate the calculation of k_e, Fitzgerald (1979) developed approximation formulas for Q_e as a function of normalized size parameter $\rho = 2\alpha(n - 1)$. For aerosols obeying a Junge size distribution of the form $n(r) = Ar^{-\nu}$, the values of k_e calculated using the approximation formulas for Q_e agreed to within 5% with those obtained by numerical integration of Eq. (16) using the exact Mie-theory values of Q_e, for wavelengths between 1 μm and 11 μm and for $3.6 \leqslant \nu \leqslant 4.4$, $1.2 \leqslant n \leqslant 1.65$, and $0 \leqslant \kappa \leqslant 0.15$.

For calculating extinction coefficients from the measured aerosol size distributions and for investigating the contribution of selected particle size ranges to the value of k_e, a program was written for the

HP-9845 desktop computer. This program, which uses the approximation formulas for Q_e, is a revised version of one developed by Gathman (1982) and was written to accept data in a more general form.

The particle-size-distribution data are put in analytic form for use in the program by fitting the data points to the sum of two or three log-normal curves of the form

$$dN/dr = C_2\, e^{C_3(\ln C_4/r)^2} \tag{17}$$

by a computer program which first fits a log-normal curve to the three (or more) data points giving the counts from the channels for the largest particles. A second log-normal curve is fitted to the data points remaining after the first log-normal curve is subtracted from the original data points. If necessary, a third log-normal curve can be fitted to obtain an adequate fit to the smallest-particle channels. The method used is that given by Gathman (1983). The computer then plots the sum of the computed log-normal curves along with the original data points.

Royco-counter data points do not always merge smoothly with mobility-analyzer data points, requiring a decision as to how to weight the data points in the overlap area. Also, when it became evident that aerosol particles less than 0.1 μm in radius make little contribution to the extinction at wavelengths greater than 0.3 μm, the best log-normal curves were selected on the basis of the fit to points for a radius of 0.089 μm or larger. For some distributions, two log-normal curves give a good fit to all points for a radius greater than 0.01 μm, and occasionally one log-normal curve would give a reasonable fit to all data points (a reasonable fit being defined as a fit that would result in a computed extinction within 20% of the value computed for the best fit).

The largest particle size used in obtaining the log-normal fits to the measured data points was a radius of 2.2 μm. In computing the extinction from Eq. (16) using the fitted size distribution, the integration was cut off at a radius of 3 μm. Thus the computed extinction at all wavelengths is that due to particles smaller than 3 μm in radius. Although particles larger than 3 μm normally make a negligible contribution to the extinction at 0.55 μm in wavelength, they can make an appreciable contribution to the extinction at wavelengths greater than 2.0 μm.

The real and imaginary parts of the index of refraction of water are well known. The complex refractive index of marine and continental particles is not as well known and is usually computed on the basis of models which assume that atmospheric aerosol particles consist of various percentages of water-soluble material, dustlike material (a portion representative of midlatitude soil conditions), and soot and that the various components are uniformly mixed with each other. The effect of relative humidity (effect of water condensed on the particle) on the refractive index is taken into account by the relation given by the equations

$$n = n_w + (n_0 - n_w)\,(r_0/r)^3 \tag{18a}$$

and

$$\kappa = \kappa_w + (\kappa_0 - \kappa_w)\,(r_0/r)^3, \tag{18b}$$

where n_w and κ_w are the real and imaginary parts of the refractive index of water, n_0 and κ_0 are the real and imaginary parts of the refractive index of the particle in the dry state, and r_0/r is the ratio of the size of a particle in the dry state (at 0% relative humidity) to the size at a particular humidity.

Index-of-refraction data for various dry aerosol components are taken from Paltridge and Platt (1976) and Shettle and Fenn (1979). Values are stored for water and the following dry components: sea salt, water-soluble residue, dustlike material, and soot. Extinction can be computed for aerosol particles composed of water and a selected dry component, excluding soot (which cannot be used exclusively as the dry component because the values of index of refraction exceed the limits for which the approximation formulas for Q_e have been shown to be valid), or for water and a mixture of dry materials including soot.

Seven relationships for the size of a particle as a function of relative humidity are available for use in computing the index of refraction from Eqs. (18). Four relationships are from Fitzgerald (1978):

$$(r/r_0)^3 = 1 + g/(1 - H/100), \tag{19}$$

where H is the relative humidity in percent and $g = 1$ (maritime aerosol), 0.6 (modified maritime), 0.3 (modified continental), or 0.1 (continental). Three relationships are from Paltridge and Platt (1976):

$$(r/r_0)^3 = 1/(1 - H/100)^{3.d}, \tag{20}$$

where H is the relative humidity and $d = 5.8$ (continental), 4.4 (normal or mixed), or 3.9 (maritime).

Extinction is computed at selected wavelengths, with the program being especially set up for computations at 0.55 μm. The extinction at selected wavelengths is stored in memory during computation and plotting of the extinction and can be printed after plotting is finished. Extinction due to a selected particle-size range can also be computed for selected wavelengths as well as being computed and plotted for all wavelengths.

Since the computed extinction may vary by 25% or more between different log-normal fits to the same data, depending on the weighting of points in the overlap region of the Royco-counter and mobility-analyzer data, variations in extinction of several percent due to uncertainties in the index of refraction of the particles are not significant. Thus the computed value of extinction is relatively insensitive to whether the growth relationships of Fitzgerald or Paltridge and Platt are used in Eqs. (18) or to the choice of aerosol type (maritime versus modified maritime, etc.). For relative humidities less than about 80%, the effect of a 10% error in the measured relative humidity on the value of the index of refraction results in only a few percent change in computed extinction.

Computation of the extinction coefficient for curve 1 in the left-hand plot of Fig. 41 illustrates the method. Figures 8 and 9 show two different log-normal fits corresponding to curve 1 of Fig. 41. Figure 8 represents a good log-normal fit to all data points of radius greater than 0.5 μm, and Fig. 9 shows a best fit when the smallest-particle Royco channel is lightly weighted. (The agreement between measured and computed extinction is usually improved if the smallest-particle Royco channel is lightly weighted. The fit to the remaining points is also improved.) Figures 10 and 11 are plots of extinction versus wavelength for the log-normal fits shown in Figs. 8 and 9 respectively. The upper curve in each figure is the total extinction, and the other curves are extinctions due to particles in selected size ranges.

The upper and lower sections of Table 1 show the computed values of the extinction coefficient for the log-normal fits in Figs. 8 and 9 respectively. Tabulated is the total extinction coefficient (bottom line in each section) and the partial extinction due to particles in selected size ranges. In this case the different log-normal fits to the same data give rise to a 28% difference in the total coefficient. The largest differences in partial extinction are, as would be expected, in the size range 0.2 to 0.4 μm, which includes the smallest-particle Royco channel at 0.24 μm. The extinction by particles below 0.1 μm is very small, although these particles are most of the particles counted.

Radon Instrumentation

Emanations of the radioactive rare gas radon (^{222}Rn) from the earth's surface and subsequent dispersal in the atmosphere are of interest in the study of vertical diffusion (Bradley and Pearson, 1970, and Hosler, 1969), in the study of dust transport (Prospero and Carlson, 1970), and as an indicator of whether or not an air mass had a trajectory recently over or near a land mass.

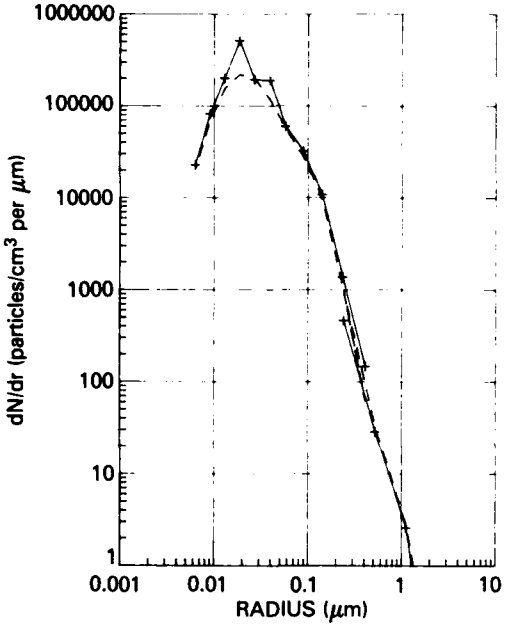

Fig. 8 — An example of the best fit of three log-normal functions to all experimental points on the size distribution shown as curve 1 in Fig. 40. The crosses are experimental data, and the dashed line is the sum of the three log-normal curves.

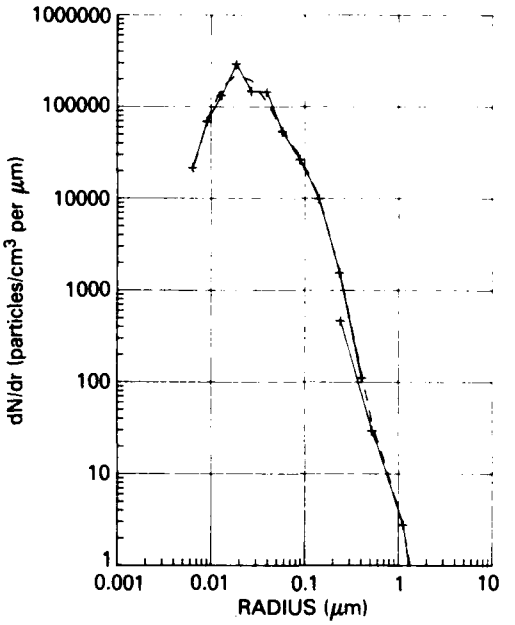

Fig. 9 — Same example as Fig. 8 except that the smallest channel of the optical counter was ignored in calculating the best fit

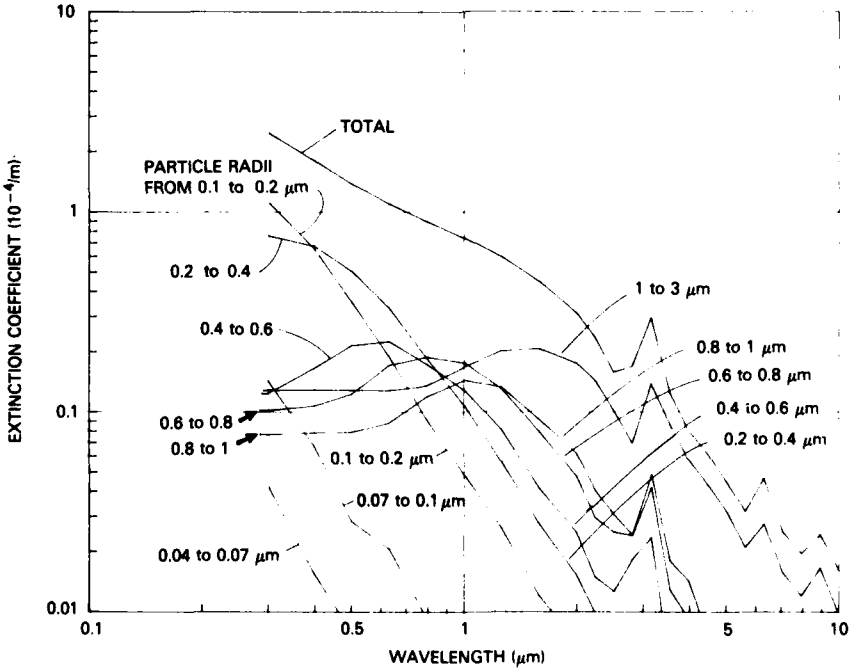

Fig. 10 — Extinction as a function of wavelength for the fitted size distribution shown in Fig. 8

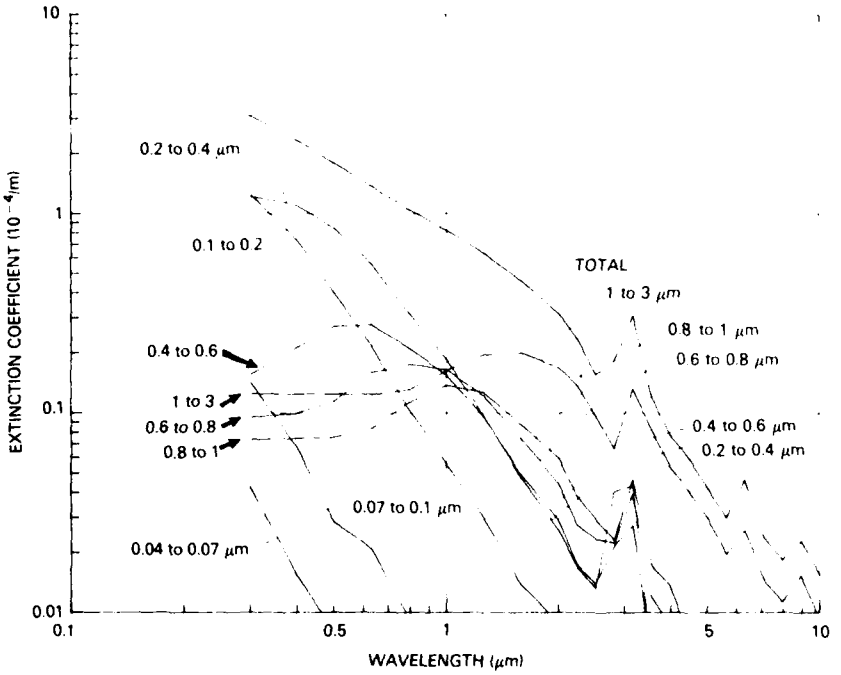

Fig. 11 — Extinction as a function of wavelength for the fitted size distribution shown in Fig. 9

Table 1 — Computed values of the extinction coefficient for the log-normal curve fits shown in Fig. 8 and 9. The measured relative humidity was 74%. The particle index of refraction at 74% relative humidity was computed from Eqs. (18) and (19) using $g = 1$.

Radius Range (μm)	Extinction Coefficient (10^{-4}/m) at Different Wavelengths (λ)					
	0.4 μm	0.5 μm	0.55 μm	0.63 μm	1 μm	2 μm
Computed for the Fit in Fig. 8 and Plotted in Fig. 10						
0.04-0.07	0.016	0.008	0.007	0.007	0.00	0.00
0.07-0.10	0.068	0.028	0.025	0.021	0.01	0.00
0.10-0.20	0.655	0.355	0.271	0.189	0.05	0.01
0.20-0.40	0.671	0.504	0.427	0.330	0.11	0.02
0.40-0.60	0.165	0.214	0.223	0.224	0.13	0.03
0.60-0.80	0.107	0.123	0.139	0.171	0.18	0.05
0.80-1.00	0.078	0.079	0.079	0.088	0.14	0.06
1.00-3.00	0.128	0.128	0.123	0.123	0.17	0.17
0.04-3.00	1.808	1.387	1.254	1.095	0.74	0.31
Computed for the Fit in Fig. 9 and Plotted in Fig. 11						
0.04-0.07	0.016	0.008	0.007	0.007	0.00	0.00
0.07-0.10	0.068	0.023	0.025	0.021	0.01	0.00
0.10-0.20	0.743	0.402	0.307	0.215	0.06	0.01
0.20-0.40	1.104	0.841	0.716	0.557	0.19	0.03
0.40-0.60	0.213	0.271	0.230	0.276	0.15	0.03
0.60-0.80	0.100	0.115	0.130	0.160	0.16	0.04
0.80-1.00	0.075	0.075	0.075	0.084	0.14	0.06
1.00-3.00	0.125	0.124	0.124	0.124	0.16	0.17
0.04-3.00	2.341	1.797	1.607	1.367	0.82	0.32

Radon is part of the uranium series, which starts with ^{238}U and ends with stable ^{206}Pb. ^{222}Rn is the daughter of ^{226}Ra. The source of atmospheric radon is the trace amounts of radium present in all soils in varying concentrations. Gaseous ^{222}Rn diffuses from the earth's surface essentially free of any daughter activity and reaches secular equilibrium with its daughter products through ^{214}Po within hours.

Radon daughter products are electrically charged and chemically reactive. These particles rapidly become attached to natural aerosol particles and can be collected on filters. Short-lived radioactive atoms can live out their lives in a free condition in clear air, but it has been demonstrated (Saunders, Patterson, and Lockhart, 1968) that these unattached radon daughters are collected by cellulose-glass-fiber and glass-fiber filters with nearly the same efficiency as aerosol particles are collected. The contribution of long-lived ^{210}Pb and subsequent daughter products in the uranium series to activity collected on the filter has been shown to be negligible (Blifford, Lockhart, and Rosenstock, 1952).

A typical sample collector consists of a filter holder and a blower to draw air through the filter. A detector consists of a plastic scintillator optically coupled by silicone grease to a photomultiplier tube. The plastic scintillator is covered with 0.05 mm of aluminum to absorb alpha particles and provide a light shield. Total beta activity on the filter changes slowly with age after about an hour. Plastic scintillators 0.25 mm thick were selected, because they have been shown to be thick enough to give adequate light output from passage of beta rays (Harley et al., 1962) and yet thin enough to be essentially transparent to gamma rays and have a low background counting rate.

The first radon counter constructed in the NRL Atmospheric Physics Branch was constructed to monitor the maritime air at a Barbados field site for possible contamination by continental air that is frequently transported across the Atlantic from Africa. Commercial instrumentation did not have the required sensitivity and portability. The first instrument combined the radon measurement techniques developed by the Chemistry Division (Lockhart et al., 1965) with sensitive beta-particle detectors developed by the Radioactivity Branch of the Nucleonics Division in response to a need for monitoring the atmosphere of the USS *Nautilus* for fission products (anonymous, 1960).

An improved version (Larson, 1973) was used by personnel of the Atmospheric Physics Branch and the Chemical Oceanography Branch on aircraft and ships to measure radon in remote areas and to relate the radon to concentrations of other materials of continental origin and to atmospheric processes. This instrumentation could measure radon down to a few tenths of a picocurie per cubic meter and thus was about two orders of magnitude more sensitive than the available commercial instruments, which were designed for monitoring continental radon levels of about 100 pCi/m^3, or the radioactivity in homes or uranium mines, where the radon is much higher.

The success of this instrumentation prompted the building of the Automatic Radon Counter (ARC) (Larson and Bressan, 1978) (U.S. Patent 4,140,912) and enabled automatic and frequent collection of data. Thus data can be collected around the clock, even when it is unsafe for personnel to go out on deck as required by the nonautomated system.

The NRL Environmental Chemistry Branch has combined the automatic radon measurement with an airborne salt measurement using the same filter papers. This instrumentation (Bressan, 1981) has enabled unattended round-trip shipboard measuring of radon and salt.

The Atmospheric Physics Branch has recently used a simplified version called the Almost Automatic Radon Counter (AARC). The ARC had a tape drive which increments the filter paper from collection position to counting position after each sample is collected and thus has a clean filter for each sample. Samples can be collected as often as every 5 or 10 minutes (with some loss of sensitivity). The AARC uses the same filter for successive samples. The blower and counter are automatically cycled to enable relatively unattended operation, but the filter must be changed every 1 to 3 days, and

the frequency of samples can be no more than one per hour. The advantage of the AARC over the ARC is greatly reduced cost and size of those components that must be exposed to the elements.

The radon data presented in this report were taken with the AARC version and are used primarily as a diagnostic tool to help identify the source of air masses.

Supporting Instrumentation

Atmospheric research requires measurements in undisturbed air free of local sources of pollution. Also required is shelter for personnel and instrumentation, and air conditioning may be required for sophisticated instrumentation and computers. As the number and complexity of our instruments increased, it became increasingly difficult to find existing locations with adequate exposure for air sampling and vents and preferably outside the ship's aerodynamic boundary layer. The time required to set up and dismantle instrumentation on site or aboard ships became increasingly costly.

To alleviate these recurring problems, it was necessary to purchase a movable equipment shelter which could be transported to the desired field sites. The shelter had to be large enough for all the present and immediately foreseeable instrumentation and operating personnel, had to be portable for easy transportation to field sites and for relocation at sites, and had to be small enough for installation on the flying bridge of the USNS *Hayes* or other research ships.

The selected design was a mobile equipment shelter 2.5 m wide and high and 5.5 m long manufactured by Ekto Corporation of Sanford, Maine. This unit was selected because it is strong enough to withstand frequent deployment, is light enough to be loaded aboard ship, and was competitive in cost. The shelter was acquired with a triple-axle transporter for trailing it to a field site. Corner jacks enable stabilizing and leveling at field sites. The shelter can easily be removed from the transporter for shipboard use.

The 200-ampere service in the shelter is more than sufficient for air conditioning and existing instrumentation. There are five data-cable/air-intake ports and an extra-wide door on one end for loading equipment. The top is flat, has a removable safety railing, and is strong enough to support a tower to further elevate instrumentation. A large window in one side and small windows in each door provide visibility of external conditions. The shelter has built-in lift and tie-down points, adequate to secure it during rough seas.

The shelter has a small area for a desk and has rails attached to the floor for securing instrument racks. Most of our equipment can be installed and checked out and altered if necessary at NRL, thus greatly reducing setup time on site. Once equipment has been installed in the shelter for one field experiment, reinstallation time for subsequent field work is minimal.

In addition to the instruments previously discussed, the shelter housed meteorological instrumentation for the measurement of temperature, dewpoint, wind speed, and wind direction. The sensors for these measurements were mounted on the roof of the shelter.

An instrument which we refer to as the variable-humidity nephelometer has been developed at NRL and was successfully used during the Washington, D.C., deployment. It was also taken on the *Hayes* cruise. This instrument in its present design is manually operated and requires full attention of at least one person during its operation. It was not operated during the cruise because of manpower shortage and enhanced awkwardness of operation due to ship's motion. This instrument and data obtained during the Washington, D.C., deployment, are described by Fitzgerald et al. (1982).

RESULTS

In early June 1979 the instrument shelter was placed near the NRL waterfront, and data were taken for a number of days to test equipment and develop procedures. From there the equipment was transported to Wallops Island, Virginia, and placed on one of the rocket launching pads about 80 m from the coast (at high tide). Data were taken at this site from 18 June until 29 June 1979. The equipment was returned to NRL, and additional data were collected during July 1979. In the fall of 1979 the opportunity to participate with the NRL Marine Biology Branch on a cruise scheduled early in the following year presented itself. The USNS *Hayes* finally cruised in April 1980, sailing from Norfolk, Virginia.

The measurements presented in this report are those taken on these three deployments. Many data were obtained, and no attempt will be made to present all of the data and required analysis. Instead selected periods will be chosen for presentation. The greatest emphasis will be on the shipboard measurements. This emphasis reflects the particular interest of the Navy in marine aerosols and the effect they have on naval systems.

Washington, D.C., Measurements

Although the aerosol program was initiated to look at the marine and coastal environment, the development and testing of the instrumentation at NRL gave us an opportunity to look at urban aerosols as well. Some samples of these data will be presented to contrast the urban environment with the marine environment. Also, an air mass advecting from the U.S. east coast over the Atlantic may have passed over some urban areas during its transit, and the urban aerosol will contribute to the history of the aerosol load in that air mass. Furthermore study of the urban aerosol will contribute to our understanding of the physical processes affecting the evolution of the size distribution.

The size distribution, scattering coefficient, and meteorological variables were measured routinely during the day between 19 July and 30 July. On several occasions measurements were also made during the night. Radon data were not taken at the NRL site, because its greatest utility is for distinguishing marine air masses from those which have recently been over land in a coastal and marine environment. Data from the variable-humidity nephelometer were obtained only at the NRL site. The hygroscopicity parameter B^0 of small particles was measured on a number of occasions using the method described earlier. The results of these hygroscopicity measurements will be presented later in this report along with results from other locations.

As is well known, the urban environment contains a large number of small particles generated by man's activity. Figure 1 shows a rather typical urban size distribution (average of four individual distributions) taken midmorning on July 30 and labeled Washington, D.C. During this particular time the scattering coefficient b_s was about 2.3×10^{-4}/m, the wind was from the north-northeast, and the total number of particles was about 33,000/cm^3. Total counts at the site during the 2-week interval were typically in the range 10,000/cm^3 to 40,000/cm^3.

Figure 12 shows size and area distributions during two different meteorological conditions with very different visibilities. The size and area distributions labeled 1 are each the average of five distributions during an interval on 23 July when conditions remained fairly stable with good visibility ($b_s = 0.7 \times 10^{-4}$/m) and a total aerosol count of 15,300 /cm^3. The wind was from the south, the sky was mostly cloudy, and the relative humidity was about 80%. A high-pressure area off the mideast Atlantic coast (Bermuda high) was causing air to flow from the Atlantic, over a portion of North Carolina and Virginia, and into the Washington, D.C., area.

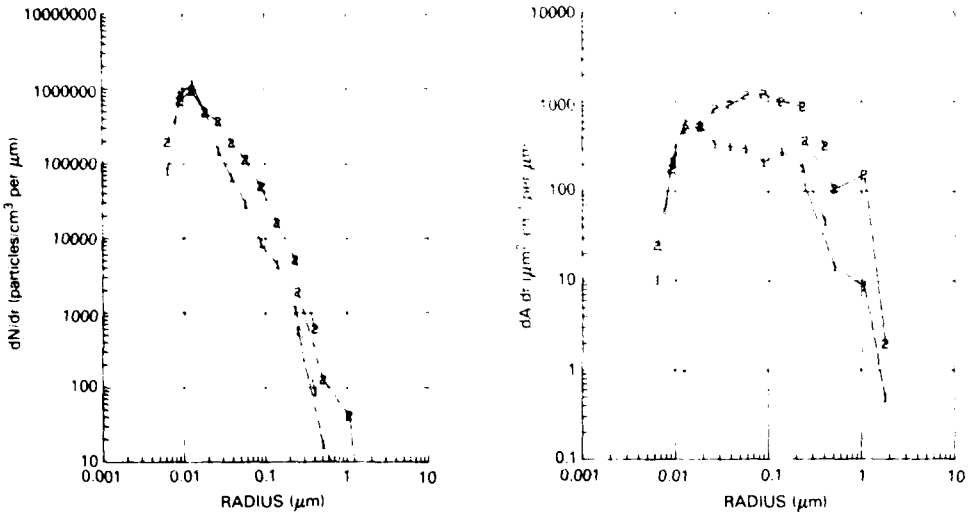

Fig. 12 — Size distributions (left-hand plot) and area distributions (right-hand plot) measured during two different meteorological conditions at Washington, D.C. Curve 1 in each plot is the average of five individual distributions on 23 July 1979 when visibility was good. Curve 2 in each plot is the average of five distributions on 30 July 1979, when visibility was poor.

The size and area distributions labeled 2 are each the average of five distributions taken on the afternoon of 30 July. The visibility was poor ($b_s = 3.6 \times 10^{-4}$/m), the total particle count was about 23,000/cm^3, and the relative humidity was about 77%. The wind was light from the north-northeast and resulted from a northerly flow around a weak high-pressure area centered over northwest Pennsylvania.

Area distributions similar (at radii greater than 0.1 μm) to the one measured on 30 July were also obtained on 20 July (not shown in the plots). On 20 July Washington was under a stagnant high-pressure ridge extending from Illinois to New York and centered over Pennsylvania, visibilities were also low ($b_s = 3.2 \times 10^{-4}$/m), and the relative humidity was 65%.

Since the measured scattering coefficients associated with curves 1 and 2 of Fig. 12 are very different, it is of interest to compare the calculated and measured values for these times. Figures 13 and 14 show the extinction coefficients, calculated from the size distributions by the method described earlier, for curves 1 and 2 respectively. The top curve of Figs. 13 and 14 is the total extinction. The other curves give the contributions of various size classes. In both cases particles in the radius range 0.1 to 0.3 μm are the largest contributors to extinction at short wavelengths. However, between 0.5 μm and 2.0 μm in wavelength the relative contribution of the different size classes in the two cases varies significantly. Table 2 compares the measured scattering coefficient and the extinction coefficient calculated from the size distributions.

Table 2 — Comparison of measured and calculated extinction coefficient

Date	Extinction (10^{-4}/m)			
	Measured	Calculated		
	0.55 μm	0.55 μm	0.50 μm	0.63 μm
23 July	0.70	0.80	0.89	0.68
30 July	3.6	4.50	4.67	4.39

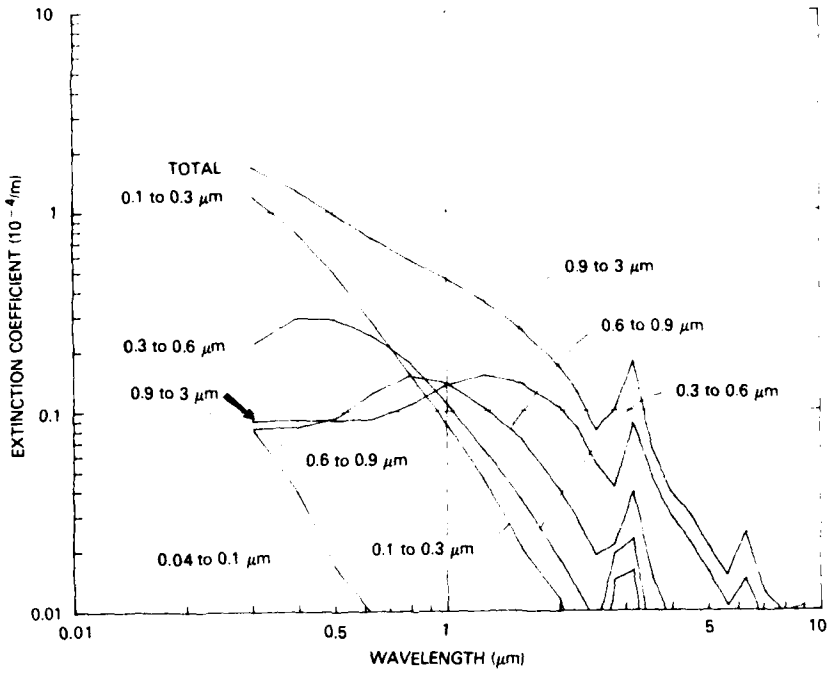

Fig. 13 — Extinction calculations based on the size distribution shown in curve 1 in the left-hand plot of Fig. 12

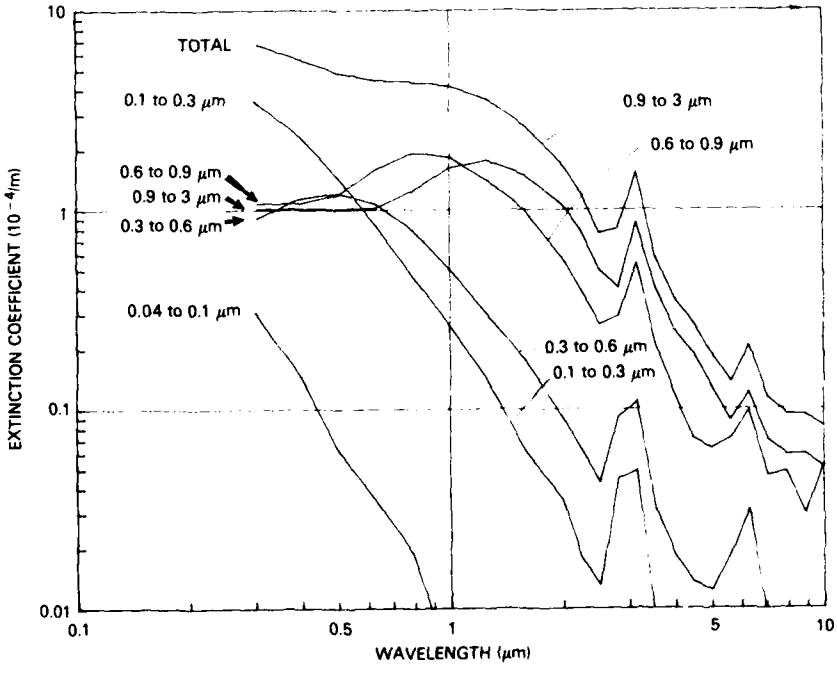

Fig. 14 — Extinction calculations based on the size distribution shown in curve 2 in the left-hand plot of Fig. 12

Wallops Island Measurements

The Site

After completion of a test period at NRL, the equipment was moved to NASA's Wallops Island rocket-launching site. The instrument shelter was placed on one of the concrete launching pads 80 m from a sand beach. The site itself is about 5 nmi from the main NASA base and tracking center (Fig. 15) and is surrounded by marshland. To the east is the Atlantic Ocean, immediately to the west is the Delmarva Peninsula, and farther to the west is the Chesapeake Bay. The Delmarva Peninsula is relatively flat farmland with no significant local sources of industrial pollution.

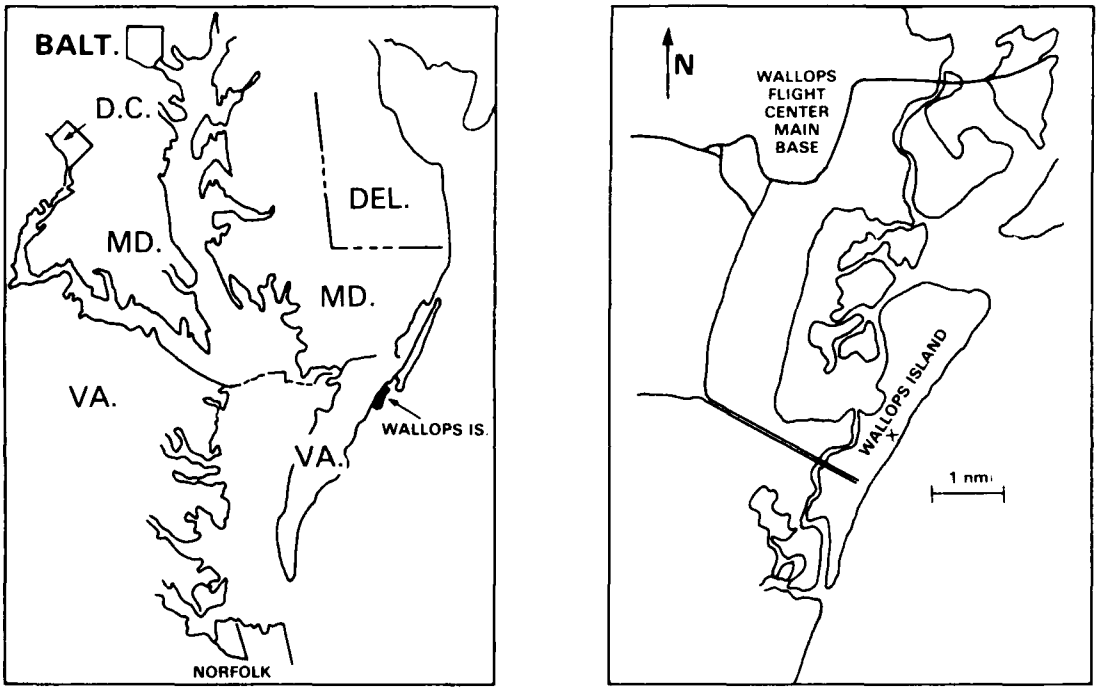

Fig. 15 — Wallops Island measurement site. The measurement location is marked by ×

The coastal site was selected to study the difference in aerosols in air masses of continental origin and of marine origin. Air masses arriving at the site from the west should represent the rural east-coast environment, whereas air masses arriving from the east would presumably represent a more marine environment. Air arriving from the east would pass over the coastal surf zone and possibly be modified by surf-generated particles. In addition a range of conditions between pure continental and pure maritime would result from air masses whose recent trajectories had passed over both marine and continental regions.

The sample air for the mobility analyzer and an Environment/One condensation-nuclei counter was drawn from about 4.5 m above ground through a 25-mm-I.D. tube at a volume flow rate of about 0.07 m^3/min. Air for the nephelometer, also housed in the shelter, had its own 38-mm-I.D. sampling duct. The sensor of the Royco optical particle counter was mounted on top of the shelter together with the radon monitor and the meteorological instrumentation.

Meteorological Conditions

The synoptic conditions over the eastern United States during the deployment were sufficiently varied that we were able to obtain aerosol samples in air masses with a variety of histories. Estimates of the recent histories of the air being measured were based on NOAA surface weather charts, local and area wind patterns, and radon concentrations. Local meteorological conditions, weather forecasts and radiosonde data were provided by the NOAA weather-service support facility at Wallops Flight Center.

Radon concentrations, CCN measurements at 0.7% supersaturation, and local winds at Wallops Island are shown in Fig. 16. (The times indicated by arrows along the top border are for use in a later discussion.) The radon concentrations of between 2 pCi/m^3 and 3 pCi/m^3 on 27 and 28 June are low and indicate that the air had a long trajectory over water. We will refer to this type of air mass as being marine. The higher concentrations near 100 pCi/m^3 indicate a recent history of continental air.

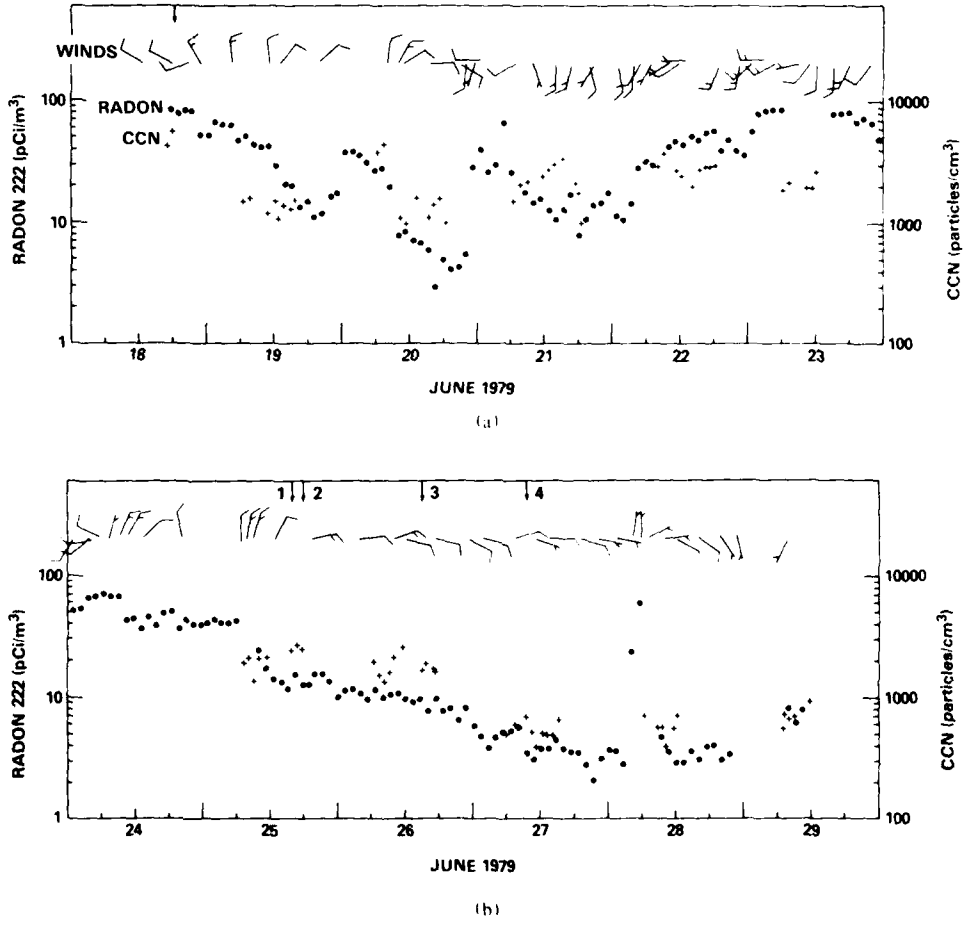

Fig. 16 — Radon concentrations, CCN concentrations at 0.7% supersaturation, and local winds at the Wallops Island site

CCN concentrations are plotted along with radon because it has been observed that radon and CCN correlate well at coastal and oceanic locations (Larson et al., 1979). The source strength of any land area will be different for radon and CCN, since the radon source strength depends on the radium content and physical nature of the soils and the CCN source strength is related to natural and anthropogenic gas and particle sources.

The first samples were taken late on 18 June in continental air behind a cold front that had moved through the area earlier that day. By the morning of 19 June, the radon concentration had decreased, and the winds and synoptic meteorology, combined with the lower radon and CCN readings, suggested some subsidence of cleaner, high-altitude air within the high-pressure area, centered over the Great Lakes. By late afternoon, the winds were from the northeast, and some maritime influence had mixed into the air.

The synoptic situation on 20 June was such that the air movements were not well defined. A high-pressure area over New York with a weak pressure gradient encouraged a northerly flow of more continental air into the area, but a weak low-pressure perturbation over North Carolina brought maritime air into the area by afternoon. On 21 June a weak high-pressure ridge over the east coast of the United States brought a mixture of maritime and continental air into the area and possibly even some industrial contamination from the Norfolk, Virginia, area.

The air became mostly continental on 22 June and remained that way through 24 June. Winds were generally southwesterly on 22 and 23 June and northerly and northeasterly on 24 June. Some rain occurred during this period.

Throughout the 3-day interval of mostly continental air, the correlation coefficient between radon and the height of the inversion was -0.85, indicating a good inverse correlation. Hsu et al. (1980) reported a correlation of -0.96 for radon and inversion height on the gulf coast of Florida near Panama City in continental air moving off the coast from the central United States. A good inverse correlation between radon and inversion height indicates that the air in the mixed layer had been of relatively uniform continental origin over the preceding day or so.

The interval 25 through 28 June was characterized by a transition from continental air early on 25 June to maritime air late on 27 June. The air was mostly maritime on 28 June, but the maritime flow was overcome by local offshore flow early on 28 June, which introduced a continental contamination to the maritime air. The synoptic transition as shown by the surface charts is shown in Fig. 17. On 25 June the clockwise circulation around a high-pressure area centered over the Great Lakes at 0500 EDT was bringing mostly continental air to the site. By late in the afternoon, the winds became onshore (easterly), and the radon concentration decreased to the teens, indicating a mixture of continental and marine air.

By 26 June, the high pressure was centered over New York State, and the continental character of the air continued to decrease. The air reaching the site had spent about 2 days over the ocean and any near surface; thus high-radon air was uniformly distributed throughout the mixed layer and may also have been diluted by subsident air or by additions of maritime air. By 27 June, the high pressure center was off Cape Cod, but the air flow at the site remained easterly, and the radon concentrations indicate maritime air by radon levels that are near background levels for the northern North Atlantic. On 28 June much of the eastern seaboard was under the influence of a large high pressure with a low gradient of pressure.

The correlation between radon and CCN was good the second 6 days (lower plot in Fig. 16), as would be expected in air that had approximately similar origin but spent an increasingly greater time away from land. The correlation was 0.82. The correlation coefficient between radon and CCN was

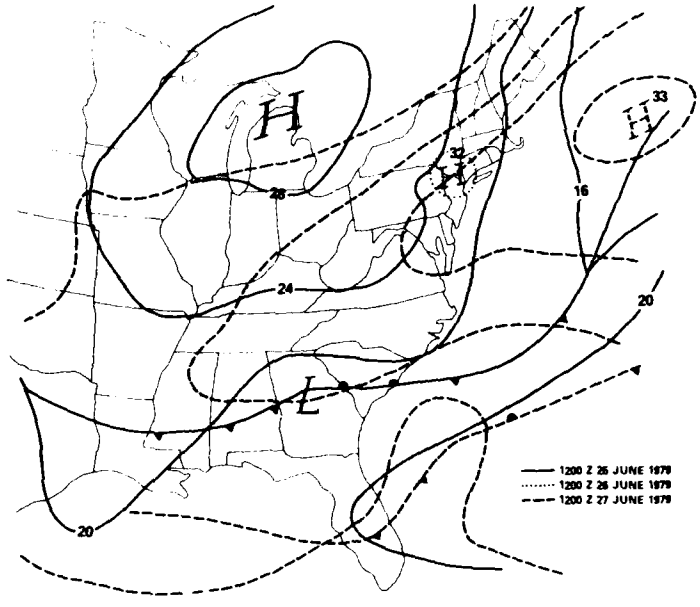

Fig. 17 — Movement of a high-pressure system across the northern United States

0.72 for the entire 12 days of operation at Wallops Island. The lower overall correlation is a consequence of the different source areas for different days.

Size Distributions

Size distributions were taken daily throughout the 12 days except on 24 June. There were periods during the morning hours when no data were obtained. The mobility analyzer would malfunction, and much time would be spent testing for nonexistent leaks in the filtered sheath air system. It was finally determined that the source of the problem was turbulent convection in the analyzer arising from transient temperature differences during warmup after a cool night. The problem was simply remedied by leaving the sheath-flow pump running continuously, maintaining the entire unit at the same temperature overnight. Even though the system was automated, data were not taken continuously throughout the night, because there was a problem with condensation in the segmented chamber which required attention every few hours. Before the cruise in April 1980 this problem was corrected.

Figure 1 illustrates differences in the size distribution obtained at Wallops Island between periods when the air was definitely from the continent and when the air arrived at the site after a long trajectory over water. The 11 smaller channels are from data taken with the mobility analyzer, and the four larger channels are from data taken with the Royco optical particle counter. In the overlapping channel it was nearly always the case that the mobility analyzer recorded more particles than the optical particle counter. The continental size distribution shown in Fig. 1 was taken on 18 June, when the visibility was the lowest recorded ($b_s = 4.0 \times 10^{-4}$/m) during our 12 days at Wallops Island.

Since the time required to obtain a single size distribution is approximately 15 minutes, any change in the absolute or relative distribution during that time would lead to a distortion of the size distribution. To help evaluate just how significant natural variations are during a measurement interval, it was useful to average a number of consecutive data sets and calculate the size distribution from the average data. To evaluate the influence of natural changes, the size distribution was also calculated

from the average data plus one standard deviation and from the average data minus one standard deviation. Figure 18 shows the result for the continental size distribution shown in Fig. 1. The average distribution is calculated from five data sets taken over about 2.5 hours. The width of the data bars represents the width of the size channel. The uppermost point on the vertical bar is the size distribution calculated from the average data plus a standard deviation, whereas the lowest point is that calculated from the average minus a standard deviation. The vertical bars are not error bars associated with the instrument but rather are an indication of atmospheric variability during that particular measurement period. The variations shown in Fig. 18 are typical in that the variations observed in the smaller-particle channels are nearly always greater than in the larger-particle channels.

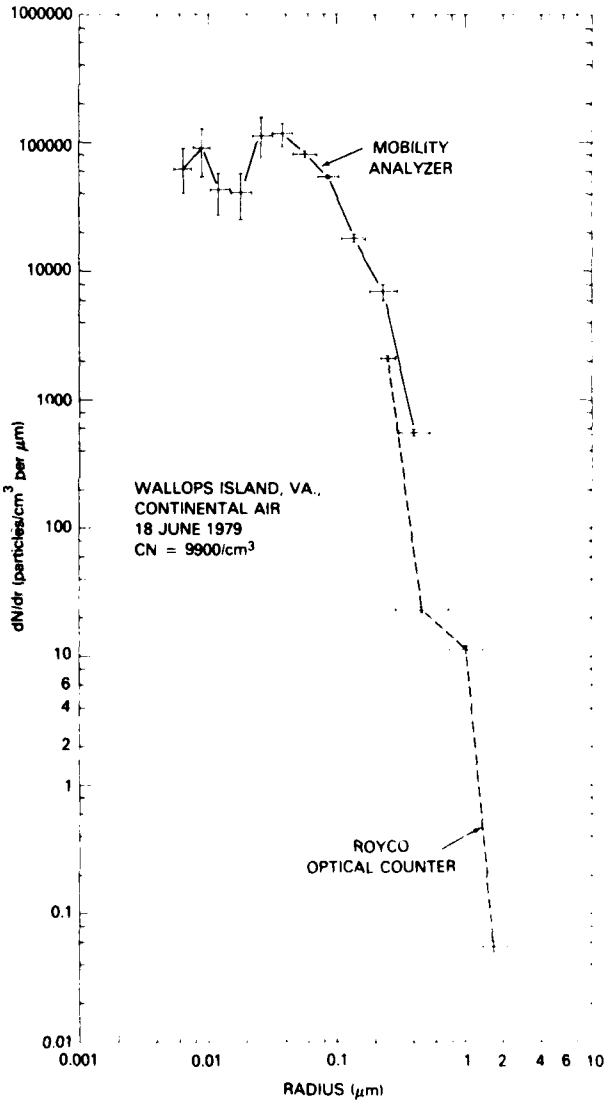

Fig. 18 — Average size distribution from five data sets taken at the Wallops Island site during a 2.5-hour interval. The vertical bars show the standard deviation in the size distribution due to real variations in the size distribution during the interval

In most of the size distributions there is an inflection (change of slope) in the optical-counter data in the size range 0.3 to 1.4 μm. In this size range there is a double-valued region in the calibration curve of the Royco optical particle counter. This double-valued region is very sensitive to the refractive index of the particle. An effort was made to adjust the channel settings such that the double-valued region was entirely within a single channel. However, we cannot be certain that this was the case, since the refractive index of natural aerosols is not well known. The inflection in the Royco size distribution may result in part from particles which belong in one size channel being assigned to the other channel.

In Fig. 1 the marine size distribution taken at Wallops Island indicates a relatively large number of particles in the third and fourth Royco channels. Whenever the wind was from the ocean, accompanied by significant surf activity, there was a large variability and increase in the number of particles in the radius range above 0.5 μm due to surf-generated particles. Hence it is doubtful that data taken at any coastal site can truly represent the open-ocean environment.

During the 12-day period at Wallops Island, over 150 valid size distributions were obtained. Interpreting the hour-to-hour changes in the distribution is difficult. Both the long-range transport and local conditions influence the changes. Even though the coastal situation offers a good opportunity to contrast continental and marine conditions in some well-defined meteorological cases (Fig. 1), at other times the coastal environment is very complex. Often it is difficult to determine whether or not the recent trajectory has been over land or water and to determine the influence of local and sea circulations and the source strength of surf-generated particles. Therefore only a selective sampling of data is presented here.

Several attempts were made to observe an increase in the number of small particles associated with an increased production due to photochemical activity at sunrise, but no clear increase was ever observed. Also, during the measurements, diurnal effects were much weaker than variations caused by changes in synoptic conditions and therefore were not observed.

The most interesting data interval occurred between 25 June and 28 June. On 25 June the clockwise circulation around a high-pressure area centered over the Great Lakes caused air to flow down the east coast to the Wallops Island site. The average of three size distributions taken between 1515 and 1645 EDT on 25 June (centered on the time indicated by arrow 1 in Fig. 16) is shown as curve 1 at the left in Fig. 19. The total number of particles exceeded 15,000/cm^3. During the next three days the high-pressure center moved eastward to a position off the New England coast, as shown in Fig. 17. The air arriving at the measuring site had increasingly longer trajectories over water (and most likely different source regions). The change in the size distribution during this period is shown at the left in Fig. 19, at times which correspond to the meteorological conditions indicated in Fig. 16 by the arrows along the top border. By 1800 EDT on 25 June, the local wind had switched from north to northeasterly, and the total count had dropped from 15,200/cm^3 to 12,700/cm^3. The decrease occurred for particles with radii smaller than 0.03 μm. The following day, 26 June, the total count had dropped below 1000/cm^3 and remained between 800/cm^3 and 1000/cm^3 for the remainder of 27 and 28 June. The total count did not go below 800/cm^3. The size distributions shown in Fig. 19 are averages of three individual size distributions taken during a 90-minute time interval centered on the times shown in Fig. 16 except for the size distribution for 1800 on 25 June (arrow 2 in Fig. 16), which was an average of only two distributions. The dip in the 27 June size distribution (curve 4) at about 0.06 μm was real and existed for at least 4 hours but was not a persistent feature of the size distribution throughout the low-count interval on 27 and 28 June. When this dip disappeared, the count was more typically about 1000/cm^3. Also, by 27 June the persistent east wind resulted in higher seas, and surf-generated particles caused a significant increase in the number of particles larger than about 1 μm.

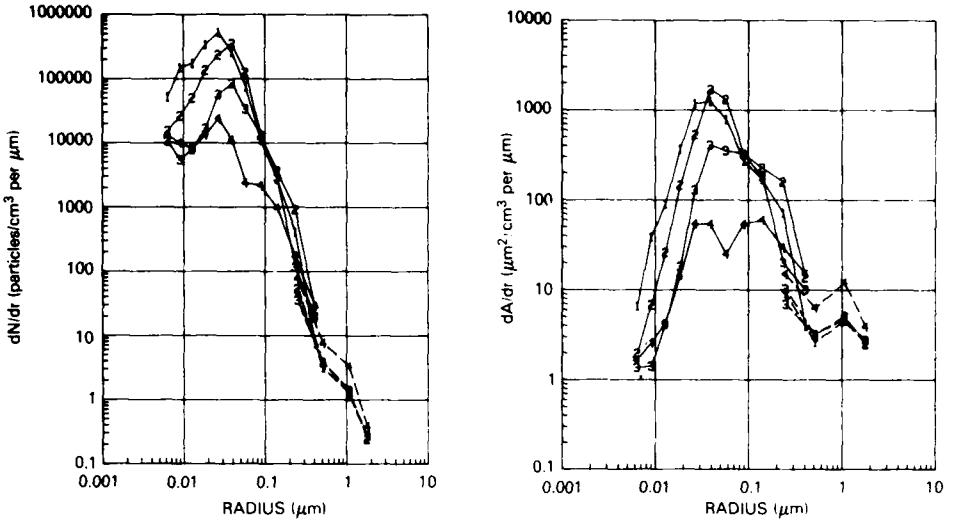

Fig. 19 — Change in the size and area distributions (corresponding to times indicated in Fig. 16 by arrows 1 through 4) as a high pressure system moved off the New England coast and brought air with increasingly long trajectory over water to the Wallops Island site

Figure 19 shows at the right the area distributions and illustrates the advantages gained by plotting different moments of the size distribution. The area distribution emphasizes the differences in the distribution at large sizes and has a tendency to decrease the steep slopes in the size distribution at larger sizes.

Unfortunately, the nephelometer failed on 25 June, and scattering coefficients were not recorded for the rest of the deployment. Some spot measurements were made with a second nephelometer used in the variable-humidity nephelometer system.

The high pressure previously described brought low relative humidities and good visibilities, and even though the relative humidity increased during the interval, as the air spent a longer time over water, the visibility remained high. The large number of small particles (presumably from the industrial northeast) recorded on 25 June had little effect on visibility. Lower visibility ($b_s \approx 2 \times 10^{-4}$/m) occurred on 22 June. The weather maps indicated that this air had passed over the Carolinas and southern Virginia before arriving at the site. A cluster of eight size and area distributions taken in late afternoon and early evening on 22 June are shown in Fig. 20. A predominant, relatively stable peak in the area distribution occurred at about 0.1 μm. This peak radius was considerably larger than the peak radius on June 25 (Fig. 19). The area distributions have not only a predominant maximum but a secondary maximum at about 1 μm. This secondary maximum cannot be attributed to locally generated surf particles. The local wind at the time was from the southwest and could not have transported surf particles from the beach, which was 80 m east of the site.

Figure 21 shows three average distributions of size and of area taken on 21, 19, and 22 June (curves 1, 2, and 3). The scattering coefficients associated with these three times were 0.40, 1.30, and 2.1×10^{-4}/m respectively. The values of the extinction coefficient at a wavelength of 0.55 μm calculated from these size distributions are 0.37, 1.42, and 3.0×10^{-4}/m respectively. As would be expected, the area associated with the number of particles greater than 0.1 μm correlates quite well with the value of the scattering coefficient. In general, we observe no correlation between the total particle count and scattering, because the total count (over land) is dominated by the smaller particles. The air reaching the site on 19 June circulated down the east coast around a high-pressure system centered over Ontario and probably originated over Canada.

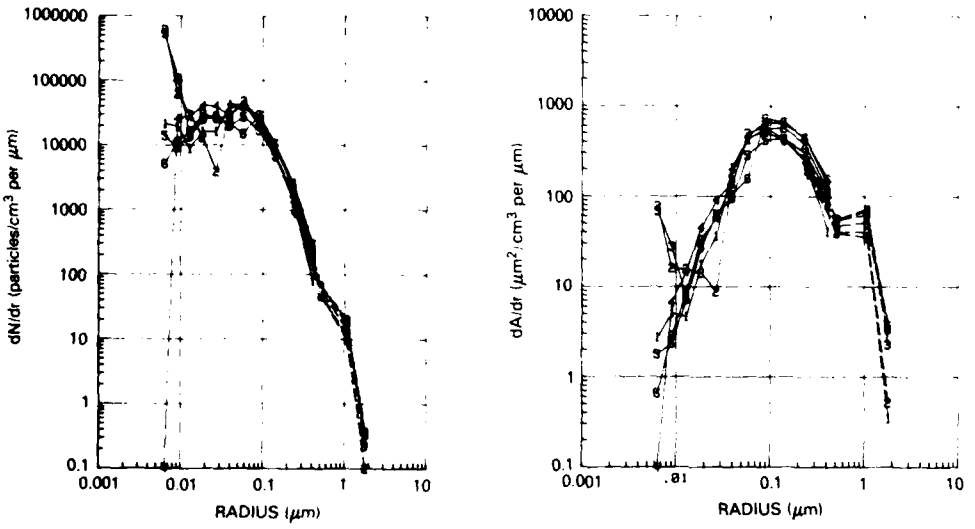

Fig. 20 — Eight distributions taken at the Wallops Island site on 22 June 1979, with a prominent secondary maximum at about 1 μm

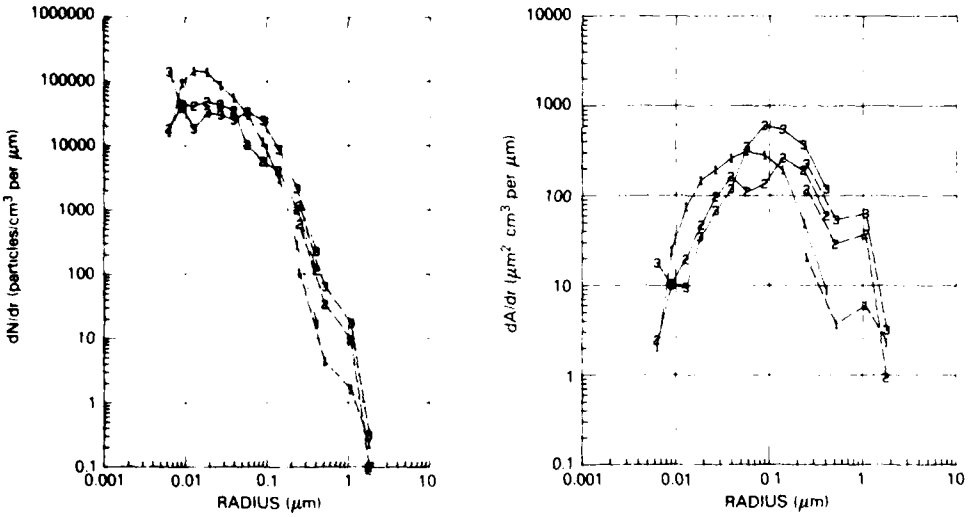

Fig. 21 — Distributions taken at the Wallops Island site on 21, 19, and 22 June 1979

Shipboard Measurements off the East Coast of the United States (1980 USNS *Hayes* Cruise)

In April 1980 a joint cruise of the NRL Marine Biology Branch and the NRL Atmospheric Physics Branch was undertaken off the east coast of the United States. The Marine Biology Branch's objectives required stops 4 to 10 hours in duration at certain stations inside and outside the Gulf Stream. The purpose of the Atmospheric Physics Branch's participation was to obtain data on aerosol size distributions along the east coast with special emphasis on the evolution of the size distribution in air advecting off the east coast. Our objective required the ship to be heading such that the wind speed and direction relative to the ship would assure uncontaminated air at the sampling location.

The USNS *Hayes* (T-AGOR 16) is a twin-hulled (catamaran) vessel designed especially for oceanographic research. The portable instrument shelter described earlier was installed on the flying bridge of the ship above the pilot house (Fig. 22). The flying bridge (roof of the pilot house) is about 14 m above the water. The air sample for the mobility analyzer and CN counter was taken through a stainless steel tube shaped like a shepherd's staff and mounted with the inlet about 5 m above the front of the pilot house. The Royco optical sensor was on the leading edge of the metal stand on the front of the shelter. Airflow measurements on a model of the USNS *Hayes* were previously made in a wind tunnel at the Naval Ship Research and Development Center, Bethesda, Maryland (Jeck, 1975). Figure 23 shows the results of these tests and indicates that the sampling sites, 3 to 5 m above the leading edge of the pilot house, provided good exposure for sampling when the relative wind was from the forward sector. In practice the CN counter provides a sensitive test of ship's contamination in the clean ocean environment. Even small traces of ship's pollution (from exhaust or galley vents) produce large numbers of CN, easily detected by the CN counter. No indication of ship's pollution was ever detected unless the relative wind was more than 70° to either side of the ship's heading.

The cruise began on the afternoon of 10 April 1980 and followed the track shown in Fig. 24. The numbered boxes are stations where the ship stopped for 2 to 12 hours for the observations by the marine biologists. Station 2 was a reference station visited on three occasions, and station 5 was visited twice. Contamination originating from the ship itself usually made it impossible to sample when the ship was on station.

Time plots of radon, CN, CCN, the scattering coefficient, and meteorological data are shown in Fig. 25a through 25d. Data for 15 April are omitted because most of the equipment was not operating on that day. Most of the breaks in the data occurred when the ship was on station.

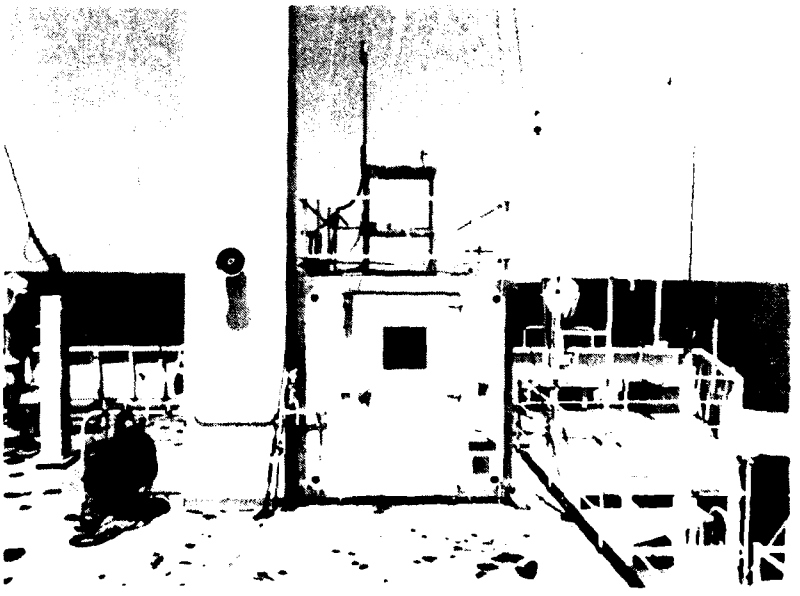

R(893)

Fig. 22 — Instrument shelter on the flying bridge of the USNS *Hayes* as viewed toward the bow. The shelter extends from alongside the mast to the bulkhead.

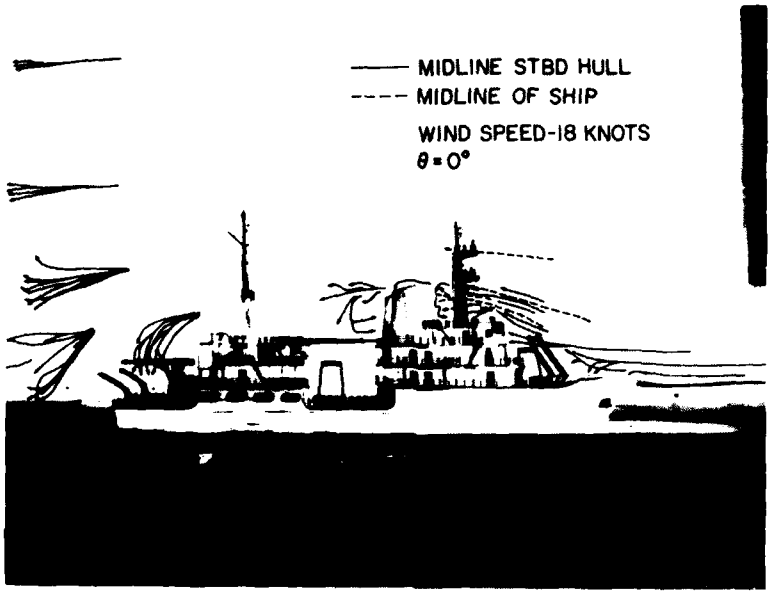

Fig. 23 — Air flow over a model of the USNS *Hayes* in a wind tunnel at NSRDC

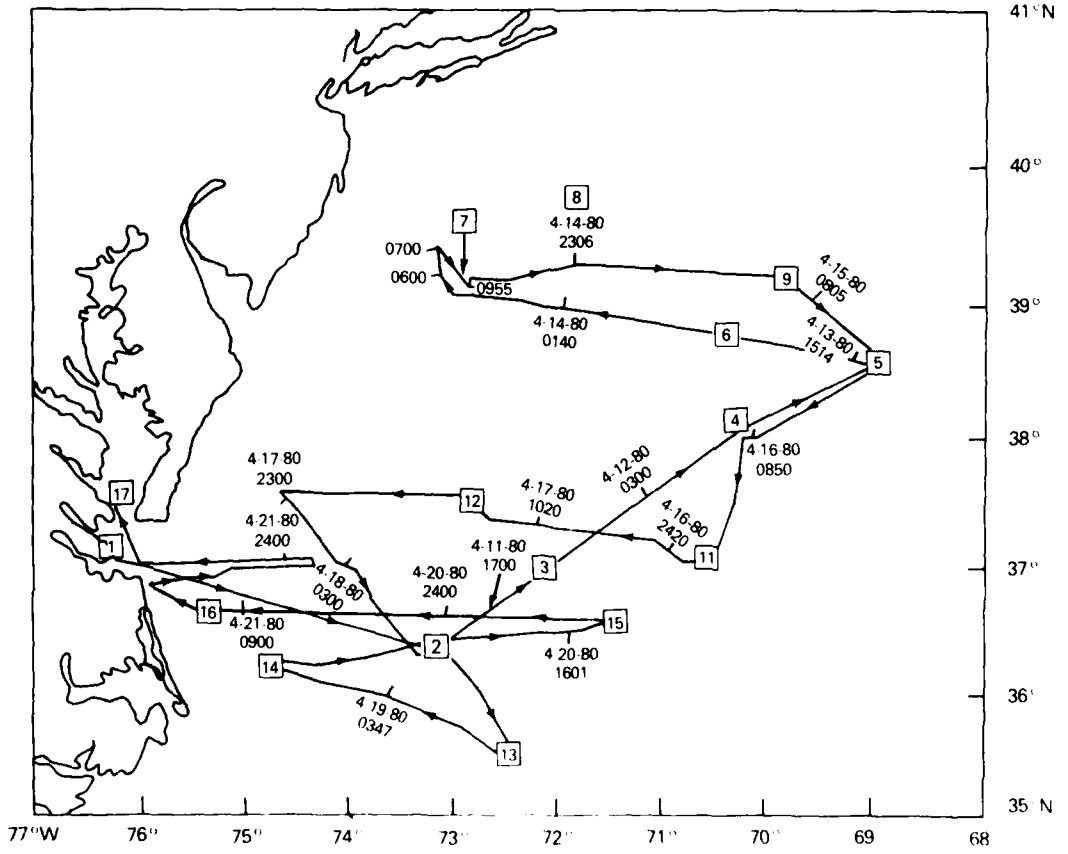

Fig. 24 — Cruise track for the USNS *Hayes* between 10 and 22 April 1980

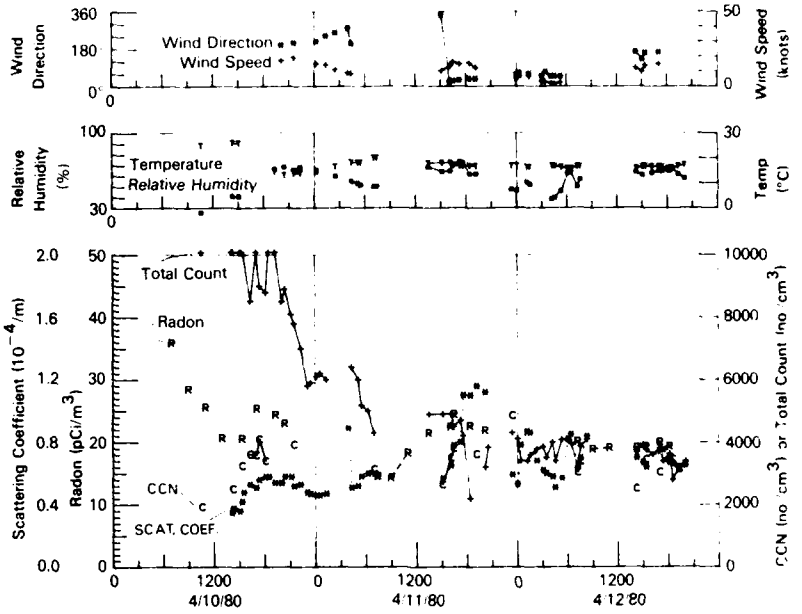

Fig. 25a — Time plots of wind speed and direction, temperature, relative humidity, radon concentration, aerosol scattering coefficient, CCN, and total aerosol concentration during the cruise

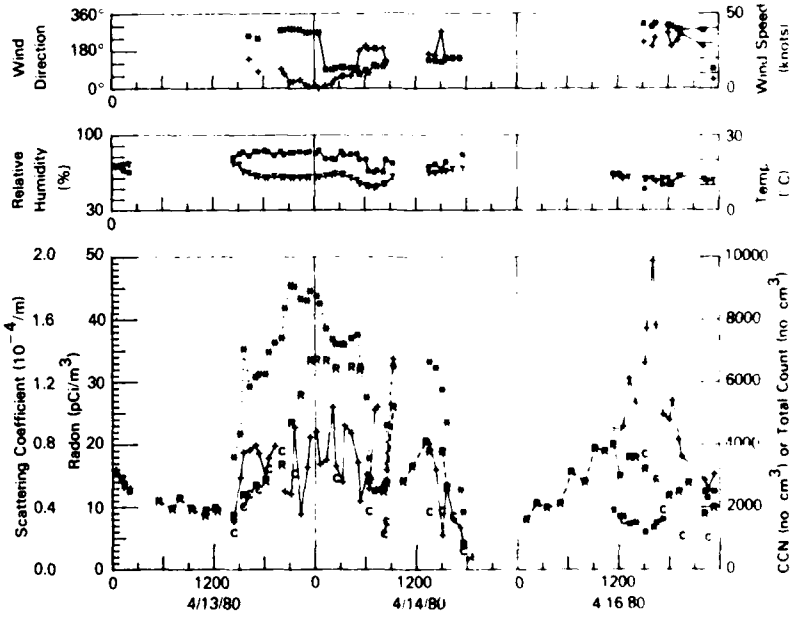

Fig. 25b — Continuation of Fig. 25a

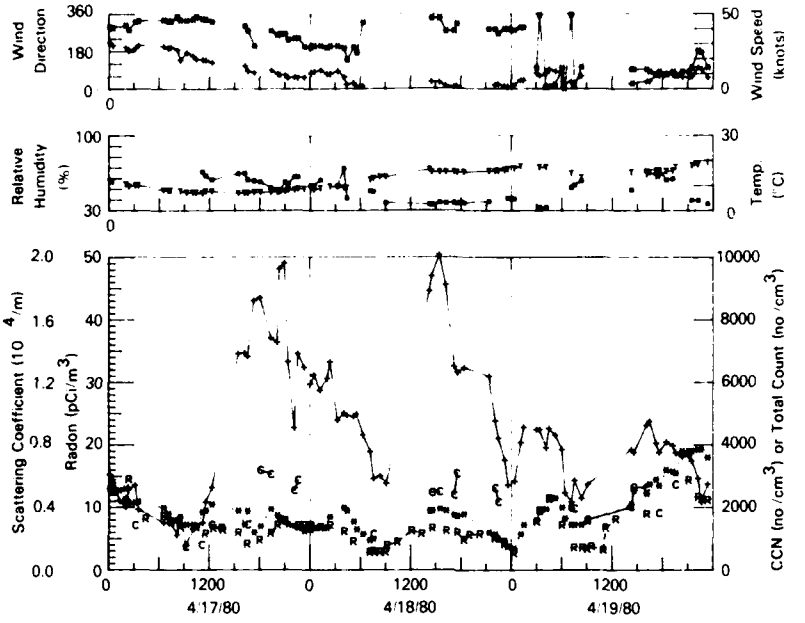

Fig. 25c — Continuation of Fig. 25b

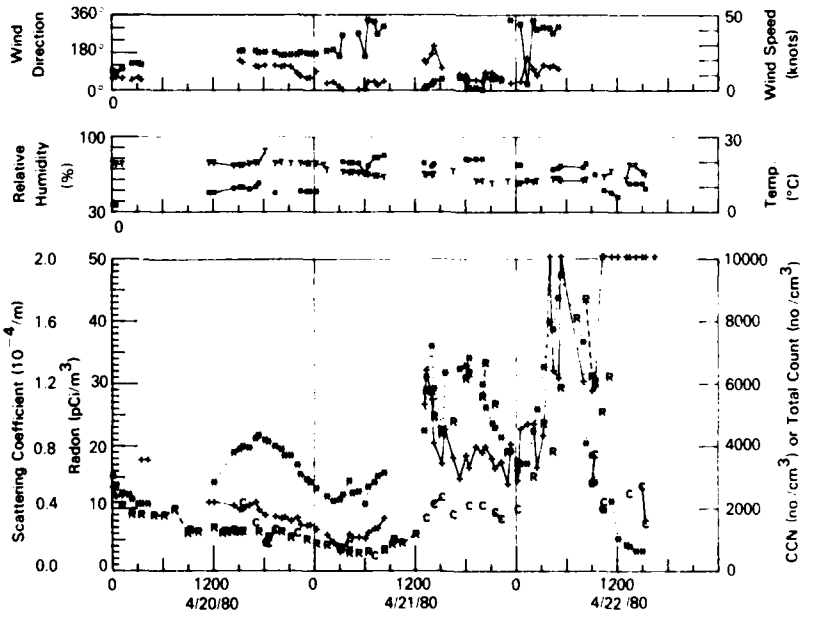

Fig. 25d — Continuation of Fig. 25c

After the ship left port on 10 April and continuing through 12 April the cruise area was under the influence of a well-defined but rather weak (5-knot) flow from off the Virginia and/or North Carolina coast. Air-mass trajectories for this interval are shown in Fig. 26. The relatively uniform radon concentrations throughout this interval (Fig. 25a) attest to the uniformity of the air mass on a synoptic scale.

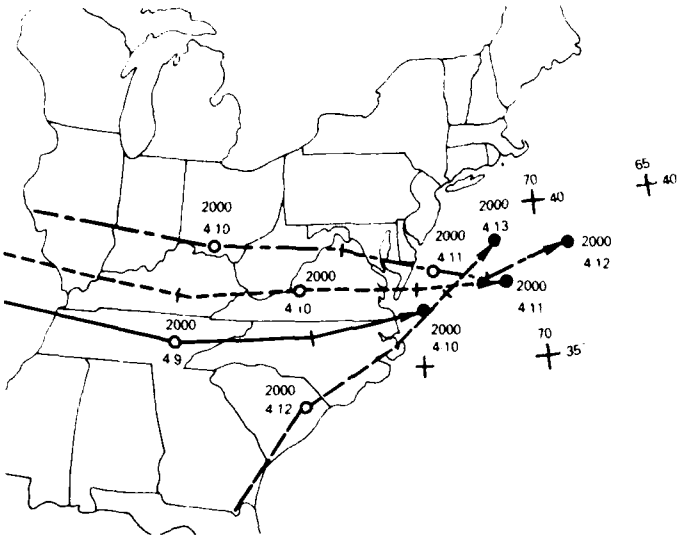

Fig. 26 — Trajectories showing the origin of the air in which the distributions were measured at 2000 EDT on 10, 11, 12, and 13 April at the locations indicated by filled circles

A well-defined cold front moved through the operations area during the night of 13-14 April. The radon, scattering-coefficient, and CCN data patterns are similar to those during previous transits of frontal areas over the ocean (Larson and Bressan, 1980). The front is shown as a line on weather maps, indicating the location of the change in wind direction, but radon data suggest that the frontal area is a broad zone where the continental materials are greatly enhanced as far as a few hundred kilometers ahead of the front. Radon, aerosol scattering, CCN, and other indicators of continental air exhibit much fine structure in these frontal zones. Sometimes the fine structure is very similar from one variable to the next, but in some cases, such as this, there is little correlation other than the overall continental enhancement. The increase in radon concentration appreciably lags the sharp increases in aerosol scattering and CCN and CN concentrations starting about 1500 EDT on 13 April, and except for a small change in scattering the abrupt change in wind direction marking the frontal boundary is not accompanied by changes in other indicators of continental air.

By 0900 EDT, 14 April, the front has changed to a warm front, and the change in wind direction from east to south is a consequence of the approach of another low-pressure area over West Virginia. Between 1500 and 1800 EDT on 14 April, the scattering coefficient and concentrations of radon and particulates dropped to low values, and the ship was in clean maritime air brought into the area by the combined influence of the low over the eastern United States and a high pressure east of Bermuda.

Data for 15 April are not included because most of the instrumentation was shut down due to heavy seas. Radon data showed maritime air until about 0900 EDT. During the remainder of the day the radon concentrations were in the range 10 to 15 pCi/m^3 that prevailed through noon on 16 April. A cold front from the west passed the ship late on 15 April, and another cold front accompanied by light rain passed over the ship just before arrival at station 11 at 2000 EDT on 16 April. The peak in total aerosol count and in CCN on 16 April, while scattering remained relatively uniform, can be attributed to larger numbers of particles with radii less than 0.07 μm which do not contribute to the scattering.

After passage of the front on 16 April, the ship came under the influence of a high-pressure system. The center of the high pressure moved from over the Great Lakes to just off Cape Hatteras on 17 April and remained stationary for the next 3 days. The combination of brisk northerly winds and relatively low radon and total particles is consistent with an assessment based on the weather maps that the air reaching the ship on the morning of the 17 April was originally maritime air brought into the area after a quick transit over New England by the high over the Great Lakes and a low off Newfoundland. The fast movement minimizes the accumulation of continental additives to the air. The winds became more westerly in the afternoon, suggesting that the large increase in small particles (increased total count but relatively unchanged scattering) results from industrial pollution from the United States or Canada. The radon concentrations were relatively low and variable on 18, 19, and 20 April, when the ship was in subsiding air near the center of the high pressure.

A cold front crossed the ship's location about noon on 21 April, accompanied by a change in wind direction and a sharp increase in radon, indicating that the air behind the front was continental. The ship remained in mostly continental air throughout the remainder of the cruise, near the coast and in the Chesapeake Bay.

Air trajectories were computed using the NOAA regional-continental scale transport, diffusion, and deposition model (Heffter et al., 1975). This model has worked well over land, where sufficient data are available, and it has worked reasonably well in remote ocean areas in that it confirmed conclusions about the continental or maritime character of air based on measured radon concentrations. Because the model does not take into account vertical air motions or discontinuities at fronts, and because data are few for areas over the ocean, the near-coastal area of this cruise, with the resulting importance of mesoscale air movements, did not suit itself well for use of this model. However, in several cases the computed trajectories confirmed the conclusions that could be drawn from particle data, radon data, and weather maps as to the origin and history of the air at the sample collection site. The trajectories from this model are used in this report only when they are supported by other meteorological data.

Overview of the Size Distribution Measurements

Over 300 aerosol size distributions were obtained during the cruise. An analysis of each size distribution in conjunction with the meteorological history of the air mass is not possible. In this subsection some general characteristics of the size distributions obtained during the cruise will be described, and in the following subsections case studies of several interesting intervals will be presented.

The size distribution over the ocean was often observed to remain remarkably stable with little change observed over the interval of hours. This is in contrast to size distributions over land, where temporal variations over similar time intervals are quite large. Figure 27 is a composite of five consecutive size and area distributions taken during 2-1/2 hours (0430 to 0700 EDT on 11 April) just prior to arrival on station 2. The five distributions are for the most part indistinguishable. At other times the distributions would change considerably over an interval of hours. These changes were usually, but not always, associated with some observable meteorological changes, with the distance the air traveled over water before arriving at the ship, or with the sea state. Since the distributions often remained stable,

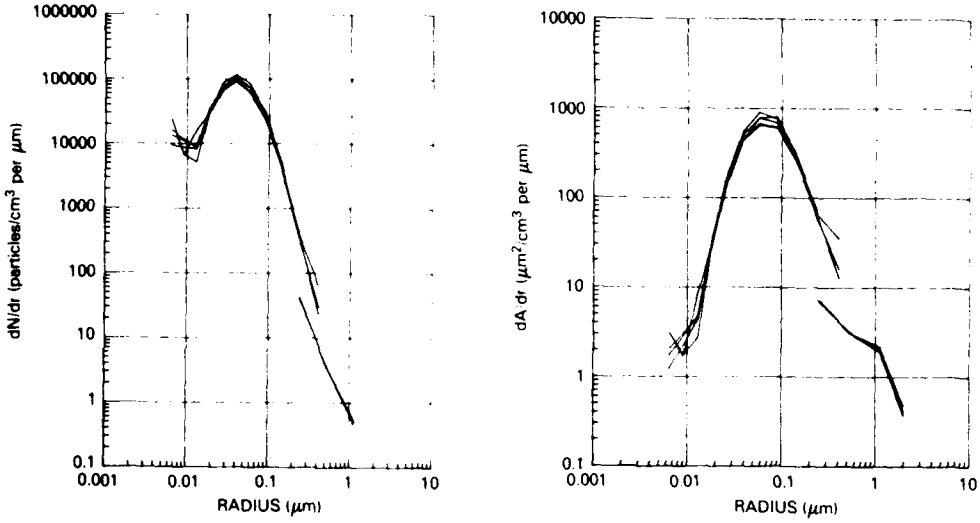

Fig. 27 — Composite of five consecutive size distributions and of the corresponding area distributions taken during a 2-1/2-hour interval, illustrating the stability of the size distribution often observed over the ocean

the data were sorted into periods when little or no change occurred, and average distributions for these periods were calculated. This was an effective way of reducing the numbers of data and of increasing their statistical significance. In the next subsections the distributions presented will be averages of two or more distributions.

The variability in the size and area distributions over longer intervals is illustrated in Figs. 28, 29, and 30 where each curve is an individual size or area distribution. The left-hand plot in Fig. 28 is a composite of 75 size distributions taken between the time the ship left the Chesapeake Bay (1700 EDT on 10 April) and 0100 EDT on 14 April, at a point between stations 6 and 7. The variability in the small particles covers about four orders of magnitude. The variability in the size distribution is remarkably low between 0.07 and 0.5 μm in radius. The region between about 0.25 and 0.4 μm is the region of overlap between the mobility analyzer and the optical particle counter, and the spread in this region is artificially increased because of the difference in the size distribution measured by the two instruments. When the value from the largest-particle channel is below the abscissa, it is not plotted. This is the reason the size distribution sometimes stops at 1.2 μm rather than about 2 μm. The average slope for the size range between 0.1 and 1 μm is nearly -4 during this time, in agreement with the slope originally proposed by Junge (1963).

The steep slope in the size distribution at radii greater than 0.08 μm tends to obscure the variations in numbers at the larger radii. At the right in Fig. 28 a composite of the same data plotted as area distributions is presented. This plot decreases the slope and magnifies the variations at larger sizes. It also magnifies the mismatch in the distributions obtained with the mobility analyzer and the optical particle counter in the overlap region between about 0.2 μm and 0.4 μm.

The air during this period was from the continental United States but with differing trajectories over water. Figure 26 shows typical trajectories during this portion of the cruise. The size distributions with the largest numbers of small particles were taken shortly after the ship had left Chesapeake Bay in air that had a short trajectory over water. As will be discussed later, there is apparently always an *initial* rapid decrease in the number of small particles as the air advects from land out over the ocean. However, beyond a certain point it is not clear that the decrease is a simple function of distance (or time)

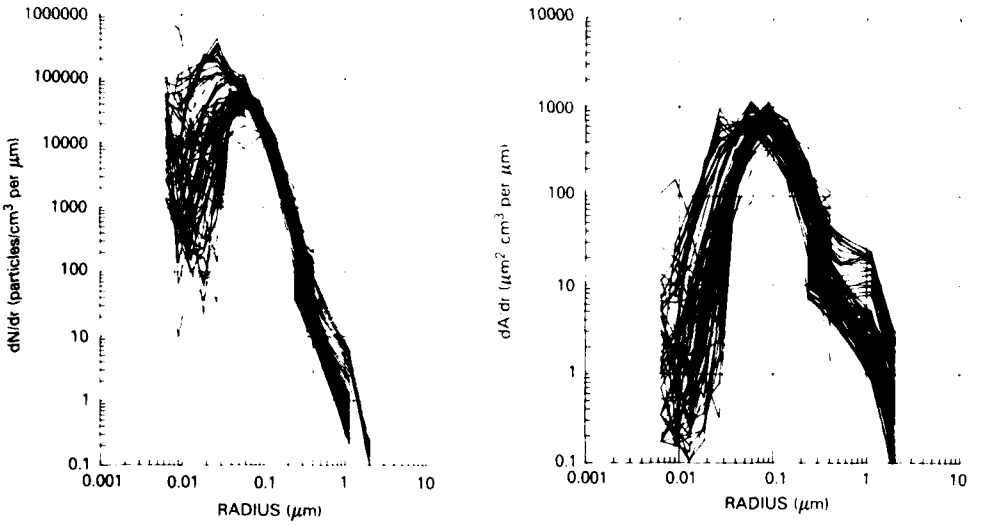

Fig. 28 — Composite of 75 size distributions and of the corresponding area distributions taken between 10 April and 14 April

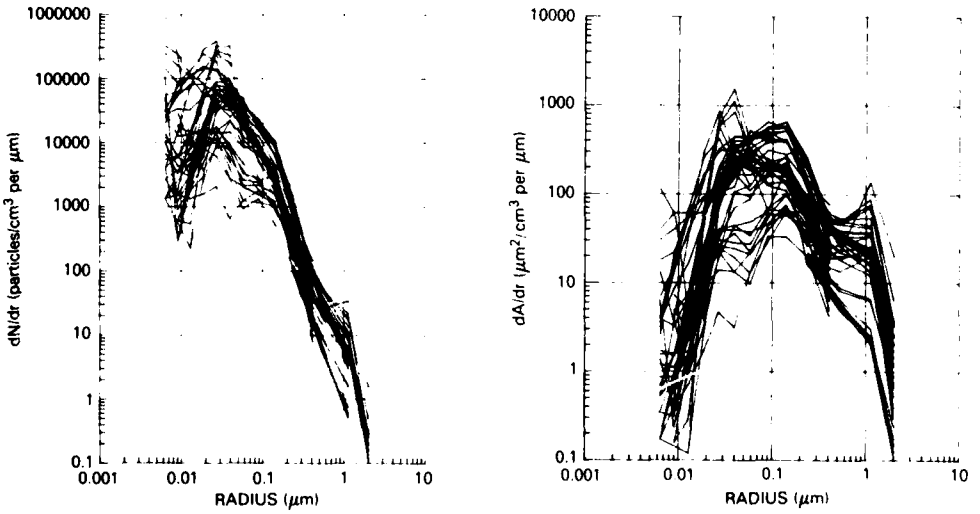

Fig. 29 — Composite of 40 distributions taken between 14 April and 16 April

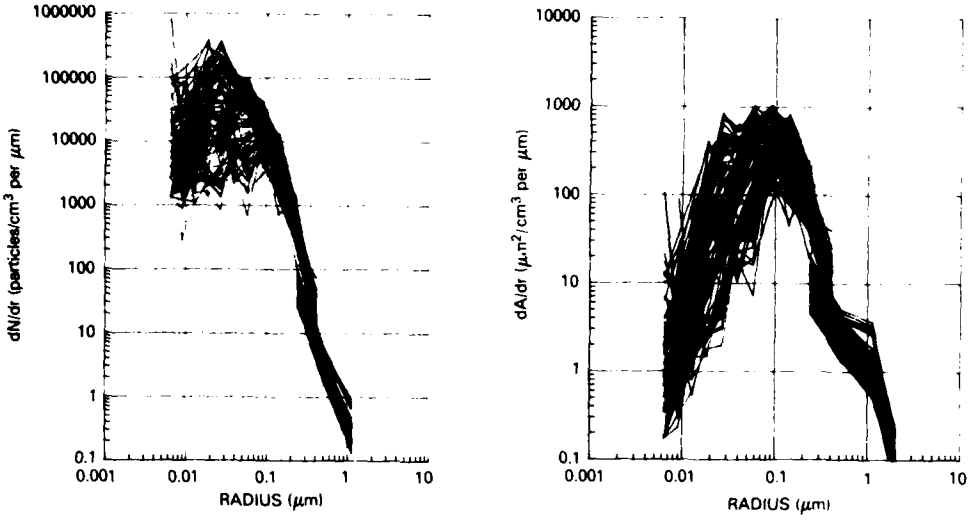

Fig. 30 — Composite of 104 distributions taken between 17 April and 21 April

over water. (Part of the problem here is the difficulty of establishing reliable back-trajectories of surface air at the ship for longer times and the difference in sources of the different samples in that the measurements are not on the same trajectory.)

The air encountered during this portion of the cruise had apparently not gone through a precipitation cycle during its transit from land to the ship. This probably plays an important role in explaining the invariance of the size distribution between 0.07 μm and 0.5 μm and the large number of particles in the size range 0.05 to 0.1 μm.

Figure 29 shows a composite of 40 size distributions taken between 0200 EDT on 14 April and 1400 EDT on 16 April (no data were taken on 15 April and on the morning of 16 April because of a storm). Again there is a large variation in small particles. Here the stability observed in the range 0.07 to 0.5 μm in Fig. 28 has degenerated. The size distributions with low concentrations in this intermediate size range were probably the result of wet removal processes associated with a frontal system. These same size distributions exhibit a large number of particles greater than 1 μm. These larger particles are surface-generated by high seas.

Figure 30 is a composite of 104 size distributions taken during the latter part of the cruise between 0800 on 17 April and 1300 on 21 April. This interval was dominated by a nearly stationary high-pressure system moving slowly off the east coast. Again there is a large variability in the small particle concentrations, and the slope between 0.1 μm and 1 μm is about -4.

Evolution of the Size Distribution in Air Masses Advecting from Land to Sea

One important objective of our participation in the 1980 cruise was to observe the change in the size distribution of small particles in air masses as they advect from the east coast out over the Atlantic. The initial decrease in the small aerosol population as continental air advects out over the water is clearly evident in a number of cases from our data. However, determination of the precise rate of decay along a given trajectory as a function of particle size is not possible from the data obtained. The main difficulties are that the complex meteorological processes cause uncertainties in the accuracy of the calculated back-trajectories of air encountered at the surface and that measurements were not along

a single trajectory. In many cases the calculated back-trajectories (for an altitude of 450 m) did not agree with analysis of surface weather charts or local observation of wind and radon concentrations. Despite the lack of knowledge of the exact trajectories of the surface air, interesting data on the decay were obtained. Two case studies will be presented: between port and station 2 and between stations 8 and 9.

The ship left Norfolk harbor about 1400 EDT on 10 April, passed through the entrance to the Chesapeake Bay at about 1530 and headed east for station 2 (Fig. 24). The night before, a front accompanied by rain passed through the area and out to sea. The air on the morning of 10 April was dry and clear. After the ship left the Bay, the air temperature dropped during the first 5 hours from 27°C to 13°C and then increased to about 21°C as the ship approached station 2. The latter warming was attributed to the influence of the Gulf Stream. Curve 1 in the left-hand plot of Fig. 31 shows the size distribution taken in the Chesapeake Bay between the James River and the mouth of the Bay. The total particulate count was about 30,000/cm^3 and highly variable.

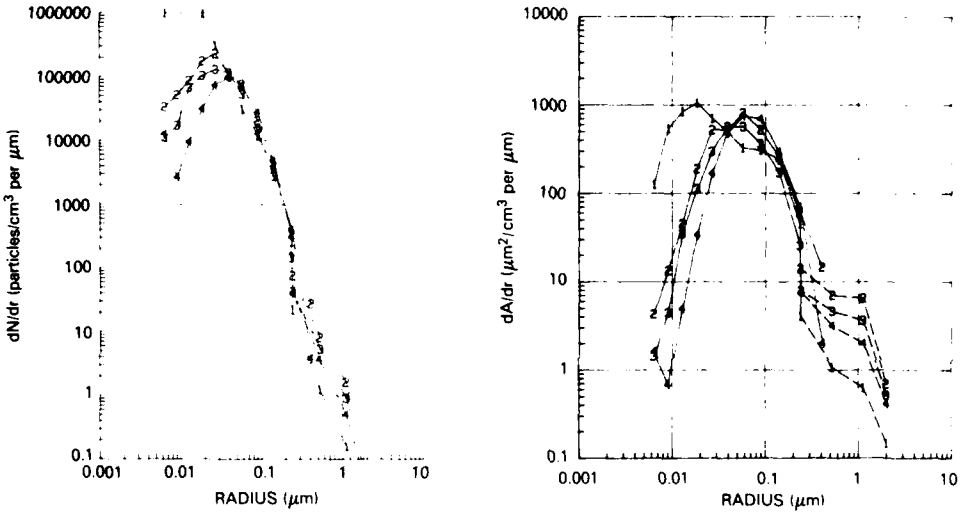

Fig. 31 — Change in the size and area distributions as the ship left Chesapeake Bay and sailed to station 2

Curve 2 is the average of ten size distributions taken between 1700 EDT and 2100 EDT about 15 to 60 nmi off shore. The total particle count was about 9000/cm^3. During this interval there was little systematic change in the size distribution. Unfortunately, the ship's speed was not recorded during this interval, so true wind speed and direction could not be accurately calculated. From estimates of the ship's speed the estimated wind direction was from the south-southwest. As the ship moved out to sea, the air encountered undoubtedly had a back-trajectory for which landfall was progressively to the south. For curves 3 and 4 landfall was probably somewhere along the North Carolina coast.

The average of three distributions taken between 2330 and 0100 EDT on 11 April about 60 to 90 nmi off the coast is shown as curve 3. Curve 4 is the average of five distributions taken between 0430 and 0700 EDT near station 2, about 130 nmi off the coast.

Figure 32 shows the calculated air-mass trajectories supplied by NOAA for 450-m level during this interval. (Surface winds would indicate that the surface air came more from the south than indicated by the trajectories for 450 m.) The weather was clear, and there was no indication that the air had passed through any region of precipitation during the previous 24 hours, and certainly not through any

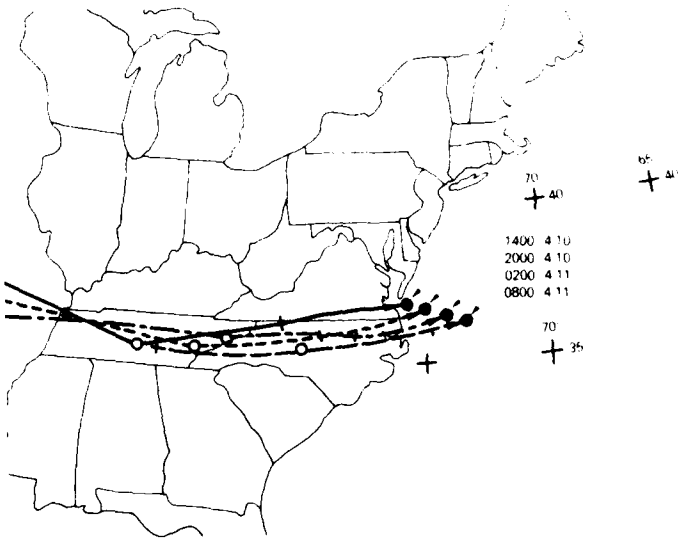

Fig. 32 — Calculated air-mass trajectories corresponding to the distributions shown in Fig. 31

precipitation after the air had been over water. If these trajectories are used to calculate the time the air spent over water between the coast and arrival at the ship, the values are 1.5 to 3 hours for curve 2, 5 hours for curve 3, and 9.5 hours for curve 4. It is suspected that these times calculated from the 450-m-level trajectories are minimal and that the real times are somewhat longer.

The decay in the number of small particles as the air spends more time over water is obvious from Fig. 31 and is undoubtedly due to the loss of small particles by coagulation with each other and with larger particles and by growth of smaller particles to larger sizes by condensation of gas-phase reaction products on their surfaces (details of the latter mechanism being given in Hoppel, 1975). These mechanisms have little effect on the particles greater than 0.08 μm in radius. The number of large particles first increased as the ship moved into the open sea and then decreased continually until the ship reached station 2. This decrease in large particles between curves 2 and 4 is more difficult to understand. The decrease occurred while the wind also decreased from about 16 knots to 7 knots, which suggests the large particles may be wind-generated particles originating at the sea surface. However, this explanation is not entirely satisfactory, because at other times on the cruise wind-speed changes of this magnitude did not cause a large change in the larger particles. The change is probably related not only to the instantaneous wind speed but also to the wind and sea-state history over the prior 24 hours or so (Gathman, 1983).

The measured scattering coefficients at the times curves 2, 3, and 4 were obtained were 0.56, 0.47, and 0.58×10^{-4}/m, respectively. This would indicate that the scattering (at 0.55 μm in wavelength) was not greatly affected by the particles larger than 0.5 μm in radius. This is in agreement with the detailed analysis of extinction discussed elsewhere in this report. Particles smaller than 0.3 μm are predominantly responsible for the scattering of visible light.

Another particularly interesting period of the cruise occurred between stations 5 and 9 (Fig. 24) from 1500 EDT on 13 April to 1100 EDT on 15 April. The number of small particles increased as the ship approached the coast and then decreased again as the ship sailed away from the coast. As the ship left station 8, a storm was encountered, and the aerosol size distribution associated with the storm was measured.

During this 2-day interval the meteorology was fairly complex. At the start of the interval a cold front, trailing from a low over Nova Scotia, passed across the ship's position. This front connected to another low-pressure system centered over southern Mississippi. A ridge of high pressure separated the two lows. During the transit from station 5 to station 7 the ship was in air behind the cold front. This air was presumably of recent continental origin. The true winds were too light to calculate accurately during most of the transit to shore but were generally from the west. The low that was over the Mississippi Gulf Coast deepened somewhat as it tracked to the north-northeast and was centered over western Kentucky by 0800 EDT on 14 April. The circulation around this low caused the wind at the ship to strengthen and shift to the east during the early morning hours of 14 April. When the ship arrived at station 7, the winds were easterly at 22 knots. The skies had become increasingly overcast during the shoreward part of the track, with heavy overcast and some mist where the track came closest to the coast.

Figure 33 shows four average size distributions and area distributions taken between stations 5 and 7 and clearly shows the increase in small particles as the ship got closer to land. Curve 1 in each plot is the average of four distributions taken between 2000 and 2230 on 13 April when the ship was between stations 5 and 6. The total count was about 3000/cm^3. Curve 2 in each plot is the average of six size distributions taken between 0350 and 0500 on 14 April. The total count was about 3500/cm^3. Curve 3 in each plot is the average of two distributions between 0600 and 0700 at the closest point to land. The total count was again about 3500/cm^3, with the increase in small particles being balanced by the decrease in the size range 0.05 to 0.2 μm. Curve 4 in each plot is the average of two distributions taken between 0700 and 0845 just prior to the ship's arrival at station 7. The total count was about 5000/cm^3. When the data for curves 3 and 4 were obtained, the wind had intensified to about 22 knots and was shifting from northwest to easterly.

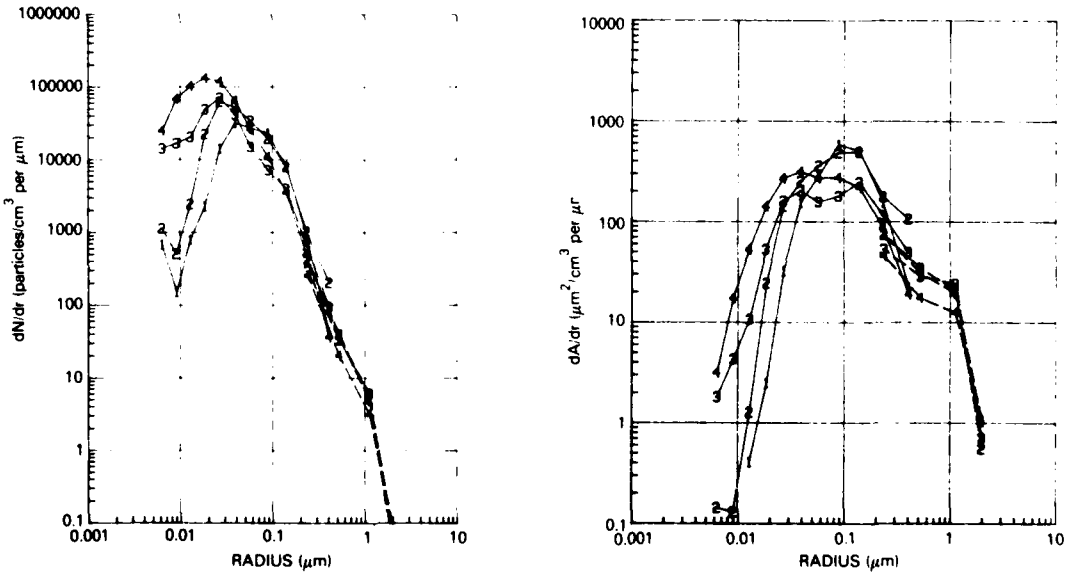

Fig. 33 — Four average size distributions and the corresponding area distributions taken between stations 5 and 7

The ship remained at station 7 from about 0800 to 1400 EDT, during which time no data were taken. At 1400 the ship left station 7 and slowly transited to station 8, where it remained from 1800 to 2400 EDT. Throughout this interval the seas became rougher, with the wind speed ranging from 17 to 25 knots from the south-southeast. As the ship sailed from station 7 to station 8, the air became noticeably cleaner, as indicated by the lower particle counts, lower radon concentrations, and smaller values of the scattering coefficient. The surface weather map showed that the warm front associated with the low over the eastern United States moved north across the ship's position at about 1430 EDT on 14 April. Curves 1 of Fig. 34 are the same as curves 4 of Fig. 33 and are the distributions upon the ship's arrival at station 7. Curve 2 in each plot is the average of two distributions taken between 1630 and 1730, just prior to the ship's arrival at station 8. The total particulate count had dropped to 1400/cm^3, but there was an increase in particles larger than 1 μm in radius, believed to be particles generated by the higher seas.

When the ship left station 8 at 0000 EDT on 15 April, the winds were very strong (30 to 35 knots) from the southeast. The seas became increasingly rough, and the wind became so strong that there was a reverse flow of air through the nephelometer due to Bernoulli suction of the wind over the air inlet. The relative humidity had increased and was between 95% and 100%. Curve 3 in each plot is the average of two distributions taken during this interval (0240 to 0330 EDT). The total particle count dropped to 350/cm^3, the lowest recorded on the cruise. There was a further increase in the number of particles larger than 0.5 μm in radius. These larger particles are believed to be salt particles generated by the high seas and wind. Rain and fog developed shortly after the curve-3 data were obtained. Because of increasingly stormy conditions, the instruments were turned off at about 0400, and all efforts were spent securing and protecting the equipment from damage. The presence of the shelter on the flying bridge makes for a particularly rough ride in heavy seas because of the long lever arm between the ship's center of gravity and the bridge. Although the storm passed that night, the seas remained heavy, and no data were taken for the next 1-1/2 days.

The dramatic change in the size distribution between curves 1 and 2 in Fig. 34 is associated with the change in air mass following the passage of the warm front. We believed that prior to the frontal passage the instruments were sampling air which recently had been over the continent. With the passage of the warm front this air was replaced by air which had a longer trajectory over water, as can be seen from Fig. 35, which shows the NOAA air-mass trajectories for 2000 EDT on 14 April and for 0200 on 15 April. These trajectories are consistent with the synoptic situation which indicated that following the passage of the warm front the air reaching the ship resulted from flow on the back side of a broad high-pressure area (102.8 kPa or 1028 mb) with one center near 30°N, 55°W. The low count in the third size distribution probably indicates air which underwent a wet-scavenging cycle. Radon concentrations of 2 pCi/m^3 indicate that the air had not been over land for some time.

Figures 36 and 37 are plots of the extinction coefficients computed for the size distributions given by curves 1 and 3 in the left-hand plot of Fig. 34. The dramatic change in the size distribution is reflected in the relative contribution of the particles in each size range to the total extinction. Curve 3 in the left-hand plot of Fig. 34 is the only size distribution we encountered such that particles in the size range 0.9 to 3 μm made a major contribution (in this case the largest contribution) to extinction at 0.55 μm in wavelength while particles smaller than about 0.3 μm made a negligible contribution.

Size Distributions Under High Pressure Off the East Coast of the United States

After the storm the seas remained rough on 15 April, with winds from the south at about 26 knots. Late in the day on 15 April, a cold front from the west passed over the ship, and the winds shifted more to the west at about 22 to 30 knots. The equipment which had been turned off early on 15 April during the storm was turned on again while the ship was on station 4. Another cold front accompanied by light rain passed over the ship just before its arrival on station 11 at 2000 EDT on 16 April. For the next 4-1/2 days the ship was under a high-pressure system which had moved down from

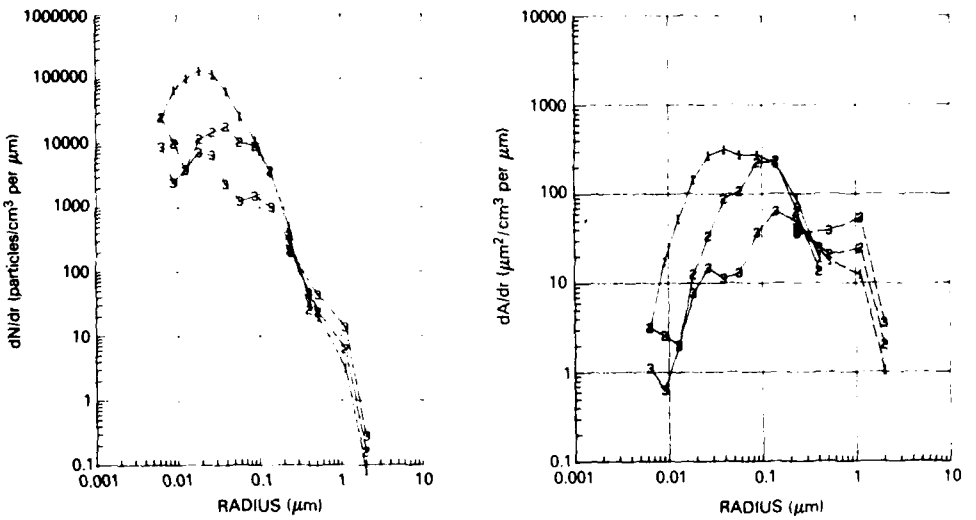

Fig. 34 — Change in distributions during the passage of a warm front on 14 April

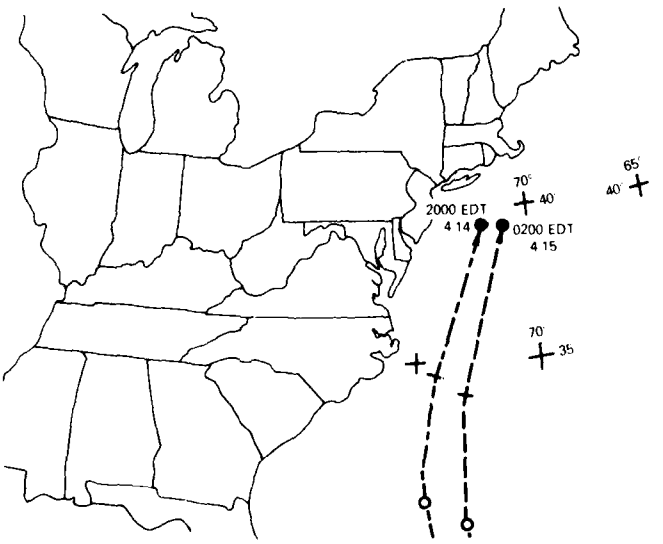

Fig. 35 — Air-mass trajectories for air encountered after the passage of the warm front on 14 April

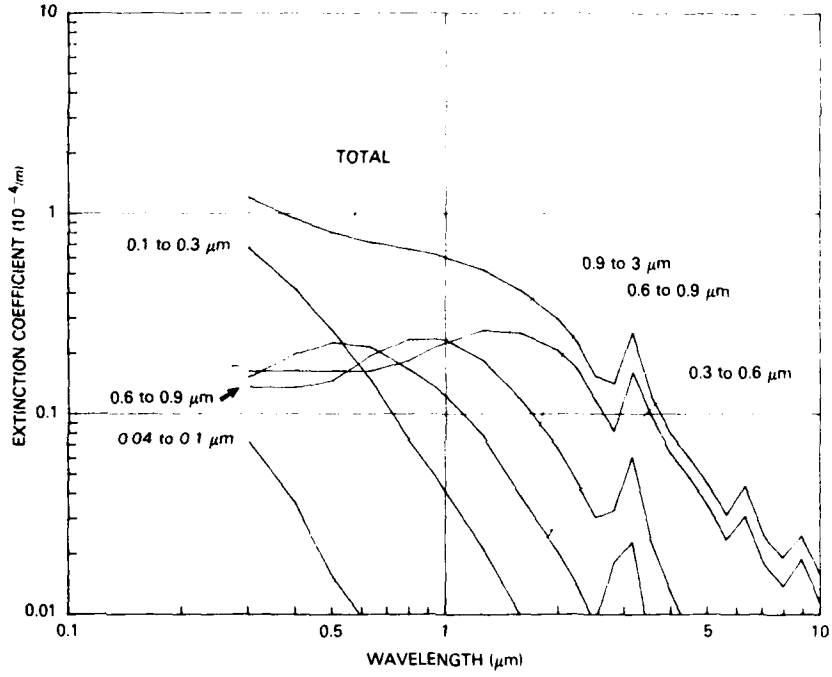

Fig. 36 — Calculated extinction for the size distribution given curve 1 of Fig. 34

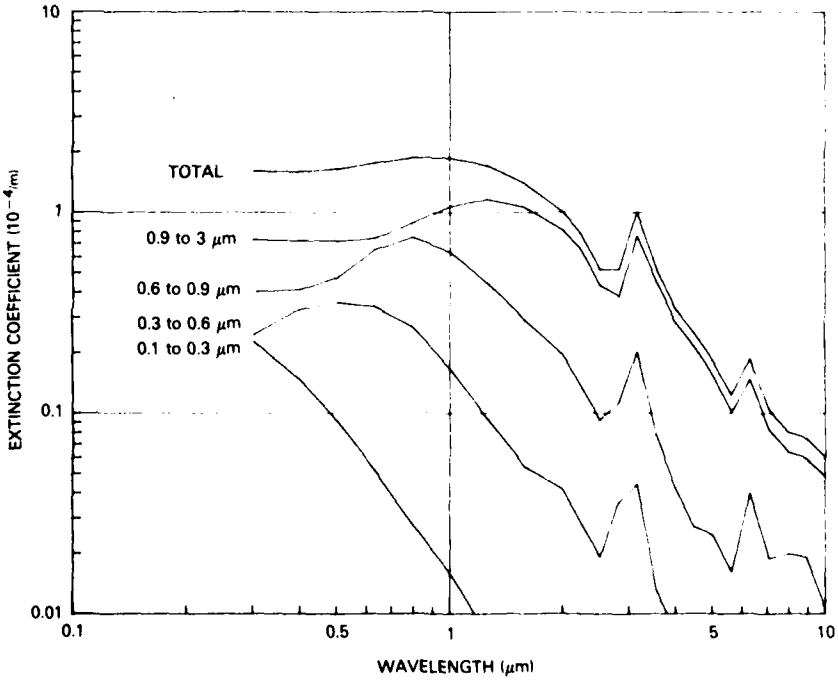

Fig. 37 — Calculated extinction for the size distribution given by curve 3 of Fig. 34

the southern Great Lakes region on 16 April to over Cape Hatteras on 17 April. At the coast, the movement slowed, and the high moved slowly out to sea, degenerating into a high-pressure ridge by 19 April.

Curve 1 in each plot of Fig. 38 is the average of eight distributions taken during a 5-hour interval before the ship arrived at station 12. Each of the eight distributions had the peculiar double peak exhibited in curve 1. The wind during this interval was from the northwest and was decreasing in speed from about 26 knots to 16 knots. The total particulate count was 1500 to 2000/cm^3. While the ship was on station 12, the total particulate count increased, and it remained high as the ship approached closer to land. Curve 2 in each plot of Fig. 38 is the average of eight size distributions taken between station 12 and the closest approach to land. The total particulate count here was about 7000 to 10,000/cm^3. The winds were from the west at about 9 knots, and the ship was just north of the center of the high pressure. From the available data it is difficult to determine the origin of the air. The trajectory for the 450-m level shows air flowing south from the North Atlantic and coming close to, but never quite over, land. The trajectory for 900 m shows the air coming from the opposite direction (from the Bahama Islands). The local winds were from the west-southwest. Although the increase in the total aerosol count would indicate a recent trajectory over land, the radon concentration was quite low, indicating that the air had not spent much time over land. Our best estimate is that the surface air had come in from the North Atlantic and had a short trajectory over land (or had mixed with continental air) before going back over the sea to the location of the ship. The air may further have been diluted with subsiding air under the high-pressure system.

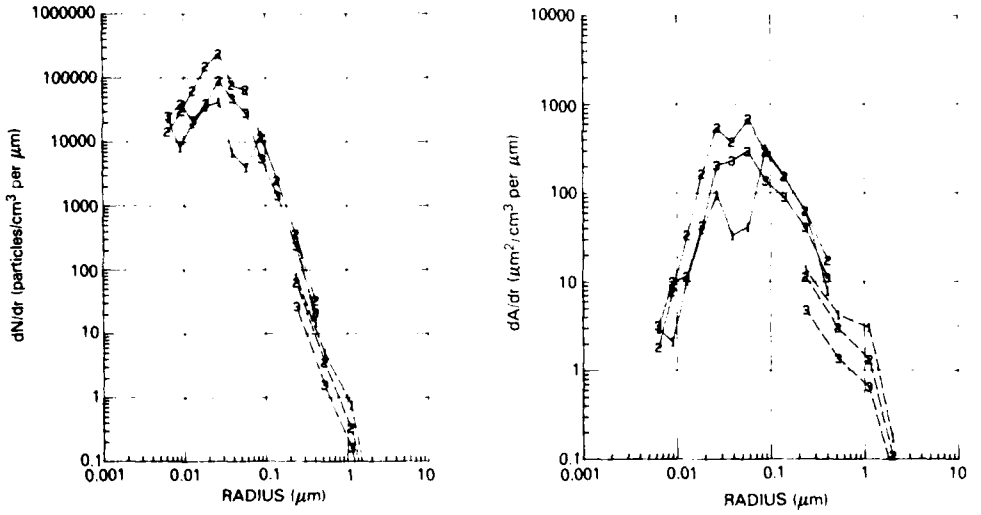

Fig. 38 — Three average distributions: (1) average of eight distributions taken just prior to the ship's arrival on station 12, with all eight exhibiting the double peak, (2) average of eight distributions between station 12 and the closest approach to land, and (3) distributions on the ship's arrival at station 2 at 0700 EDT on 18 April

As the ship turned southeast away from land at about 2300 EDT on 17 April and headed toward stations 2 and 13, the number of small particles began a slow decrease. When the ship arrived at station 2, 7 hours later, the size distribution was as shown by curve 3 in the left-hand plot with a total particulate count of about 3000/cm^3. The air was dry compared to typical oceanic humidities, reflecting the influence of the high pressure. The relative humidity was about 60% at station 12 and dropped to 37% on station 2, when the ship was at the center of the high.

The distributions obtained from 18 April to 20 April are difficult to interpret in terms of the meteorology and air-mass origin. In Fig. 39 the average distributions during two periods when the distributions remained quite stable are shown. Curve 1 in each plot is the average of seven size distributions taken between 1700 and 2400 on 18 April near and on station 13. All of the size distributions individually exhibited the double peak. The wind was weak from the north-northwest, seas were calm, and the particulate count was 4500 to 5500/cm^3.

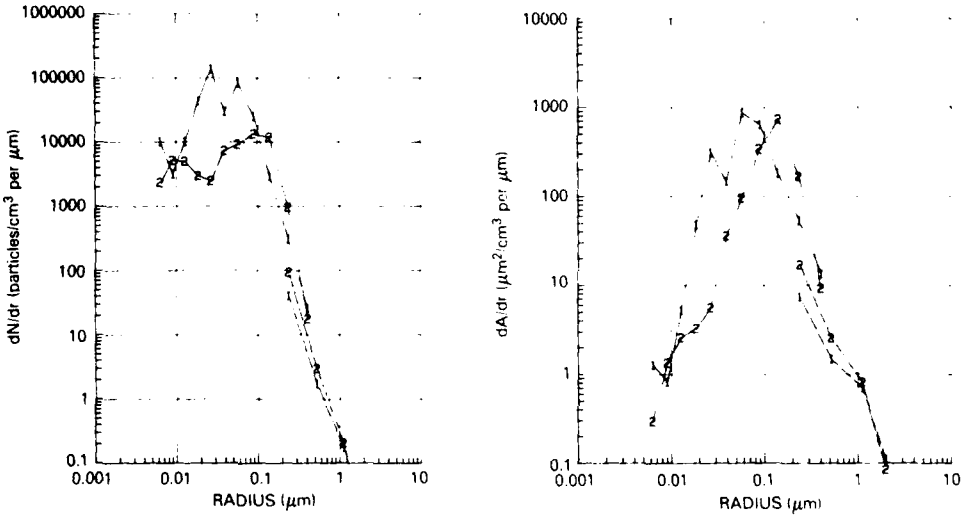

Fig. 39 — Two average distributions: (1) average of seven distributions taken on 18 April with all seven exhibiting the double peak, and (2) average of 16 distributions which remained nearly unchanged from 1400 EDT on 20 April until 0030 EDT on 21 April

Curve 2 in each plot of Fig. 39 is the average of 16 similar distributions measured between 1430 EDT on 20 April and 0030 on 21 April (the first half of the transit between stations 15 and 16). The wind was from the south at about 13 knots, and the total count was in the range 1500 to 2000/cm^3. Here the peak of the area distribution occurred at a radius exceeding 0.1 μm, which was about the largest radius at which the peak occurred on the cruise and much larger than ever observed over land.

Return to the Chesapeake Bay

The weather maps for 21 April showed a cold front moving across the location of the ship in early afternoon while the ship was on station 16, about 40 nmi off Cape Hatteras. There was no significant change in temperature or cloudiness associated with the passage of the front that was observed at the ship. However, there was a significant increase in wind speed, scattering coefficient, and total aerosol count (which increased from 1500 to 5000/cm^3) as shown in Fig. 25d at about 1300 EDT on April 21. The increase in radon concentrations from about 3 to 25 pCi/m^3 confirms that after the passage of the front the air had a more recent (and/or longer) trajectory over land than air preceding the front. (This change was not evident from NOAA air-mass trajectories.) The change in the size and area distributions associated with the passage of the front is shown in Fig. 40, where curve 1 in each plot is the average of three distributions taken between 0715 and 0830 EDT just prior to the ship's arrival on station 16 and curve 2 is the average of six distributions taken between 1330 and 1650 EDT after the ship left station 16 en route to the mouth of the Bay.

Starting at 1600 EDT on 21 April the ship sailed eastward away from the Chesapeake Bay until 2300 EDT, when it turned 180° and headed back toward the Bay. During most of this interval, the total aerosol count remained in the range 3000 to 5000/cm^3, and the size distribution was similar to

that shown by curve 2 in the left-hand plot of Fig. 40. During the 6 hours from 0600 to 1200 EDT (22 April) as the ship approached the mouth of the Bay and proceeded to station 17 inside the Bay, there was a dramatic decrease in the aerosol scattering coefficient and a corresponding change in the size distribution. The number of particles larger than 0.06 μm decreased dramatically, and the number of small particles increased, such that the total concentration increased from about 6000/cm^3 to about 20,000/cm^3. The temperature increased during this time, and the relative humidity decreased from about 70% to about 50%. There were no navigational data available from which to calculate wind speed and direction during transit in the Bay, but the interval ended on station 17, where the ship maintained a position with its bow into the wind, which was from the north at 16 to 24 knots. While the ship was on this station, the aerosol scattering coefficient continued to drop from 0.40×10^{-4}/m to 0.16×10^{-4}/m, and the relative humidity remained constant at about 50%. The changes in the size and area distributions are shown in Fig. 41, where curve 1 in each plot is the average of two distributions taken outside the Bay. Curve 2 is the size distribution measured at the entrance to the Bay. Curves 3 and 4 are averages of three distributions upon the ship's arrival at and departure from station 17 respectively.

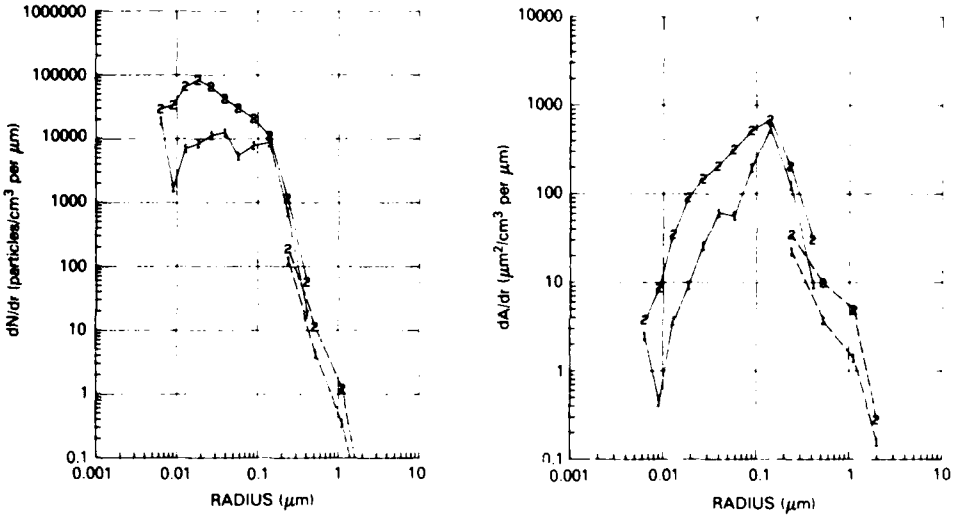

Fig. 40 — Change in the size and area distributions associated with the passage of a weak cold front on 21 April

If the 450-m-level air-mass trajectory for this interval can be trusted to indicate the origin of the surface air, then the air had moved rather rapidly (in the prior 12 hours) from upper New York State down the east coast to the Chesapeake Bay. The observed change in the size distribution for larger particles was probably more related to the changing trajectory of the air mass and only incidently related to the entrance of the ship into the Chesapeake Bay.

The rapid change in the scattering coefficient makes this an interesting interval for looking at the extinction in more detail. The measured scattering coefficient corresponding to curves 1 through 4 of Fig. 41 were 1.85, 0.74, 0.40, and 0.16×10^{-4}/m respectively. The values of the extinction coefficient calculated from the four size distributions shown in Fig. 41 for 0.55 μm in wavelength are 1.60, 0.70, 0.40, and 0.16×10^{-4}/m respectively and are in excellent agreement with the measured values of the scattering coefficient.

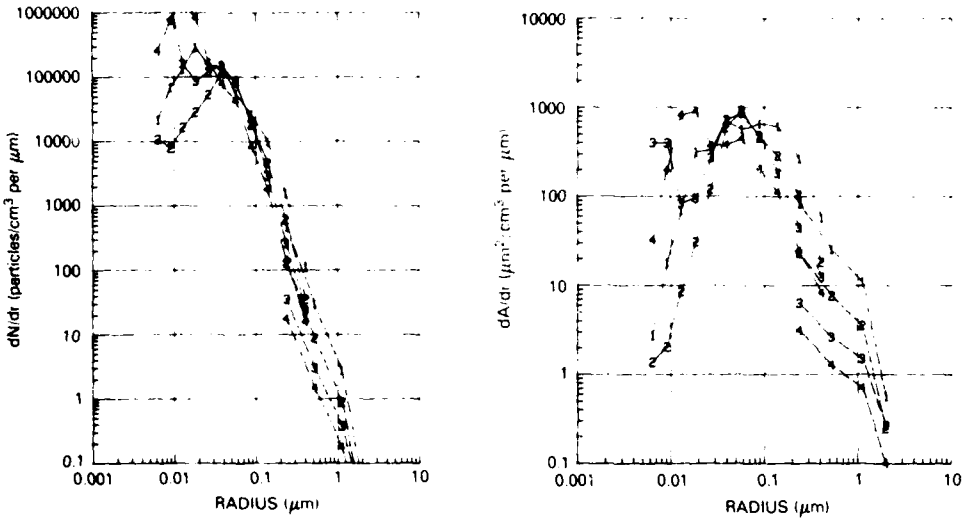

Fig. 41 — Change in the size and distributions as the ship returned to the Chesapeake Bay

DISCUSSION

Summary of the Hygroscopicity Results

In the subsection from page 10 to page 15 we described the theory and experimental method used to determine the value of the particle activation parameter (B^0) from measurements of the supersaturation at which a particle of known dry size is activated. In this subsection we summarize and discuss the results of these measurements.

Figure 42 shows the results of our measurements of the dry size (r_0) and critical supersaturation (S_c) of atmospheric aerosol particles. Each data point represents the values of S_c and r_0 at the center of an S_c-r_0 block, such as is shown in Fig. 7. These measurements were made at Washington, D.C., during 1978 to 1980 and off the east coast of the United States during the cruise of the USNS *Hayes* in April 1980. Figure 42 also shows the relationship between S_c and r_0 for sodium chloride particles ($B^0 \simeq 1.3$), ammonium sulfate particles ($B^0 \simeq 0.65$), and particles having a B^0 value of 0.2. The S_c-r_0 relationships for other electrolytes commonly found in atmospheric aerosol particles, such as ammonium nitrate, sodium nitrate, and sodium sulfate, lie between the curves for sodium chloride and ammonium sulfate. Since the measured values of critical supersaturation are higher than those calculated for pure particles of the salts commonly present in atmospheric particulates, we may conclude that a significant fraction of the dry mass of the atmospheric aerosol particles was insoluble. If we assume, for instance, that the soluble material in atmospheric aerosol particles is ammonium sulfate, then a value of B^0 of 0.2 implies that 70% of the mass of the dry particles is insoluble.

Although critical supersaturation was measured for only two or three values of particle radius for *any given* aerosol sample, there is some indication in the results presented in Fig. 42 that the slope of the S_c-r_0 relationship is not as steep as predicted by theory (Eq. (15)) for the case when particle composition is independent of particle size. One possible explanation of these results is that the mass fraction of soluble material in the particles increased with decreasing particle size. At this time, however, such a conclusion must be regarded as tentative. Also, a number of approximations were made in deriving Eq. (14). In particular, it was assumed that at the critical supersaturation r^3/r_0^3 is large compared to unity. This approximation becomes less tenable as r_0 and ϵ assume small values. However, the error introduced by the approximation will not be large when $r_0 > 0.02$ μm and $\epsilon > 0.1$.

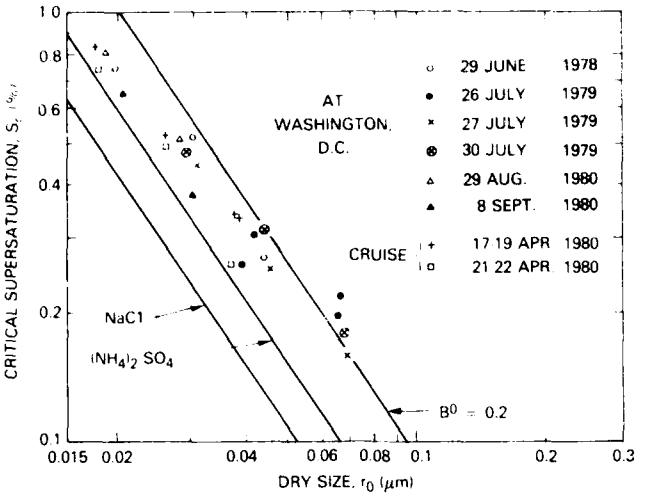

Fig. 42 — Summary of the hydroscopicity measurements in comparison with calculated values for pure particles (25°C)

Table 3 lists the values of B^0 computed from Eq. (15) and the measured values of S_c and r_0. The value of B^0 was found to range from 0.11 to 0.55, with the average of all 24 values being 0.32. Except for the data of 21 April the indicated particle-size range encompasses two or three size ranges transmitted by the mobility analyzer. While 0.55 is the largest value of B^0 we have measured to date, Hänel and Lehmann's (1981) data on ρ_0 and η^0 (Fig. 5) for aerosol samples yield values of B^0 as high as 0.98 for particles 0.15 μm to 5.0 μm in radius which were 90% sea salt. The number of measurements of B^0 which we have made is not sufficient to allow us to draw conclusions regarding differences in the value of B^0 between continental and maritime air for particles smaller than 0.1 μm. However, if the ocean surface is not a significant source of particles in this size range, then we would not expect large systematic differences in B^0 between continental and maritime air masses.

Table 3 — Values of B^0 for atmospheric aerosol particles

Location of Measurements	Date	Particle Size Range Measured (μm)	B^0
Washington, D.C.	29 June 1978	0.020-0.052	0.23-0.40
Washington, D.C.	26 July 1979	0.043-0.079	0.11-0.39
Washington, D.C.	27 July 1979	0.029-0.079	0.19-0.27
Washington, D.C.	30 July 1979	0.029-0.079	0.16-0.29
Washington, D.C.	29 Aug. 1980	0.020-0.035	0.29-0.38
Washington, D.C.	8 Sept. 1980	0.020-0.035	0.44-0.46
200 km off the Virginia coast	17-19 Apr. 1980	0.015-0.047	0.28-0.42
Norfolk harbor	21 Apr. 1980	0.032-0.047	0.51
Chesapeake Bay	22 Apr. 1980	0.015-0.032	0.40-0.55

Figure 43 shows the dependence of particle size on relative humidity for $B^0 = 0.1$, 0.3, and 0.55. These curves were computed from Eqs. (5), (10), (12), and (15) using $B = 0.8B^0$ and $\beta = 20.2$ μN/mm. The figure shows that the observed range in B^0 gives rise to large differences in the equilibrium size of particles at high relative humidity. The figure also shows the effect of dry particle radius on the particle growth curves. If we assume simply that the aerosol extinction coefficient varies as the square of particle radius, then a factor-of-2 difference in particle radius means a factor-of-4 difference in visibility.

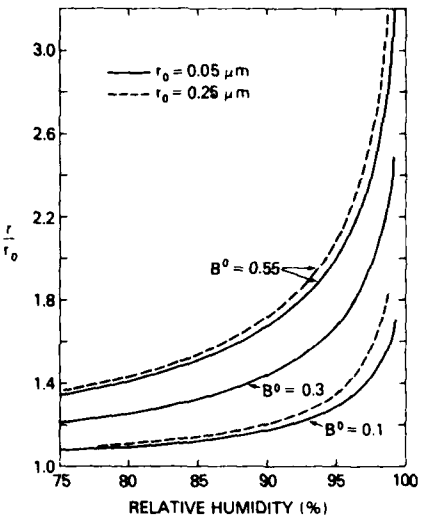

Fig. 43 — Dependence of particle size on relative humidity

Relationship Between the CCN Supersaturation Spectrum and the Size Distribution

There is a unique relationship between the dry size of a particle and its critical supersaturation S_c. This relationship can be formulated in terms of the activation parameter B^0 and is given by Eq. (15). It is plotted for various B^0 values (chemical compositions) in Fig. 42. By use of the expression given in Eq. (15) it is possible to convert all size distributions to CCN supersaturation spectra. The supersaturation spectrum is defined as the cumulative number of particles activated at a given supersaturation; therefore the differential size distribution must first be integrated to obtain the cumulative size distribution. Curves 1, 2, and 3 of Fig. 44 show supersaturation spectra calculated for a size distribution taken on 19 April at 0900 EDT assuming values of B^0 of 0.1, 0.2, and 0.3, respectively. The CCN concentrations taken concurrently are plotted as individual points and lie below those calculated from the size distribution. The degree of agreement shown between calculated CCN concentrations and those measured with the TGDCC are typical of those obtained during the cruise. The shape of the two curves in the overlap region usually agreed better than the number concentration. Another comparison between measured and calculated CCN supersaturation spectra for different times on the cruise is given by Fitzgerald and Hoppel (1982).

The measured concentration of CCN was nearly always less than the concentration inferred from the size distribution. In the past (Hoppel and Wojciechowski, 1976), we have observed that the CCN concentrations obtained from the video recording were about 10 to 15% below that obtained from simultaneous photographs. The photographic method has a smaller minimum detectable size. The TGDCC data presented in this report were taken with the videotape system. Other limitations of the TGDCC also tend to make the measured CCN concentrations on the low side (Hoppel and Wojciechowski, 1976).

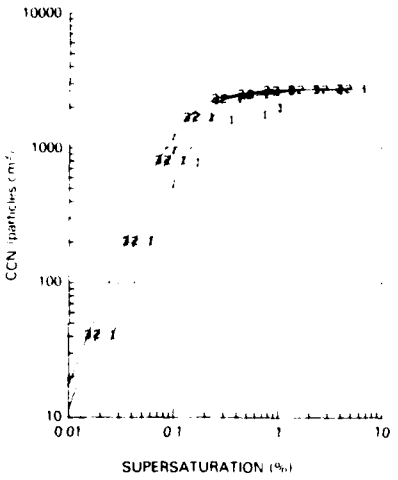

Fig. 44 — Supersaturation spectra calculated from a single size distribution for the assumed values $B^0 = 0.1$ (curve 1), 0.2 (curve 2), and 0.3 (curve 3). CCN concentrations measured concurrently with the IGDCC are plotted as the four numerals 1s that are unconnected to the curve.

Figure 45 shows the correlation of the concentrations of CCN active at 0.7% supersaturation with the number of particles in channels larger than 0.0318 μm obtained from the size distribution taken closest in time to the CCN data. Figure 45 shows the high concentrations of CCN observed during the cruise. The majority of the concentrations are greater than 2000/cm^3 and account for a large fraction of the total aerosol concentration on many occasions. The reason CCN concentrations are often a large fraction of the total concentration is obvious from the size distributions and is a result of the small number of particles at radii below 0.04 μm in air masses that have been over water for a number of hours. These conditions over water are in strong contrast to conditions usually found over land. Large CCN concentrations were also observed on a 1977 trans-Atlantic cruise as the ship left Norfolk and moved northeast along the east coast. On the 1977 cruise the CCN count remained high until the ship was beyond Nova Scotia, where it encountered a polar air mass (Hoppel, 1979). The CCN count at that point dropped to levels well below 400/cm^3.

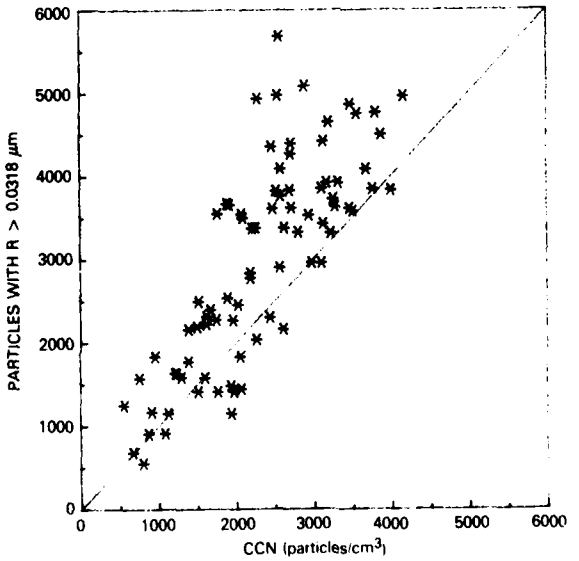

Fig. 45 — Correlation of the concentration of CCN active at 0.7% supersaturation with the number of particles larger than 0.0318 μm obtained from the size distribution.

It is generally accepted that the effects of water-vapor depletion in the TGDCC due to growing droplets is small for concentrations of CCN below 1000/cm^3. As the concentration increases, vapor depletion becomes an increasingly serious problem (Chodes et al., 1974, and others). It is evident from Fig. 45 that the measured concentration of CCN tends to be smaller than the number of particles larger than 0.0318 μm in radius when the CCN concentration is large. Since the direct measurements of B^0 would indicate that particles as small as 0.025 μm should be activated at 0.7% supersaturation, the CCN concentration should be at least as large as the concentration of particles larger than 0.0318 μm. The low CCN concentration at larger concentration is probably the result of vapor depletion in the TGDCC causing a depressed supersaturation. If we attempt to determine B^0 by matching the supersaturation spectrum inferred from the size distribution with that from the TGDCC, the value of B^0 would be considerably smaller than that determined from the more direct method used in the preceding subsection. We believe the more direct method is more accurate, because it does not depend on the absolute accuracy of the measured CCN and particle concentrations but only on the accuracy of the size interval transmitted by the mobility analyzer and the accuracy of the measurement of the critical supersaturation in the TGDCC.

Mechanisms Which Determine the Aerosol Size Distribution in Air Masses Advecting Off the East Coast

In principle it should be possible, starting with a given size distribution at some point on an airmass trajectory, to predict the future size distribution along that trajectory. In practice this is generally not possible, because one cannot accurately quantify the sources, sinks, and transformations of aerosol material, and the limitations of models to accurately predict the trajectory and meteorological conditions along that trajectory. The very simple case of an air mass advecting directly off the coast in the absence of precipitation and fronts is a possible exception. In this latter case the rapid initial decay of small particles during the first 24 hours can be explained by coagulation of particles less than 0.03 μm with larger particles and by growth of small particles due to condensation of newly formed gas-phase reaction products of low volatility on their surfaces. An example of the decay of small particles as an air mass moves off the coast is shown in Fig. 31.

Once the meteorological processes become more complex, the quantitative interpretation of the observed changes in the size distribution becomes difficult. Some of the important but difficult processes are: the effect of a capping inversion on the boundary layer, mixing within the planetary boundary layer, the cycling of air through clouds which subsequently evaporate (this mechanism perhaps having an important effect on the size distribution and to be discussed later), removal of aerosols by precipitation scavenging, formation of new particles by gas-to-particle conversion, and the generation of new particles at the sea surface during high seas and strong wind. Presently there are few marine aerosol data and supporting meteorological data available to sort out the relative contributions of the various mechanisms.

Our observations in air masses advecting off the east coast (in the absence of a precipitation cycle) are consistent for the most part with what would be expected from aerosol theory:

- There is a rapid decay of small particles (<0.05 μm) during the first hours as the air mass moves out over the ocean away from local sources of particulates. The time associated with this decay is such that the particle lifetime increases as the size increases. For particles 0.05 μm in radius and larger, coagulative decay was not observed over the interval of about 12 hours.

- The absence of local sources makes the size distribution remarkably stable, often over the interval of hours (after the initial decay of small particles). Although this observation is entirely reasonable, the observed stability is quite remarkable to anyone experienced in measuring urban aerosols. The temporal stability of the size distribution measured from a

moving platform in an atmosphere in which there is obviously turbulent mixing implies a degree of spatial uniformity as well. This spatial homogeneity must have extended at least 10 to hundreds of kilometers horizontally and 10 to hundreds of meters vertically on some occasions.

- Particles in the range 0.08 to 0.5 μm in radius were less variable than the smaller particles. This region of the size distribution has aptly been referred to as the accumulation mode, because the mass lost by coagulation from smaller sizes is transferred to this region of the distribution within a time comparable to the lifetime of particles in the troposphere. Even though the transfer of particles to the accumulation mode greatly reduces the concentration of small particles, the mass transfer is small and produced no consistent observable effect on the size range 0.08 to 0.5 μm, over the hours when the decay in the small-size range was greatest. The temporal stability of the accumulation mode also implies that ocean surface deposition of particles in this size range is small, as would be expected.

The decay time for aerosols smaller than 0.05 μm strongly depends on their size, as is evident from Fig. 31, and it makes little sense to discuss a residence or lifetime of atmospheric aerosols without specifying the size range of interest. For example, the total particulate count dropped from about 9000/cm^3 to 5500/cm^3 between curves 2 and 4 of Fig. 31, during which time the air had spent 7 hours over water. This would imply a rather short lifetime for aerosols. This loss occurred almost entirely in the size range smaller than 0.03 μm. There was no observable loss of mass and only a small change in the measured CCN concentration. For particles between 0.08 and 0.5 μm in radius the lifetime depends less on the properties of the aerosol and more on the meteorological conditions to which the air is subjected; for example, these particles are removed by wet-scavenging processes.

Possible Mechanisms Which Would Produce the Double-Peaked Size Distributions

On several occasions size distributions occurred with prominent double peaks in the small-particle size range (below 0.1 μm) and were quite constant for a number of hours. Averages during two of these occasions were shown as curve 1 in the left-hand plot of Fig. 38 and curve 1 in the left-hand plot of Fig. 39; each individual distribution of the average displayed the double peak. Figure 46 shows a composite of five of the eight size distributions from which the average shown as curve 1 in the left-hand plot of figure 38 was calculated. We can suggest at least four physical mechanisms which might produce a double-peaked size distribution: mixing of two air masses with very different aerosol populations, heterogeneous nucleation and growth of larger particles by condensation of gas-phase reaction products, homogeneous heteromolecular nucleation of new small particles in air initially deficient of particles (the peak at the smaller size resulting from newly formed small particles and the peak at the larger sizes representing the remnant of the size distribution in an aged air mass), and increase in mass of CCN which have been through a cloud condensation-evaporation cycle.

The first of the mechanisms which might produce a double peak is the mixing of two air masses with very different size distributions. It is certainly possible to invent two size distributions which, when added together, will result in a size distribution such as those shown in Fig. 46. However, the two size distributions (assuming each is singly peaked) must be much different from what we have ever observed. To reproduce the strong minimum, the size distribution exhibiting the peak at the smaller size must decrease with increasing size much more rapidly than has ever been observed. Therefore, it is highly unlikely that the size distribution of Fig. 46 was formed by the mixing of air masses.

The second mechanism which might produce a double peak is the continual formation of new gaseous species in the atmosphere by gas-phase reactions (including photochemical reactions). Some of these reaction products are of low volatility and will diffuse to and condense on existing particles. If the particles are larger than a critical size, they will be nucleated and grow (details of the mechanism being given in Hoppel, 1975). This causes a separation in the size distribution at the critical radius and

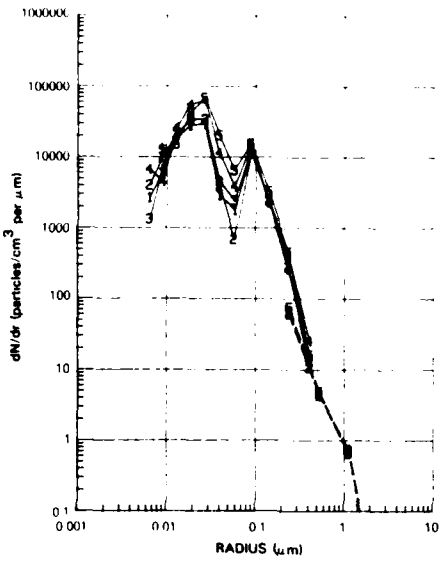

Fig. 46 — Composite of five consecutive size distributions over a 3-hour interval which all exhibited a double peak

could lead to the double-peaked size distribution. Use of estimated gas-phase reaction rates for the marine environment to quantitatively estimate the growth rate of particles with radii from 0.03 to 0.06 μm by this mechanism, however, yields growth times which are much longer than the lifetimes of atmospheric aerosols. It is therefore doubtful that this mechanism produced the size distributions shown in Fig. 46.

The third mechanism which might produce a double peak is the production of new particles at small sizes (<0.005 μm). They are produced when the surface area of the existing particles is insufficient to absorb the newly formed involatile products and the concentration of these involatile products increases to the level required for spontaneous nucleation of new particles. These newly formed particles grow by condensation of additional gas-phase reaction products and by coagulation with other particles. This growth becomes slow as the particle radius increases above 0.01 μm. The newly formed particles produce a new peak at a smaller radius, in addition to the residual peak, and could certainly produce a double-peaked size distribution. This mechanism has been suggested by others and possibly has been observed by Haaf and Jaenicke (1980) on a mountain site (Schauinsland in the Black Forest), *where the increase in small particles in the morning was strongly correlated with solar radiation.* Haaf and Jaenicke found a weak suggestion in their data of small particle formation in the eastern North Atlantic on sunny days. We looked in vain for a correlation between small particles and solar radiation throughout the *Hayes* cruise and could find none. If there were solar influences on the concentration of small particles, they were not immediate and were masked by the more prominent meteorological effects. Furthermore the total aerosol load off the east coast of the United States during our cruise was considerably greater than that usually encountered in the middle and eastern Atlantic. Thus the surface area available to absorb newly formed gas-phase-reaction products is larger than in more remote regions of the Atlantic. In regions where the aerosol load is less, the probability of new particle formation is greater. The double-peaked size distribution shown in Fig. 46 exhibited few particles with a radius less than 0.01 μm. This would indicate that if nucleation of new particles occurred, then the mechanism acted earlier and new particle formation had either ceased or was weak at the time the measurements were made. These measurements were made on a clear sunny morning.

The fourth mechanism which might produce a double peak is the enhancement of involatile material in a droplet during formation and reevaporation of cloud droplets. Pruppacher and Klett (1978) estimate that globally the residence time of water in the troposphere is about 9 days before

removal by precipitation and that there are about ten condensation-evaporation cycles before a precipitating system is formed. This would indicate that moisture goes through a cloud formation-and-evaporation cycle about once a day. In a well-mixed lower troposphere this would imply that air (with aerosols) is also filtered through clouds at about the same frequency. When a cloud forms, aerosols larger than a critical size will be activated and grow to cloud drop sizes. Typically the change in size will be from 0.05 μm to 5.0 μm, which is an increase in mass of the order of 10^6. The increased size of cloud droplets makes them effective surfaces to which smaller aerosol particles can diffuse and effective centers for absorbtion of various trace gases. Some of these dissolved gases react with other dissolved gases and water to form new substances which will remain as additional residue when the cloud droplet reevaporates. The process of this type most widely studied is the conversion of SO_2 to sulfate in the cloud droplet, by Easter and Hobbs (1974) and Hegg and Hobbs (1979). If only one foreign molecule in 10^6 condensed water molecules is retained as new nuclear material, then upon reevaporation of the droplet, the mass of the residue will be increased by as much as a factor of 2 and the radius will be increased by the cube root of 2 (being less for larger CCN).

To illustrate how this process might work to form a double-peaked size distribution, a typical size distribution shown as curve 1 in Fig. 47 has been subjected to a simulated 1-hour cloud cycle. The maximum supersaturation in the cloud is assumed to be about 0.3%, so that all particles greater than about 0.04 μm are activated to form a cloud with a droplet concentration of 500/cm^3 and a liquid water content of 0.3 g/m^3. Nuclei smaller than 0.04 μm are not activated and are allowed to diffuse to the cloud droplets according to the following formula by Twomey (1977):

$$\frac{n(r)}{n_0(r)} = e^{-7.85W^{1/3}N^{2/3}D(r)t}, \tag{21}$$

where $n(r)$ is the number of particles of radius $r (r < 0.04\ \mu\text{m})$ that diffuse to the cloud droplets, $n_0(r)$ is the initial number of particles of radius r, W is the liquid water content of the cloud, N is the cloud droplet concentration, $D(r)$ is the diffusion coefficient for particles of radius r, and t is the time. Upon reevaporation, particles initially bigger than 0.04 μm in radius were assumed to have arbitrarily increased their mass by a factor of 2, due to the in-cloud processes mentioned. Curve 2 of Fig. 47 is the size distribution obtained from curve 1 when unactivated particles are lost to cloud droplets by diffusion according to Eq. (21) and the mass of cloud nuclei has been increased by a factor of 2 during the condensation/evaporation cycle. The depth of the minimum between the double peak of curve 2 was drawn in arbitrarily. Ideally the minimum would be even less, but any mixing with air which had not been through a cloud cycle has a strong tendency to destroy the minimum. If this mechanism is responsible for the double-peaked size distribution of Fig. 46, then the strong minimum observed implies that the air had been through a cloud cycle at least once and was not mixed with air which had not been through a cloud cycle.

The size distributions of Fig. 46 were obtained under clear conditions just behind a cool front. However, the NOAA back-trajectories indicated that the air had originated in a cloudy overcast region just behind the front within the prior 12 hours. The reliability of the trajectories under these conditions is unknown. It is interesting that Haaf and Jaenicke (1980) observed on Schauinsland (at 1230 m) on "days with complete cloud cover" size distributions somewhat similar to some of our double-peaked distributions.

Of the four mechanisms discussed which may produce double-peaked distributions, the latter two are probably both important at times in the marine atmosphere. However, our discussion is speculative, and more aerosol measurements and supporting meteorological measurements are needed to resolve specific mechanisms.

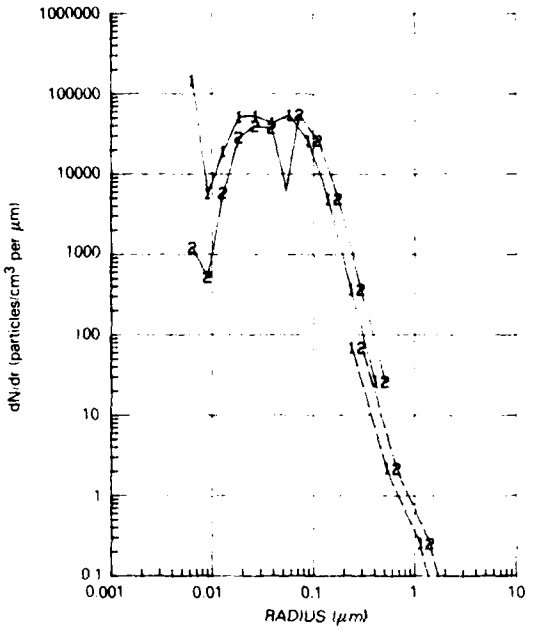

Fig. 47 — Illustrative example of how air passing through a cloud cycle could produce a double-peaked size distribution. Curve 1 is the size distribution entering the cloud, and curve 2 is the size distribution in the evaporated cloud

Summary of Electromagnetic Extinction Results

The extinction coefficients at 0.55 μm in wavelength for those size distributions from the 1980 USNS *Hayes* cruise that are given in the figures of this report (excluding composites) are tabulated in Table 4. The extinction is computed by use of approximation formulas for the Mie theory extinction efficiency factor Q_e (Fitzgerald, 1979), analytic approximations to the particle distributions in the form of the sum of three log-normal distributions, index-of-refraction data from Paltridge and Platt (1976) and Shettle and Fenn (1979), and the relative amounts of water and dry material in the particles as a function of relative humidity, as given by Fitzgerald (1978). The details of the computations were discussed in the subsection beginning on page 15.

The agreement between measured and computed extinction as given in Table 4 is good for the intervals when the ship was under high pressure off the east coast (Fig. 38, curve 1), and for the interval of rapid change in extinction coefficients just before the return to Chesapeake Bay (Fig. 41). The agreement was also good for the interval when the distributions were stable and double-peaked (Fig. 39, curve 1). Further, although the computed values of extinction for before and after passage of a cold front on 21 April (Fig. 40) were lower than the measured extinctions, the ratio of the extinction after passage of the front to that before passage is nearly the same for measured and computed extinction.

The percentage of the computed extinction at 0.55 μm in wavelength due to particles in selected size ranges shown in Table 4 is plotted in Fig. 48. There are wide variations in the contributions of the individual size ranges to the total extinction, although the contribution from particles with a radius less than 0.1 μm is small. However, the variation during unchanging weather conditions is much less. Only in the rapidly changing air masses after the ship left Chesapeake Bay (Fig. 31) and in the changing air masses associated with passage of a warm front (Fig. 34) were there appreciable changes in the relative contribution of different size ranges, as can be seen from Table 4.

Table 4 — Extinction coefficients at 0.55 μm in wavelength for particle distributions shown in this report

Figure-Curve	Extinction (10^{-4}/m)		RH[‡] (%)	Extinction (%) in Particle-Radius Ranges[†]				
	Measured*	Computed[†]		0.04 to 0.1 μm	0.1 to 0.3 μm	0.3 to 0.6 μm	0.6 to 0.9 μm	0.9 to 3 μm
31-1	0.36	0.28	42	7	75	7	5	6
31-2	0.55	0.51	65	6	38	23	16	19
31-3	0.46	0.33	65	7	36	17	18	22
31-4	0.55	0.39	52	8	55	9	9	18
33-1	1.76	1.10	86	2	30	26	23	18
33-2	1.51	1.54	80	2	26	33	23	16
33-3	1.01	1.23	80	1	18	28	30	23
33-4(34-1)	0.80	0.73	72	1	23	30	24	21
34-2	—	0.88	95	1	14	20	31	34
34-3	—	1.69	95	0	4	21	33	42
38-1	0.34	0.35	64	4	47	25	12	11
38-1	0.31	0.32	60	6	49	31	8	6
38-1	0.19	0.19	45	5	61	23	5	5
39-1	0.30	0.31	38	7	68	18	3	3
39-2	0.70	0.64	50	3	79	14	2	2
40-1	0.61	0.46	84	1	67	22	5	4
40-2	1.10	0.93	75	3	60	23	8	6
41-1	1.8	1.60	74	2	39	35	15	9
41-2	0.74	0.70	70	4	47	34	8	6
41-3	0.41	0.36	55	8	53	29	4	6
41-4	0.15	0.16	58	5	54	29	5	7

*The measured extinction is really the scattering coefficient measured with an integrating nephelometer.
†The total extinction and extinction due to particles in selected size ranges were computed by the method outlined in the subs tion beginning on page 15.
‡The relative humidity was determined from dew point and temperature.

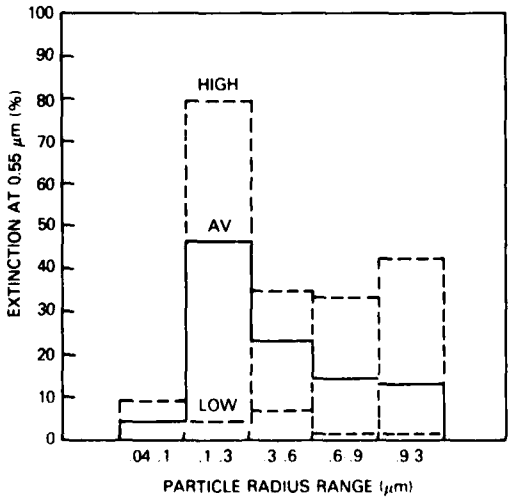

Fig. 48 — Contribution of various size ranges to the total aerosol extinction at 0.55 μm in wavelength

Particles 0.1 to 0.3 μm in radius contributed the most to the extinction in 16 of the 21 distributions. The least variability in percent contribution to total extinction was observed in the range 0.3 to 0.6 μm. This is consistent with Figs. 27, 29, and 30, which show that the variations in the size distribution at intermediate sizes are much less than the variations at smaller and larger sizes. In only one distribution did particles 0.3 to 0.6 μm in radius make the largest contribution to total extinction.

The contribution to total extinction at 0.55 μm from particles greater than 0.6 μm in radius was also highly variable from case to case, with a minimum of 4% and a maximum of 75% of the extinction. The contribution from particles 0.6 to 0.9 μm in radius and 0.9 to 3 μm in radius were usually nearly equal and tracked each other in their contribution to the total extinction. This can be attributed to the origin of many of the particles in these size ranges being from wind and wave action. The two distributions in which particles 0.9 to 3 μm in radius made the largest contribution to total extinction were composites of distributions in high winds, as was discussed with regard to the distributions shown in Fig. 34.

Waggoner et al. (1981) have reported a good correlation between fine-particle mass and visibility for rural and urban air. To test this correlation for the *Hayes* cruise, the mass was computed from the log-normal fit to the data points. A particle density of 2.0 g/cm^3 and a large-radius cutoff of 1.25 μm were selected for comparison with the results of Waggoner et al. (1981).

The correlation between the fine-particle mass and extinction at 0.55 μm is shown in Fig. 49, where the extinction as measured with a nephelometer is plotted against the mass of particles of radius between 0.05 and 1.25 μm calculated from the size distributions. The correlation coefficient is 0.89, and the ratio of mass concentration to extinction is 0.60 g/m^2, which is within the range of 0.2 to 0.7 g/m^2 indicated by the data of Charlson et al. (1968).

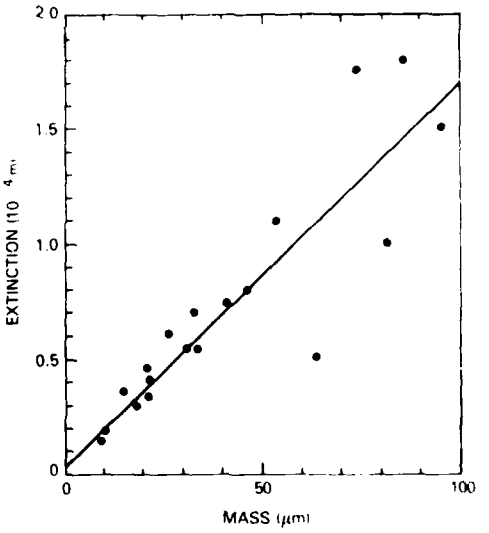

Fig. 49 — Correlation between fine-particle mass ($r < 1.25$ μm) and extinction (scattering coefficient) at 0.55 μm

The correlation coefficient between the extinction computed from the size distribution and the mass of the particles ($0.05 < r < 1.25$ μm) is 0.98, whereas the correlation between the calculated and measured extinction at 0.55 μm in wavelength is 0.91. The mass is relatively independent of the lower radius cutoff, with a change in the lower radius cutoff of from 0.01 to 0.1 μm, resulting in a few percent change in mass. The mass is much more dependent on the large-radius cutoff, with the increase in mass resulting from an extension of the large-radius cutoff to 3 μm ranging from less than 20% to well over 100%.

Waggoner et al. (1981) also present a historic perspective to the optical characteristics of atmospheric aerosols before discussing the results of their measurements of aerosols in rural and urban air. The correlations between fine-particle mass and extinction for their measurements were greater than 0.95, and their mass-to-extinction ratio was about 0.3 g/m^2 for the continental aerosols they measured.

CONCLUSIONS

In this report we have described the instruments and methods developed at NRL to measure submicrometer particles and have presented the results of size distributions and solubility measurements along the east coast of the United States both at a shore site (Wallops Island) and from a ship within 300 km of the coast. Some measurements made at Washington, D.C., are included to contrast submicrometer aerosol properties in urban air with those in aged continental air off the east coast.

Earlier measurements of the marine size distribution were of such poor quality that it was impossible to determine if different distributions were real or an artifact of the measurement technique (Jaenicke, 1978). The size distributions presented in this report are sufficiently accurate and numerous to assure that the observed changes were real and that the data can be used with confidence in the search for physical mechanisms causing the changes.

Some of the observed changes can be understood in general qualitative terms:

- The rather rapid decay of small particles as an air mass leaves land and advects over the ocean is due mainly to coagulation of small particles with particles greater than 0.06 μm in radius and indicates little to no production of new submicrometer particles;

- The observed termporal stability of the size distribution over many hours would be expected in air masses in which the initial decay of small particles had already occurred and no wet-scavenging of particles is occurring;

- The decrease in particles in the range 0.08 to 1.0 μm in an air mass which appeared to go through a precipitation cycle can qualitatively be explained in terms of wet-scavenging of particles;

- An increase in particles larger than 0.5 μm during heavy seas and high winds is undoubtedly caused by surface-generated sea-salt particles.

Many observed changes in the size distribution are difficult to explain even qualitatively. Some of the difficulty in understanding the changes may originate with our inability to determine the history of the air encountered and the role which condensation and reevaporation of cloud droplets play. The existence of two distinct peaks on several occasions is an interesting example of a phenomenon which we were unable to explain adequately.

Efforts to quantify or model mechanisms believed to be responsible for the changes have not yet been attempted for specific cases given in this report. In principle it should be possible to start with a size distribution at one point on the air mass trajectory and predict the size distribution at a later time. In practice this task is extremely difficult, because a prior size distribution on the same trajectory is not usually known and the trajectories and the meteoroligical history along a trajectory cannot be predicted accurately. Nevertheless a comparison of model predictions including various known mechanisms applied to specific cases given by our data could help sort out the relative importance of mechanisms. Such studies are planned.

Since the measurements given in this report were all taken within 300 km of the coast, the air masses encountered were not sufficiently aged that the aerosol load could be considered to represent "marine" or "background" levels. "Marine" aerosol and/or "background" aerosol are poorly defined descriptions often used to indicate low submicrometer concentrations found at locations remote from land and thus from anthropogenic sources of pollution. Measurements in air masses farther removed from land are necessary to observe the change from the aged-continental size distributions found near the east coast of the United States to background levels believed to exist in more remote regions. Measurements farther from land were made on a cruise during March and April of 1983 and will be an important addition to the measurements reported here.

Measured values of the aerosol solubility (activation) parameter B^0 ranged from 0.1 to 0.55. The effect of the value of B^0 on the growth of particles as a function of relative humidity was shown in Fig. 43. A particle having $B^0 = 0.55$ and a dry radius of 0.05 μm will swell to twice its dry size at 95% relative humidity, whereas a particle with $B^0 = 0.1$ will grow to only 1.3 times its dry size at 95% relative humidity. If it is assumed that the soluble component of atmospheric particles is ammonium sulfate and that the particles have a dry density of 1.8 g/cm^3, then a B^0 value of 0.1 implies that 15% of the dry mass of the particle is soluble and a B^0 value of 0.55 implies that 80% of the mass is soluble.

Electromagnetic extinction in the wavelength range 0.3 to 12 μm was calculated from the measured size distributions using approximation formulas for the Mie extinction efficiency factor. The agreement between the calculated extinction at 0.55 μm and the measured scattering coefficient is good. Particles in the size range 0.1 to 0.3 μm made the largest contribution to the extinction on nearly all occasions. A high correlation was found between fine-particle mass (calculated from the measured size distribution using a particle density of 2.0 g/cm^3 and a large-radius cutoff of 1.25 μm) and the measured scattering coefficient. The mean value of the ratio of mass concentration to the scattering coefficient at 0.55 μm was 0.60 g/m^2.

ACKNOWLEDGMENTS

We thank Dr. Michel Vietti, associate professor of physics at the University of Maine, who was at NRL under the Intergovernmental Personnel Program from January to August 1979 and then returned to NRL in the spring of 1980 to accompany us on the USNS *Hayes* cruise. His help was invaluable in automating the mobility analyzer and data-aquisition system and in acquiring the data on all three of the deployments discussed in this report.

T. A. Wojciechowski was also part of our team during the three deployments and was responsible for the mechanical design and construction of much of the equipment,which worked so well during the deployments. He has been sorely missed since his retirement in early 1981.

P. J. Hannan of the Environmental Biology Branch was senior scientist during the cruise. His good humor, helpfulness, and effective liaison with the officers and crew of the *Hayes* was deeply appreciated.

We also thank J. L. Heftner of NOAA's Air Resources Laboratory for providing the air mass trajectory analysis used in this presentation and J. J. Mullaney of the forecast division of NOAA for providing surface weather maps.

The use of the facilities at Wallops Island was through the courtesy of NASA. We thank Raymond Atkins for his cooperation and others for providing us with local meteorlogical data.

Lastly we thank the officers and the crew of the USNS *Hayes* as well as the NRL Ships Facility Group, whose splendid cooperation made it possible to obtain the shipboard data.

REFERENCES

Alofs, D.J., and J.C. Carstens (1976), "Numerical simulation of a widely used cloud nucleus counter," *J. Appl. Meteor.* **15**, 350-354.

Anonymous (1960), "IM 161 (XB-1)/WDQ Radiac Meter," NRL Instruction Book 29.

Blifford, L.B., L.B. Lockhart, Jr., and H.B. Rosenstock (1952), "On the natural radioactivity of the air," *J. Geophys. Res.* **57**, 499-509.

Bradley, W.E., and J.E. Pearson (1970), "Aircraft measurements of the vertical distribution of radon in the lower atmosphere," *J. Geophys. Res.* **74**, 5890-5894.

Bressan, D.J. (1981), "Maritime Atmosphere Salt Load Monitoring System," NRL Memorandum Report 4581.

Charlson, R.J., N.C. Ahlquist, and H. Horvath (1968), "On the generality correlation of aerosol mass concentration and light scatter," *Atmos. Envir.* **2**, 455-464.

Chodes, N., J. Warner, and A. Gagin (1974), "A determination of the condensation coefficient of water from the growth rate of small cloud droplets," *J. Atmos. Sci.* **31**, 1351-1357.

Dinger, J.E., H.B. Howell, and T.A. Wojciechowski (1970), "On the source and composition of cloud condensation nuclei in the subsident air mass over the North Atlantic," *J. Atmos. Sci.* **27**, 791-797.

Easter, R.C., and P.V. Hobbs (1974), "The formation of sulfates and the enhancement of cloud condensation nuclei in clouds," *J. Atmos. Sci.* **31**, 1586-1594.

Fitzgerald, J.W., (1975), "Approximation formulas for the equilibrium size of an aerosol particle as a function of its dry size and composition and the ambient relative humidity," *J. Appl. Meteor.* **14**, 1044-1049.

Fitzgerald, J.W. (1978), "On the Growth of Aerosol Particles with Relative Humidity," NRL Memorandum Report 3847.

Fitzgerald, J.W. (1979), "Approximation formulas to calculate infrared extinction by an aerosol having a Junge size distribution," *J. Appl. Meteor.* **18**, 931-939.

Fitzgerald, J.W., and W.A. Hoppel (1982), "Measurements of the relationship between the dry size and critical supersaturation of natural aerosol particles," *Idöjaros* **86** 242-248.

Fitzgerald, J.W., C.F. Rogers, and J.G. Hudson (1981), "Review of isothermal haze chamber performance," *J. Rech. Atmos.* **15**, 333-346.

Fitzgerald, J.W., W.A. Hoppel, and M. Vietti (1982), "The size and scattering coefficient of urban aerosol particles at Washington, D.C., as a function of relative humidity," *J. Atmos. Sci.* **39**, 1838-1852.

Gathman S.G. (1982), private communication.

Gathman, S.G. (1983), "Navy hygroscopic aerosol model," in *Proceedings of the Workshop on Hygroscopic Aerosols in the Planetary Boundary Layer,* 13-15 Apr. 1982, Vail, Colorado, Spectrum Press, Hampton, Va.

Gerber, H.E., W.A. Hoppel, and T.A. Wojciechowski (1977), "Experimental verification of the theoretical relationship between size and critical supersaturation of salt nuclei," *J. Atmos. Sci.* **34**, 1836-1841.

Grant, L.O. (1971), editor, *The Second International Workshop on Condensation and Ice Nuclei.* Dept. Atmos. Sci., Colorado State Univ., Ft. Collins.

Haaf, W., and R. Jaenicke (1980), "Results of improved size distribution measurements in the Aitken range of atmospheric aerosols," *J. Aerosol Sci.* **11**, 321-330.

Hänel, G. (1976), "The properties of atmospheric aerosol particles as functions of the relative humidity at thermodynamic equilibrium with the surrounding moist air," *Advances in Geophys.* **19**, 73-188.

Hänel, G., and M. Lehmann (1981), "Equilibrium size of aerosol particles and relative humidity: New experimental data from various aerosol types and their treatment for cloud physics applications," *Contr. Atmos. Sci.* **28**, 382-390.

Harley, J.H., N.A. Hallden, and I.M. Fisenne (1962), "Beta scintillation counting with thin plastic phosphors," *Nucleonics* **20**, 59-61.

Heffter, J.L., A.D. Taylor, and G. Ferber (1975), "A regional-continental scale transport, diffusion, and deposition model: Part I, Trajectory model, and Part II, Diffusion-deposition models," NOAA TM ERL ARL-50.

Hegg D.E., and P.V. Hobbs (1979), "The homogeneous oxidation of sulfur dioxide in cloud droplets," *Atmos. Environment* **13**, 981-987.

Hidy, G.M. (1972), editor, *Aerosols and Atmospheric Chemistry*, Academis Press, New York, Part III.

Hoppel, W.A. (1975), "Growth of condensation nuclei by heteromolecular condensation," *J. Rech. Atmos.* **9**, 167-180.

Hoppel, W.A. (1978), "Determination of the aerosol size distribution from the mobility distribution of the charged fraction of aerosols," *J. Aerosol Sci.* **9**, 41-54.

Hoppel, W.A. (1979), "Measurement of the size distribution and CCN supersaturation spectrum of submicron aerosols over the ocean," *J. Atmos. Sci.* **36**, 2006-2015.

Hoppel, W.A. (1981a), "Measurement of the aerosol size distribution with NRL's mobility analyzer," *J. Rech. Atmos.* **15**, 313-319.

Hoppel, W.A. (1981b), "Description of the NRL isothermal haze chamber," *J. Rech. Atmos.* **15**, 263-266.

Hoppel, W.A. (1982), "Measurement of size distributions and solubility of submicron particles," pp. 345-360 in *Atmospheric Aerosols: Their Formation, Optical Properties, and Effects*, A. Deepak, editor, Spectrum Press, Hampton, Va.

Hoppel, W.A., and T.A. Wojciechowski (1976), "Accuracy limitations on CCN measurements with thermal gradient diffusion chambers," *J. Applied Meteor.* **15**, 107-112.

Hoppel, W.A., and T.A. Wojciechowski (1981), "Description and discussion of the NRL TGDCC," *J. Rech. Atmos.* **15**, 209-213.

Hoppel, W.A., J.E. Dinger, and R.E. Ruskin (1973), "Vertical profiles of CCN at various geographical locations," *J. Atmos. Sci.* **30**, 1410-1420.

Hoppel, W.A., S. Twomey, and T.A. Wojciechowski (1980), "A segmented thermal diffusion chamber for continuous measurement of CN," *J. Aerosol Sci.* **10**, 369-373.

Hosler, C.R. (1969), "Vertical diffusivity from radon profiles," *J. Geophys. Res.* **74**, 7018-7026.

Hsu, S.A., R.E. Larson, and D.J. Bressan (1980), "Diurnal variations of radon and mixing heights along a coast: A case study," *J. Geophys. Res.* **85**, 4107-4110.

Jaenicke, R. (1978), "Aitken particle size distributions in the Atlantic north-east trade winds," "*Meteor*" *Forsch.-Ergebnisse*, Reihe **B**, No. 13, 1-9.

Jeck, R.K. (1975), "*A Study of the Airflow over the Research Ship USNS Hayes*," unpublished.

Junge, C.E. (1963), *Air Chemistry and Radioactivity*, Academic Press, New York.

Junge, C., and E. McLaren (1971), "Relationship of cloud nuclei spectra to aerosol size distribution and composition," *J. Atmos. Sci.* **47**, 155-171.

Katz, U., and W.C. Kocmond (1973), "An investigation of the size-supersaturation relationship of soluble condensation nuclei," *J. Atmos. Sci.* **30**, 160-165.

Knutson, E.O., and K.T. Whitby (1975), "Aerosol classification by electric mobility: apparatus, theory, and application," *J. Aerosol Sci.* **6**, 443-451.

Larson, R.E. (1973), "Measurement of radioactive aerosols using thin plastic scintillators," *Nuc. Inst. and Meth.* **108**, 467-470.

Larson, R.E., and D.J. Bressan (1978), "Automatic radon counter for continual unattended operation," *Rev. Sci. Instrum.* **49**, 965-969.

Larson, R.E., D.J. Bressan, K.W. Marlow, T.A. Wojciechowski, and J.L. Heffter (1979), "A comparison of concentrations of fission products, radon 222, and cloud condensation nuclei over the North Atlantic," *Pageoph* **117**, 874-882.

Larson, R.E., and D.J. Bressan (1980), "Air mass characteristics over coastal areas as determined by radon measurements," pp. 94-100 in Preprint Vol., *Second Conference on Coastal Meteorology*, Am. Metro. Soc., Boston.

Liu, B.Y.H., and D.Y.H. Pui (1974), "A submicron aerosol standard and the primary, absolute calibration of the condensation nuclei counter," *J. Colloid and Interface Sci.* **47**, 155-171.

Lockhart, L.B., Jr., R.L. Patterson, Jr., and C.R. Hosler (1965), "Determination of Radon Concentration in the Air Through Measurement of its Solid Decap Products," NRL Report 6229.

Lundgren, D.A., F.S. Harris, W.H. Marlow, M. Lippmann, W.E. Clark, and M.D. Durham (1979), editors, *Aerosol Measurements*, University Presses of Florida, Part 3.

Paltridge, G.W., and C.M.R. Platt (1976), *Radiative Processes in Meteorology and Climatology*, Elsevier, Amsterdam-Oxford-New York.

Prospero, J.M., and T.N. Carlson (1970), "Radon-222 in the North Atlantic Trade Winds: Its Relationship to Dust Transport From Africa," *Science* **167**, 974-977.

Pruppacher, H.R., and J.D. Klett (1978), *Microphysics of Clouds and Precipitation*, D. Reidel, Boston.

Saunders, A.W., Jr., R.L. Patterson, Jr., and L.B. Lockhart, Jr. (1968), "The Interaction of Radon Decay Products with Aerosols," NRL Report 6802.

Shettle, E.P., and R.W. Fenn (1979), "Models for the Aerosols of the Lower Atmosphere and the Effects of Humidity Variations on their Properties," Air Force Geophysics Laboratory, AFGL-TR-79-0214.

Twomey, S. (1965), "Size measurements of natural cloud nuclei," *J. Rech. Atmos.* **2**, 113-119.

Twomey, S (1967), "Remarks on the photographic counting of cloud nuclei," *J. Rech. Atmos.* **3**, 85-90.

Twomey, S. (1968), "On the composition of cloud nuclei in the northern United States," *J. Rech. Atmos.* **3**, 281-285.

Twomey, S. (1971), "The vaporization of submicron aerosol particles," *J. Rech. Atmos.* **5**, 93-99.

Twomey, S. (1977), *Atmospheric Aerosols*, Elsevier, New York.

Waggoner, A.P., R.E. Weiss, N.C. Ahlquist, D.S. Covert, S. Will, and R.J. Charlson (1981), "Optical characteristics of atmospheric aerosols," *Atmos. Environ.* **15**, 1891-1909.

Winkler, P. (1973), "The growth of atmospheric particles as a function of relative humidity, II — An improved concept of mixed nuclei," *J. Aerosol Sci.* **4** 373-387.


DATE
ILME